THERMODYNAMICS OF AQUEOUS 2-AMINO-2-METHYL-1-PROPANOL AND 2-AMINO-2-METHYL-1-PROPANOL HYDROCHLORIDE OVER A WIDE RANGE OF TEMPERATURE AND PRESSURE: APPARENT MOLAR VOLUMES, HEAT CAPACITIES, EXCESS MOLAR HEAT CAPACITIES, VOLUMES, AND EXPANSIBILITIES

KAI ZHANG

Your file Votre référence
ISBN: 0-612-84056-5
Our file Notre référence
ISBN: 0-612-84056-5

Canada

THERMODYNAMICS OF AQUEOUS 2-AMINO-2-METHYL-1-PROPANOL AND 2-AMINO-2-METHYL-1-PROPANOL HYDROCHLORIDE OVER A WIDE RANGE OF TEMPERATURE AND PRESSURE: APPARENT MOLAR VOLUMES, HEAT CAPACITIES, EXCESS MOLAR HEAT CAPACITIES, VOLUMES, AND EXPANSIBILITIES

by

Kai Zhang

A thesis submitted to the
School of Graduate Studies
in partial fulfilment of
the requirements for the
degree of Master of Science

Department of Chemistry
Memorial University of Newfoundland

September 2001

St. John's Newfoundland

Abstract

Aqueous alkanolamines have wide applications in steam generators and natural and refinery gas streams. 2-amino-2-methyl-1-propanol (AMP), $(CH_3)_2C(CH_2OH)NH_2$, is a sterically-hindered primary amine because of the bulky group adjacent to the amino nitrogen. In this study, apparent molar volumes ($V_{\phi,2}$) and apparent molar heat capacities ($C_{p,\phi,2}$) for very dilute aqueous AMP and $AMPH^+Cl^-$ were determined from relative densities and specific heat capacities measured in a Sodev vibrating-tube densimeter and a Sodev Picker flow microcalorimeter, at the pressure of 0.1 MPa over the temperature range 283 K ≤ T ≤ 328 K. Apparent molar volumes ($V_{\phi,2}$) of aqueous AMP and $AMPH^+Cl^-$ at temperatures up to 556 K were measured at two pressures with a high-temperature platinum vibrating tube densimeter. Functions were fitted to the molality-dependent apparent molar properties, and extrapolated to infinite dilution to obtain standard partial molar volumes V_2^o and standard partial molar heat capacities $C_{p,2}^o$.

At elevated temperatures, the standard partial molar properties of aqueous AMP appear to approach strong positive infinities at the critical point, and those of aqueous $AMPH^+Cl^-$ appear to approach strong negative infinities. These observations are typical for neutral and ionic species. Three models were fitted to the standard partial molar properties: the revised Helgeson-Kirkham-Flowers (HKF) model, the "density" model, and a hybrid model. The standard partial molar volumes V_2^o were represented well by all of the three models, for both aqueous AMP and $AMPH^+Cl^-$. Values for the standard

partial molar heat capacity $C^{o}_{p,2}$ at high temperatures are predicted by these models through thermodynamic relationships. The predictions from these models agree on the direction of the divergence near the critical temperature, that is, positive for AMP and negative for $AMPH^{+}Cl^{-}$. However, the magnitude of the predicted $C^{o}_{p,2}$ is different.

The heat capacities of (AMP + H_2O) were measured in a CSC 4100 differential scanning calorimeter at temperatures from 278.15 K ≤ T ≤ 368.15 K, to yield excess molar heat capacities $C^{E}_{p,m}$ over the whole mole fraction range. Densities of (AMP + H_2O) were determined over the whole mole fraction range at temperatures from 293.15 K ≤ T ≤ 353.15 K, using a DMA 5000 vibrating tube densimeter. Excess molar volumes V^{E}_{m} and excess molar thermal expansibilities $E^{E}_{m} = (\partial V^{E}_{m}/\partial T)_{p}$ were derived. A modified Redlich-Kister treatment was employed to describe the excess functions. Reduced excess molar properties $C^{E}_{p,m}/\{x_2(1-x_2)\}$ were employed to reveal solute-solvent and solute-solute interactions, and the properties of (AMP + H_2O) were compared with those of (methyldiethanolamine + H_2O) from an earlier study in this laboratory. Values of $C^{o}_{p,2}$ and V^{o}_{2} for AMP from measurements at low mole fractions ($x \leq 0.03$) differ from the Redlich-Kister extrapolations, suggesting that specific interactions took place in dilute solutions. The mole-fraction dependence of the reduced excess heat capacities is most pronounced below 298.15 K. These observations were interpreted using Lumry's model [Faraday Symp. Chem. Soc., 17, 93-108 (1982)]. Further studies to examine other thermodynamic properties would be of interest, particularly at temperatures below 298.15 K.

Acknowledgments

First of all, I wish to thank my supervisor, Dr. Peter Tremaine, for his guidance, encouragement, and patience in every part of this work. It is my fortune to be his student, and as a supervisor he has done everything he could to benefit students.

I wish to thank Dr. Raymond Poirier and Dr. Michael Mackey, for being my supervisor committee members, giving time and support all along, and teaching me courses.

I wish to express my gratitude to Dr. Caibin Xiao and Dr. Rodney Clarke for helpful discussions and suggestions. I am also grateful to my wonderful colleagues for their help and the good times: Dr. Liliana Trevani, Dr. Richard Bartholomew, Brent Hawrylak, Wei Xie, Chris Collins, Wanda Aylward, Rosemarie Harvey, Jenene Roberts, and Sean Keating.

I am grateful to the following people who kindly helped me during the course of this work: Randy Thorn from the machine shop and Carl Mulcahy from the electronics shop for the equipment repairs; Dr. Peter Pickup and Dr. Gregory Dunning for teaching me courses; Dr. Rom Palepu in St. Francis Xavier University for providing the access and introduction to the DMA 5000 densimeter; Dr. Jacques Desnoyers (INRS-Énergie et Matériant) for his valuable comments on excess properties; Dr. Robert Helleur for GC-MS analysis of the AMP materials; and Linda Thompson for her help on the measurements of the index of refraction. Also, I thank the amino acid analysis facility in

Memorial University of Newfoundland for their analysis on my solutions.

I cannot forget the love and inspiration from my parents, Wanhua Zhang and Lianqing Deng, and my brother E Zhang. They have cheered up my life constantly. Special thanks to my husband, Lu Xiao, whose love, encouragement, and support are so important to me.

I appreciate the help and support from Department of Chemistry and School of Graduate Studies in Memorial University of Newfoundland. The financial support from Natural Sciences and Engineering Research Council of Canada (NSERC) and Memorial University of Newfoundland is gratefully acknowledged.

Table of Contents

Page

Abstract i

Acknowledgments iii

Table of Contents v

List of Figures viii

List of Tables xi

List of Abbreviations and Symbols xiii

1. Introduction 1

1.1 The Importance of 2-Amino-2-Methyl-1-Propanol 1

1.2 Thermodynamics of Dilute Solutions 5
- 1.2.1 Apparent Molar and Partial Molar Properties 5
- 1.2.2 Young's Rule 7
- 1.2.3 Chemical Relaxation 8
- 1.2.4 Standard State (Henry's Law) 11
- 1.2.5 Standard Partial Molar Properties 12
- 1.2.6 Thermodynamic Relationships 15

1.3 Solvation and Equations of State for Dilute Solutions 17
- 1.3.1 Solute Hydration 17
- 1.3.2 Born Equation 22
- 1.3.3 The Revised Helgeson-Kirkham-Flowers Model 24
- 1.3.4 The "Density" Model 30
- 1.3.5 A Hybrid Model 33

1.4 Thermodynamics of Concentrated Solutions 34
- 1.4.1 Standard State (Raoult's Law) 34
- 1.4.2 Excess and Reduced Excess Molar Properties 35
- 1.4.3 Lumry's Model 38

1.5 Literature on AMP Decomposition 39

1.6 Objectives 41
1.6.1 Standard State Properties of Dilute Solutions 41
1.6.2 Properties of Concentrated Solutions 42

2. Experimental 44

2.1 Picker Flow Microcalorimeter 44

2.2 Differential Scanning Calorimeter 47

2.3 Vibrating Tube Densimeters 49
2.3.1 Sodev Flow Densimeter 49
2.3.2 High-Temperature Densimeter 50
2.3.3 DMA 5000 Densimeter 54

3 Thermodynamics of Dilute Aqueous 2-Amino-2-Methyl-1-Propanol (AMP) and 2-Amino-2-Methyl-1-Propanol Hydrochloride ($AMPH^+Cl^-$): Apparent Molar Volumes and Heat Capacities 56

3.1 Introduction 56

3.2 Experimental Methods 56
3.2.1 Materials 56
3.2.2 Experiments on the Picker Flow Microcalorimeter 60
3.2.3 Experiments on the Sodev Flow Densimeter 61
3.2.4 Measurements on the High-Temperature Densimeter 62
3.2.5 Hydrothermal Stability of AMP 62

3.3 Results 65
3.3.1 Apparent Molar Properties 65
3.3.2 Standard Partial Molar Properties 80
3.3.3 Uncertainty Estimation 86
3.3.4 Comparison with Literature Data 88

3.4 "Equations of State" for Aqueous AMP and $AMPH^+Cl^-$ 89
3.4.1 The Revised HKF Model 89
3.4.2 The "Density" Model 92
3.4.3 A Hybrid Model 94

3.5 Discussion on Standard Partial Molar Properties at Elevated Temperatures and Pressures 96

3.6 Discussion on Equations of State 102
3.6.1 The Revised HKF Model 102
3.6.2 The "Density" Model 103
3.6.3 The Hybrid Model 103

3.7 AMP Ionization 104

4 Excess Molar Properties of [2-Amino-2-Methyl-1-Propanol + Water] Mixtures at Finite Concentrations from 278 to 368 K 110

4.1 Introduction 110

4.2 Experimental Methods 110
4.2.1 Materials 110
4.2.2 Experiments on Differential Scanning Calorimeter 111
4.2.3 Vapor Corrections 112
4.2.4 Experiments on DMA 5000 Densimeter 114

4.3 Results 115
4.3.1 Molar Heat Capacities and Volumes 115
4.3.2 Excess Molar Heat Capacities and Volumes 118

4.4 Discussion 128

4.5 Conclusions 137

5 Bibliography 138

6 Appendices 145

Appendix 1: Experimental Data Tables of Apparent Molar Properties for Dilute Aqueous AMP and $AMPH^+Cl^-$ 146

Appendix 2: Experimental Data Tables of Molar Properties for Pure AMP and Pure Water 161

Appendix 3: Experimental Data Tables of Molar Properties and Excess Molar Properties for the System (AMP + H_2O) 163

Appendix 4: Excess Molar Properties of (MDEA + H_2O) Mixtures from the Literature 170

List of Figures

		Page
Figure 1.1	Structures: (i) 2-amino-2-methyl-1-propanol (AMP); (ii) 2-amino-2-methyl-1-propanol hydrochloride ($AMPH^+Cl^-$)	2
Figure 1.2	Schematic diagram of the solvation process and the formation of three regions	19
Figure 1.3	Standard partial molar volumes V_2^o at 20 MPa plotted against temperature (Hawrylak, 1999)	29
Figure 2.1	Schematic of Picker flow microcalorimeter	45
Figure 2.2	Schematic of CSC 4100 differential scanning calorimeter	48
Figure 2.3	Schematic of the high-temperature vibrating tube densimeter	52
Figure 3.1	The apparent molar volumes $V_{\phi,2}$ of AMP solutions at 0.1 MPa from 283.15 to 328.15 K plotted as a function of molality	71
Figure 3.2	The apparent molar volumes $V_{\phi,2}$ of AMP (Fluka) solutions at 20 MPa plotted as a function of molality	72
Figure 3.3	Pressure effects on the apparent molar volumes $V_{\phi,2}$ of AMP (Fluka) solutions as a function of molality	73
Figure 3.4	The apparent molar heat capacities $C_{p,\phi,2}$ of AMP solutions at 0.1 MPa from 283.15 to 328.15 K plotted as a function of molality	74
Figure 3.5	The apparent molar volumes $V_{\phi,2}$ of $AMPH^+Cl^-$ solutions at 0.1 MPa from 283.15 to 328.15 K plotted as a function of ionic strength after subtracting the Debye-Hückel limiting law term	75
Figure 3.6	The apparent molar volumes $V_{\phi,2}$ of $AMPH^+Cl^-$ (Fluka) solutions at 20 MPa plotted as a function of ionic strength after subtracting the Debye-Hückel limiting law term	76
Figure 3.7	Pressure effects on the apparent molar volumes $V_{\phi,2}$ of $AMPH^+Cl^-$ (Fluka) solutions as a function of ionic strength after subtracting the Debye-Hückel limiting law term	77

Figure 3.8 The apparent molar heat capacities $C_{p,\phi,2}$ of $AMPH^+Cl^-$ solutions at 0.1 MPa from 283.15 to 328.15 K plotted as a function of ionic strength after subtracting the Debye-Hückel limiting law term 78

Figure 3.9 Decomposition effects: the apparent molar volumes $V_{\phi,2}$ of $AMPH^+Cl^-$ solutions at 555.59 K and 19.63 MPa plotted as a function of ionic strength after subtracting the Debye-Hückel limiting law term 79

Figure 3.10 Standard partial molar volumes V_2^o of AMP at 20 MPa plotted as a function of temperature 97

Figure 3.11 Standard partial molar volumes V_2^o of $AMPH^+Cl^-$ at 20 MPa plotted as a function of temperature 98

Figure 3.12 Standard partial molar heat capacities $C_{p,2}^o$ of AMP at 20 MPa plotted as a function of temperature 99

Figure 3.13 Standard partial molar heat capacities $C_{p,2}^o$ of $AMPH^+Cl^-$ at 20 MPa plotted as a function of temperature 100

Figure 3.14 Contributions to the standard partial molar volume change $\Delta_r V^o$ for Equation (3.27) 108

Figure 3.15 Contributions to the standard partial molar heat capacity change $\Delta_r C_p^o$ for Equation (3.27) 109

Figure 4.1 Molar heat capacities of pure AMP 117

Figure 4.2 Excess molar heat capacities of aqueous AMP from 278.15 K to 368.15 K (at 5 K intervals) plotted against mole fraction 124

Figure 4.3 Excess molar volumes V_m^E of aqueous AMP from 293.15 K to 353.15 K (at 10 K intervals) plotted against mole fraction 125

Figure 4.4 Experimental excess molar thermal expansibilities E_m^E of aqueous AMP from 303.15 K to 328.15 K (at 5 K intervals) plotted against mole fraction 127

Figure 4.5 Idealized schematic of typical reduced excess molar heat capacity plot, showing regions (i), (ii), and (iii) according to Lumry *et al.* (1982) . . . 130

Figure 4.6 Reduced excess molar heat capacities of aqueous AMP from 278.15 K to 368.15 K (at 5 K intervals) plotted against mole fraction 131

Figure 4.7 Reduced excess molar volumes of aqueous AMP from 298.15 K to 348.15 K (at 10 K intervals) plotted against mole fraction 132

Figure 4.8 Reduced excess molar heat capacities of aqueous AMP at 298.15 K plotted against mole fraction 134

Figure 4.9 Reduced excess molar volumes of aqueous AMP at 298.15 K plotted against mole fraction 135

Figure A.4.1 Structure of methyldiethanolamine (MDEA) 171

Figure A.4.2 Excess molar heat capacities $C^{E}_{p,m}$ of aqueous MDEA from 278.15 K to 323.15 K (at 5 K intervals) plotted against mole fraction (Hawrylak, 1999) 172

Figure A.4.3 Excess molar volumes V^{E}_{m} of aqueous MDEA at 298.15 K (Hawrylak *et al.*, 2000) 173

Figure A.4.4 Reduced excess molar heat capacities of aqueous MDEA from 283.15 K to 328.15 K (at 15 K intervals) plotted against mole fraction (Hawrylak, 1999) 174

List of Tables

Page

Table 3.1 Physical properties of AMP from the literature 58

Table 3.2 Thermal decomposition for AMP and $AMPH^+Cl^-$ solutions after measurements of densities with the high-temperature vibrating tube densimeter at T = 555.6 K and p = 19.6 MPa 64

Table 3.3 Parameters for $V_{\phi,2}$ of AMP and $AMPH^+Cl^-$ solutions at low temperatures from isothermal fits of Equations (3.12) and (3.14), respectively.. 82

Table 3.4 Parameters for $C_{p,\phi,2}$ of AMP and $AMPH^+Cl^-$ solutions from isothermal fits of Equations (3.13) and (3.15), respectively 83

Table 3.5 Parameters for $V_{\phi,2}$ of AMP solutions at high temperatures from isothermal fits of Equation (3.12) 84

Table 3.6 Parameters for $V_{\phi,2}$ of $AMPH^+Cl^-$ solutions at high temperatures from isothermal fits of Equation (3.14) 85

Table 3.7 Revised HKF model parameters in the fits of V_2^o and $C_{p,2}^o$ of aqueous AMP and $AMPH^+Cl^-$ in Equations (3.18) and (3.20) 91

Table 3.8 "Density" model parameters for the fits of V_2^o and $C_{p,2}^o$ of aqueous AMP and $AMPH^+Cl^-$ in Equations (3.23) and (3.24) 93

Table 3.9 Hybrid model parameters for the fits of V_2^o and $C_{p,2}^o$ of aqueous AMP and $AMPH^+Cl^-$ in Equations (3.25) and (3.26). 95

Table 3.10 Standard partial molar volumes of aqueous $AMPH^+$ $[(CH_3)_2C(CH_2OH)NH_3^+]$ on the conventional scale, $V^o(H^+, aq) \equiv 0$. . . . 105

Table 3.11 Standard partial molar heat capacities of aqueous $AMPH^+$ on the conventional scale, $C_p^o(H^+, aq) \equiv 0$ 106

Table 4.1 Coefficients of Equations (4.5) and (4.6) for molar heat capacities $C_{p,m,2}^*$ and molar volumes $V_{m,2}^*$ of pure AMP, respectively. 116

Table 4.2 Comparison of densities ρ_1^* of water from NIST compilations (Harvey *et al.*, 1996) and those from Bettin and Spieweck (1990) 119

Table 4.3 Properties of (amine + water) mixtures and T = 298.15 K 120

Table 4.4 Parameters from Equation (4.8) for the excess molar heat capacities of aqueous AMP. 122

Table 4.5 Parameters from Equation (4.8) for the excess molar volumes of aqueous AMP 123

Table A.1.1 Apparent molar volumes $V_{\phi,2}$ for aqueous AMP (ACROS) 146

Table A.1.2 Apparent molar heat capacities $C_{p,\phi,2}$ for aqueous AMP (ACROS) . . . 148

Table A.1.3 Apparent molar volumes $V_{\phi,2}$ for aqueous AMP (Fluka) 150

Table A.1.4 Apparent molar heat capacities $C_{p,\phi,2}$ for aqueous AMP (Fluka) 151

Table A.1.5 Apparent molar volumes $V_{\phi,2}$ for aqueous $AMPH^+Cl^-$ 152

Table A.1.6 Apparent molar heat capacities $C_{p,\phi,2}$ for aqueous $AMPH^+Cl^-$ 155

Table A.1.7 Apparent molar volumes $V_{\phi,2}$ for aqueous AMP (Fluka) at high temperatures 157

Table A.1.8 Apparent molar volumes $V_{\phi,2}$ for aqueous $AMPH^+Cl^-$ (Fluka) at high temperatures 159

Table A.2.1 Experimental molar heat capacities of water $C^*_{p,m,1}$ and AMP $C^*_{p,m,2}$ . . . 161

Table A.2.2 Densities ρ and molar volumes V_m^* of pure AMP 162

Table A.3.1 Molar heat capacities $C_{p,m}$ and excess molar heat capacities $C^E_{p,m}$ of aqueous AMP 163

Table A.3.2 Relative densities $(\rho - \rho_1^*)$ and excess molar volumes V_m^E of aqueous AMP 167

List of Abbreviations and Symbols

Abbreviations

aq	aqueous
AMP	2-amino-2-methyl-1-propanol
$AMPH^+Cl^-$	2-amino-2-methyl-1-propanol hydrochloride
DHLL	Debye-Hückel limiting law
exp	experimental
HKF	Helgeson-Kirkham-Flowers
id	ideal
rel	relaxation
RTD	resistance temperature detector
sp	species
TED	thermo-electric device

Symbols

μ	chemical potential
α	degree of dissociation; degree of ionization
α_1^*	thermal expansion coefficient of water
ε_r	solvent dielectric constant
ε_o	permittivity of free space
ξ	extent of a reaction
η	constant defined in Born equations ($\eta = e^2N_A/8\pi\varepsilon_o$)
β_1^*	compressibility coefficient of water
^{o}	standard state
$\gamma_{H,m,2}$	activity coefficient of solute 2 in terms of Henry's Law
$\gamma_{H,m,\pm}$	geometric mean activity coefficient of electrolytes (Henry's Law)
$\gamma_{R,2}$	activity coefficient of component 2 in terms of Raoult's law
δ	excess mixing term in Young's rule
Θ	solvent parameter in HKF equations (Θ = 228 K)
ν	stoichiometric coefficient
ν_k	stoichiometric coefficient of species k
ρ	density
ρ_1^*	density of water
τ	resonance period of the vibrating tube densitometers
Ψ	solvent parameter in HKF equations (Ψ = 2600 bars)
ω	valence factor
ω_e	effective Born coefficient

a_i	activity of component i
A_C	DHLL slope for apparent molar heat capacity
A_V	DHLL slope for apparent molar volume
A_ϕ	osmotic slope in the DHLL
c_p	specific heat capacity
$c^*_{p,1}$	specific heat capacity of water
C^o_p	standard partial molar heat capacity
$C^o_{p,1}$	standard partial molar heat capacity of water
$C^o_{p,2}$	standard partial molar heat capacity of component 2 (solute)
$C_{p,\phi}$	apparent molar heat capacity
$C^*_{p,m,1}$	molar heat capacity of water
$C^*_{p,m,2}$	molar heat capacity of component 2 (solute)
$C^*_{p,i}$	heat capacity of pure component i (default: the same as $C^*_{p,m,i}$)
C^{comp}_p	conventional compositional contribution
C^{rel}_p	chemical relaxation contribution
$C^E_{p,m}$	excess molar heat capacity
e	the charge on an electron
E^E_m	excess molar thermal expansibility
f_m	mass flow rate
ff	heat leak correction factor
G	Gibbs free energy
H	enthalpy
I	ionic strength
K	equilibrium constant; densimeter calibration constant; Kelvin
m	molality of solute (default: component 2)
M	molar mass
N_A	Avogadro's number
n_i	number of moles of species i
p	pressure
p_c	pressure at critical point
Q	Born function in HKF equations
r_e	effective radius
r_x	crystallographic radius
R	gas constant, 8.314 $J \cdot K^{-1} \cdot mol^{-1}$
s	standard deviation
S	entropy
T	temperature (in Kelvins)
T_c	temperature at critical point (in Kelvins)
V	volume
V^o	standard partial molar volume

V_1^o	standard partial molar volume of water
V_2^o	standard partial molar volume of component 2 (solute)
V_ϕ	apparent molar volume
$V_{m,1}^*$	molar volume of water
$V_{m,2}^*$	molar volume of component 2 (solute)
V_m^E	excess molar volume
W	electric power input to heater
X	Born equation derivative in HKF equations
x_1	mole fraction of water
x_2	mole fraction of component 2 (amine)
$\overline{Y}_i$	partial molar property of component i
$Y_{\phi,i}$	apparent molar property of component i
Y_i^o	standard partial molar property of component i
Z	the charge an ion has
Z_e	the effective charge

Chapter1: Introduction

1.1 The Importance of 2-Amino-2-Methyl-1-Propanol

The alkanolamine, 2-amino-2-methyl-1-propanol (AMP) has found practical use in many industrial processes. These include natural gas processing, oil refining, thermal power generation, and coal gasification. As shown in Figure 1.1, AMP has a -OH group that increases water solubility, and a $-NH_2$ group that provides alkalinity in aqueous solutions. It is used as a pH-controlling additive and corrosion inhibitor in steam generators. In gas processing, AMP has been used with much success in the removal of bulk CO_2 from natural and refinery gas streams.

High temperature boiler water can be corrosive to many metals and alloys commonly used for construction of steam generating systems in nuclear and thermal power stations, especially when acidic impurities are present. Currently ammonia is widely used as a corrosion inhibitor and pH-controlling additive. However, the high concentrations of ammonia needed to achieve the high pH required for corrosion control are not compatible with the copper-alloy tubing in the system. Volatile organic amines, which have higher base strengths and lower volatilities, have been considered as prospective alternatives to ammonia. AMP has been used as a corrosion inhibitor in the boilers at the nuclear power station at Wylfa (Lewis and Wetton, 1987).

Aqueous alkanolamines are used in many commercial processes for the removal of bulk CO_2 in gas processing. Accurate physical-chemical properties of concentrated

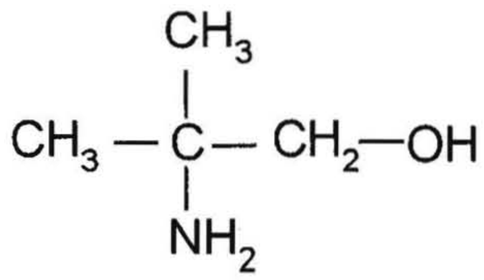

(i)

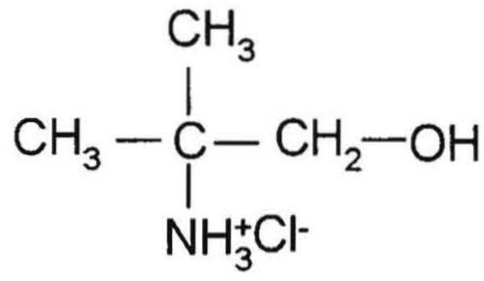

(ii)

Figure 1.1 Structures: (i) 2-amino-2-methyl-1-propanol (AMP);

(ii) 2-amino-2-methyl-1-propanol hydrochloride ($AMPH^+Cl^-$).

amine solutions are required for the engineering design and operation of gas processing plants, as described by Astarita *et al.* (1983). Generally, primary and secondary amines react with CO_2 to produce stable carbamates (Sartori and Savage, 1983):

$$2R_1R_2NH(aq) + CO_2(aq) \leftrightarrows R_1R_2NCOO^-(aq) + R_1R_2N^+H_2(aq) \qquad (1.1)$$

The loading capacity is limited by stoichiometry to 0.5 mole of CO_2 per mole of amine. Although carbamate hydrolysis can cause the loading to exceed 0.5 especially at high pressures, the loading capacity is not improved significantly.

Tertiary amines are unable to form carbamates when reacted with CO_2. This leaves bicarbonate ion formation as the predominant CO_2 adsorption reaction:

$$CO_2(aq) + R_1R_2R_3N(aq) + H_2O \leftrightarrows HCO_3^-(aq) + R_1R_2R_3N^+H(aq) \qquad (1.2)$$

Therefore, the loading capacity can reach 1 mole of CO_2 per mole of amine. However, the reaction rate of absorption is low, which limits its practical use.

Because AMP is sterically hindered, it cannot form a carbamate (Sartori and Savage, 1983). As a result, bicarbonate ion formation is the major reaction. This leads to a high loading capacity of 1 mole of CO_2 per mole of amine. With fast absorption rates, comparable to those achieved by common primary and secondary amines, AMP is very attractive in these gas processing applications. Heat capacities and volumes of aqueous

AMP solutions over the whole mole fraction range are then important to investigate for this application.

Because the AMP molecule is small, ionizable, and thermally stable, it can be used as a "molecular probe" to investigate hydration phenomena at high temperatures, and to examine the accuracy of various models for the prediction of standard partial molar properties (Tremaine *et al.*, 1997).

The equilibrium constant K (or the value of Gibbs free energy $\Delta_r G^\circ$) of the amine dissociation reaction at elevated temperatures is needed for calculating speciation and basicity:

$$AMP\ (aq) + H_2O\ (l) \rightleftharpoons AMPH^+\ (aq) + OH^-\ (aq) \qquad (1.3)$$

$$K = a_{AMPH+} \cdot a_{OH-} / (a_{AMP} \cdot a_{H2O}) \qquad (1.4)$$

$$\Delta_r G^\circ = - RT\ln K \qquad (1.5)$$

Here a_{AMPH+}, a_{OH-}, a_{AMP}, and a_{H2O} are the activities of $AMPH^+$, OH^-, AMP, and H_2O, respectively. Because of the difficulty in making direct measurements under such conditions, the temperature dependence of the Gibbs free energy is often calculated through the thermodynamic relationship:

$$\Delta_r G^o(T,p) = \Delta_r G^o(T_r,p_r) - \Delta_r S^o(T_r,p_r) + \int_{T_r}^{T} \Delta_r C_p^o dT - T\int_{T_r}^{T} \frac{\Delta_r C_p^o}{T} dT + \int_{p_r}^{p} \Delta_r V^o dp \quad (1.6)$$

where $\Delta_r C_p^o$, $\Delta_r V^o$ and $\Delta_r S^o$ are the changes in the standard partial molar heat capacity, volume, and entropy of the reaction, respectively. These properties are straightforward to measure at the reference conditions $T_r = 298.15$ K and $p_r = 0.1$ MPa. Therefore, if the temperature dependence and pressure dependence of the standard partial molar heat capacities and volumes for AMP and $AMPH^+Cl^-$ can be estimated, values of Gibbs free energy can be calculated under process conditions.

1.2 Thermodynamics of Dilute Solutions

1.2.1 Apparent Molar and Partial Molar Properties

In binary systems, such of those considered in this study, the partial molar properties and apparent molar properties are related to extensive properties through the expressions:

$$Y_{sol} = n_1\overline{Y}_1 + n_2\overline{Y}_2 = n_2 Y_{\phi,2} + n_1 Y_1^* \quad (1.7)$$

where Y_{sol} is the extensive property of solution; n_i is the number of moles of component i; Y_1^* is the property of pure water; and $\overline{Y}_i$ and $Y_{\phi,i}$ are the partial molar property and apparent molar property, respectively.

The partial molar property is defined as:

$$\overline{Y}_i = (\partial Y_{sol} / \partial n_i)_{T,p,n_{j\neq i}} \tag{1.8}$$

where $n_{j\neq i}$ means that the amounts of all species other than i are held constant. When Y_{sol} is the Gibbs free energy, $\overline{Y}_i$ is the chemical potential μ_i.

The apparent molar property $Y_{\phi,2}$ (e.g., apparent molar volume or apparent molar heat capacity) is defined as the change in property Y of solution per mole of solute when n_2 moles of solute are added to n_1 moles of solvent (water). It can be expressed as:

$$Y_{\phi,2} = \frac{Y_{sol} - n_1 Y_1^*}{n_2} = \frac{Y_{sol} - (1000 Y_1^* / M_1)}{m} \tag{1.9}$$

where M_1 is the molar mass of water; and m is the molality of solute in the solution.

Apparent molar properties are calculated from bulk quantities that can be measured directly, such as specific heat capacities and densities. The equations for apparent molar volumes $V_{\phi,2}$ and heat capacities $C_{p,\phi,2}$ can be expressed as follows:

$$V_{\phi,2} = \frac{1000(\rho_1^* - \rho)}{m\rho_1^*\rho} + \frac{M_2}{\rho} \tag{1.10}$$

$$C_{p,\phi,2} = \frac{c_p(1000 + mM_2) - 1000c_{p,1}^*}{m} \tag{1.11}$$

where M_2 is the molar mass of the solute; ρ_1^* and $c_{p,1}^*$ are the density and specific heat capacity of water, respectively; and ρ and c_p are the density and specific heat capacity of the solution, respectively.

1.2.2 Young's Rule

In measurements of the apparent molar properties of neutral amines and amine salts, additional species added for suppressing speciation or produced from speciation contribute to the experimental results. For example, in this study a small amount of NaOH was added to some of the AMP solutions to suppress hydrolysis, and a small amount of HCl was added to all the $AMPH^+Cl^-$ solutions to suppress the formation of the neutral amine. Young's rule (Young and Smith, 1954) provides a method to separate contributions to the apparent molar properties from the different species in a mixture of electrolytes. The experimental apparent molar properties Y_ϕ^{exp} for a solution with two solutes, as in this study, is expressed as:

$$Y_{\phi}^{exp} = Y_{\phi,2} \cdot m_2 / (m_2 + m_3) + Y_{\phi,3} \cdot m_3 / (m_2 + m_3) + \delta \qquad (1.12)$$

where $Y_{\phi,2}$ and $Y_{\phi,3}$ are the values for the hypothetical solutions of the pure components 2 and 3, respectively, with speciation and ionic strength identical to that of the total solution; m_i is the molality of solute i; and δ is an excess mixing term. This mixing term can be ignored in this study because of the large ratio of m_2 to m_3 and the presence of a common cation or anion.

1.2.3 Chemical Relaxation

If the solute under investigation is in a solution containing dissociation equilibria, the contributions of the resulting "additional" species can be subtracted by Young's rule, as discussed in Section 1.2.2. Another contribution to the experimental apparent molar heat capacity is the shift in the dissociation, which is caused by the temperature increment in the heat capacity measurement. This is the so-called "chemical relaxation" effect, described by Woolley and Hepler (1977) and Mains *et al.* (1984). The effect is present for both endothermic and exothermic reactions.

The total molar enthalpy of a mixture (H) can be expressed as:

$$H = \sum n_k H_k \qquad (1.13)$$

where H_k is the enthalpy of component k; and n_k is the number of moles of that

component. Woolley and Hepler (1977) considered the heat capacity contributions from H to derive expressions for the effect of chemical relaxation on heat capacities:

$$C_{p,\phi}^{\exp} = \sum_k n_k \left(\frac{\partial H_k}{\partial T} \right)_p + \sum_k H_k \left(\frac{\partial n_k}{\partial T} \right)_p \qquad (1.14)$$

The first term is the sum of the conventional compositional contributions C_p^{comp}, while the second term is defined as the relaxation effect C_p^{rel}.

The extent of reaction ξ for a general chemical equilibrium is defined as:

$$d\xi = dn_k / \nu_k \qquad (1.15)$$

where ν_k are the stoichiometric coefficients of the equilibrium. From its definition, C_p^{rel} can be expressed as:

$$C_p^{rel} = \sum \nu_k H_k (\partial \xi / \partial T)_p = \Delta H^o (\partial \xi / \partial T)_p \qquad (1.16)$$

Here ΔH^o is the enthalpy of reaction in an ideal solution or in an ideal gas mixture. According to the van't Hoff equation (where K is an equilibrium constant):

$$(\partial \ln K / \partial T)_p = \Delta H^o / RT^2 \qquad (1.17)$$

the ΔH^o and $(\partial\xi/\partial T)_p$ should have the same sign: both positive or both negative. Therefore, the value of C_p^{rel} is always positive.

Combination of Equation (1.17) and the relationship between K and ξ gives:

$$(\partial\xi / \partial T)_p = \Delta H^o / (RT^2B) \qquad (1.18)$$

$$B = [-(\sum\nu)^2 / (n_{t,i} + \xi\sum\nu)] + \sum(\nu_k)^2 / (n_{k,i} + \nu_k\xi) \qquad (1.19)$$

where $\sum\nu$ is the sum of the stoichiometric coefficients in the equilibrium, "t" means "total", "i" means "initial", and "k" stands for each species. Since B is known for any specific reaction, C_p^{rel} can be determined by Equations (1.13)-(1.19).

In this study, the ionization reaction of AMP is considered:

$$AMP + H_2O \rightleftharpoons AMPH^+ + OH^- \qquad (1.20)$$

Besides the Young's rule correction to remove the effect of "unwanted" species, a correction for chemical relaxation effect C_p^{rel} is also required in the heat capacity calculations:

$$C_p^{rel} = (\Delta_r H)^2\alpha(1 - \alpha) / [RT^2(2 - \alpha)] \qquad (1.21)$$

where α is the degree of the ionization of AMP; $\Delta_r H$ is the partial molar enthalpy of the ionization reaction, which is close to ΔH° as the solutions are very dilute.

1.2.4 Standard State (Henry's Law)

The standard states used in this section are defined in terms of Henry's Law for solutes in dilute solutions. Here, both neutral solutes and ionic solutes are considered. The chemical potential of a neutral solute at temperature T and pressure p is given by the expressions:

$$\mu_2(T, p) = \mu_2^\circ(T, p) + RT\ln a_2(T, p)$$

$$= \mu_2^\circ(T, p) + RT\ln [\gamma_{H,m,2}(T, p)\cdot m_2] \qquad (1.22)$$

where $\mu_2^\circ(T, p)$ is the standard state, referring to a hypothetical 1.0 $mol\cdot kg^{-1}$ ideal solution that obeys Henry's law; a_2 is the activity of the solute; and $\gamma_{H,m,2}(T, p)$ is the activity coefficient of solute 2 in terms of Henry's Law. At the standard state and when $m_2 \rightarrow$ zero, the activity coefficient $\gamma_{H,m,2}$ approaches unity.

Electrolyte solutes also use the Henry's law standard state with provisions to account for the stoichiometry of the salt. For a 1:1 strong electrolyte MX, the chemical potential is considered to be the sum of the chemical potentials of individual cation, M^+, and anion, X^-.

$$\mu_{MX}(T, p) = \mu^{o}_{MX}(T, p) + RT[\ln a_{+}(T, p) + \ln a_{-}(T, p)]$$

$$= \mu^{o}_{MX}(T, p) + RT[\ln \gamma_{H,m,+}(T, p)\cdot m_{+} + \ln \gamma_{H,m,-}(T, p)\cdot m_{-}]$$

$$= \mu^{o}_{MX}(T, p) + RT[\ln \gamma_{H,m,\pm}(T, p)\cdot m_{2}] \qquad (1.23)$$

where $\mu^{o}_{MX}(T, p)$ is the standard state, referring to a hypothetical 1.0 $mol\cdot kg^{-1}$ ideal solution that obeys Henry's law (so that all of the interactions between ions due to their charge, size and other properties are absent); $a_{+}(T, p)$ and $a_{-}(T, p)$ are the activities of the corresponding ions, respectively; $\gamma_{H,m,+}(T, p)$ and $\gamma_{H,m,-}(T, p)$ are the activity coefficients of M^{+} and X^{-} in terms of Henry's Law, respectively; $m_{+} = m_{-} = m_{2}$; and $\gamma_{H,m,\pm}$ is the geometric mean activity coefficient, $\gamma_{H,m,\pm} = (\gamma_{H,m,+}\gamma_{H,m,-})^{1/2}$.

1.2.5 Standard Partial Molar Properties

Standard partial molar properties can be related to apparent molar properties by the differential equations:

$$\overline{Y}_2 = Y_{\phi,2} + n_2\left(\frac{\partial Y_{\phi,2}}{\partial n_2}\right)_{n_1,T,p} = Y_{\phi,2} + m\left(\frac{\partial Y_{\phi,2}}{\partial m}\right)_{T,p} \qquad (1.24)$$

Therefore, when m approaches zero (infinite dilution), the apparent molar property $Y_{\phi,2}$ is equal to the standard partial molar property Y^{o}_{2}.

$$Y_2^o = \lim_{m\to 0} \overline{Y}_2 = \lim_{m\to 0} Y_{\phi,2} \tag{1.25}$$

Generally, in solutions of neutral molecules, only short-range solute-solute interactions exist. If a linear function can be fitted to the experimental apparent molar properties, the extrapolation of experimental apparent molar properties to m = 0 mol·kg^{-1} yields the standard partial molar properties, according to Equation (1.24):

$$Y_{\phi,2} = Y_2^o + B_Y m \tag{1.26}$$

where B_Y is an adjustable parameter that represents the molality dependence.

In electrolyte solutions, besides the short-range forces, long-range electrostatic interactions between ions are present. The magnitude of the electrostatic ion-ion interactions is related to the ionic charges, the dielectric constant of solvent, thermal energy, and the concentration. Although other properties of ions and solvent may affect the chemical potential at finite concentrations, these effects would disappear more quickly than the electrostatic effects with decreasing concentration.

In 1923, Debye and Hückel presented a theory of long-range interaction effects in dilute solutions, which can be used for the extrapolation of partial molar properties to infinite dilution. The result from this theory has been proved by mathematically sophisticated theories to be exact at infinite dilution (Pitzer, 1995). The Debye-Hückel limiting law has been applied in many practical cases satisfactorily. Millero (1979) has

successfully used Guggenheim's form of the extended Debye-Hückel equations for extrapolations from higher concentrations to I = 0:

$$Y_\phi = Y^o + 1.5\frac{\omega A_Y}{I}\left[I - 2I^{1/2} + 2\ln(1 + I^{1/2})\right] + C_Y I \qquad (1.27)$$

Here A_Y is the Debye-Hückel limiting slope for apparent molar properties, which can be obtained from the compilation of Archer and Wang (1990); ω is the valence factor; C_Y is an adjustable parameter; and I is the ionic strength: $I = \omega m = \frac{1}{2}\cdot\sum m_i Z_i^2$.

The Pitzer ion-interaction model (Pitzer, 1973, 1991) has been widely used to interpolate and model experimental data for aqueous electrolyte solutions. In the Pitzer treatment, total excess Gibbs energy was expanded in a virial series, which included terms for long-range electrostatic forces, short-range forces between two ions and among three ions. For a pure electrolyte $M_{\nu M}X_{\nu x}$ which has charges z_M and z_X, the apparent molar volumes $V_{\phi,MX}$ and apparent molar heat capacities $C_{p,\phi,MX}$ can be derived through the thermodynamic relations:

$$\begin{aligned} V_{\phi,MX} = V^o_{MX} &+ v|z_M z_X|(A_v / 2b)\ln(1 + bI^{1/2}) \\ &+ 2v_M v_X RT[mB^V_{MX} + m^2(v_M z_M)C^V_{MX}] \end{aligned} \qquad (1.28)$$

$$C_{p,\phi,MX} = C^{o}_{p,MX} + v|z_M z_X|(A_J / 2b)\ln(1 + bI^{1/2}) - 2v_M v_X RT^2[mB^{J}_{MX} + m^2(v_M z_M)C^{J}_{MX}] \quad (1.29)$$

Here V^{o}_{MX} and $C^{o}_{p,MX}$ are the standard molar volume and the standard molar heat capacity, respectively; $v = v_M + v_X$; A_v and A_J are the Debye-Hückel limiting slopes; $b = 1.2$ $kg^{1/2}\cdot mol^{-1/2}$; m is the overall molality; and B^{V}_{MX}, B^{J}_{MX}, C^{V}_{MX} and C^{J}_{MX} are interaction parameters. For example, the B^{V}_{MX} has the following expression:

$$B^{V}_{MX} = \beta^{(0)V} + \beta^{(1)V} g(\alpha_1 I^{1/2}) + \beta^{(2)V} g(\alpha_2 I^{1/2}) \quad (1.30)$$

where

$$g(x) = \frac{2[1 - (1 + x)\exp(-x)]}{x^2} \quad (1.31)$$

Here $\beta^{(o)V}$, $\beta^{(1)V}$, $\beta^{(2)V}$, α_1, and α_2 are adjustable parameters.

1.2.6 Thermodynamic Relationships

The equilibrium constant K (or the Gibbs free energy $\Delta_r G^{o}$) is one of the state functions used in the application of thermodynamics to chemical or phase equilibria. Because the direct measurement of K under hydrothermal conditions is difficult to carry

out, an alternative is to calculate K from measurements of other properties.

$$\Delta_r G^o = - RT\ln K \tag{1.32}$$

$$\left(\frac{\partial \Delta_r G^o}{\partial T}\right)_p = -\Delta_r S^o \tag{1.33}$$

$$\left(\frac{\partial}{\partial T}\frac{\Delta_r G^o}{T}\right)_p = -\frac{\Delta_r H^o}{T^2} \tag{1.34}$$

$$\left(\frac{\partial \Delta_r H^o}{\partial T}\right)_p = \Delta_r C_p^o \tag{1.35}$$

$$\left(\frac{\partial \Delta_r G^o}{\partial p}\right)_T = \Delta_r V^o \tag{1.36}$$

Here $\Delta_r S^o$, $\Delta_r H^o$, $\Delta_r C_p^o$, and $\Delta_r V^o$ are the changes in the standard partial molar entropy, enthalpy, heat capacity, and volume of the reaction, respectively.

The equilibrium constant K can be obtained from the above five equations, if the standard partial molar volumes and heat capacities are known as functions of temperature and pressure, as described in Section 1.1. The expression for $\Delta_r G^o$ at temperature T and

pressure p is:

$$\Delta_r G^o(T,p) = \Delta_r G^o(T_r,p_r) - \Delta_r S^o(T_r,p_r) + \int_{T_r}^{T} \Delta_r C_p^o dT - T\int_{T_r}^{T} \frac{\Delta_r C_p^o}{T} dT + \int_{p_r}^{p} \Delta_r V^o dp \quad (1.37)$$

The first two terms are properties at the reference state (T_r = 298.15 K, p_r = 0.1 MPa), which are generally available. The last three terms are complex functions of temperature and pressure.

Various models (Helgeson *et al.*, 1981; Tanger and Helgeson, 1988; Sedlbauer *et al.*, 2000; Mesmer *et al.*, 1988; Tremaine *et al.*, 1997) have been proposed to represent experimental data at elevated temperatures, and to predict thermodynamic properties over a wide range of temperature and pressure. These models were based either on theoretical models or on empirical fitting equations.

1.3 Solvation and Equations of State for Dilute Solutions

1.3.1 Solute Hydration

Water has many unusual thermodynamic properties, such as a maximum in density, and minima in isothermal compressibility and molar heat capacity. It is widely agreed that the hydrogen bond interactions between water molecules play a major role

(Poole *et al.*, 1994). These hydrogen bonds cause open four-coordinated structures to form in water. The presence of ionic or non-ionic solutes perturbs these hydrogen-bonded structures.

One structural treatment of ion-solvent interactions was presented by Bockris and Reddy (1998). They considered the existence of tetrahedral bonding, and the character of the network structure around the ion, which has been confirmed by an X-ray study, as follows. When an ion enters into water, the electric field of the ion may orient water dipoles and alter the bulk water "lattice". The ion-solvent interactions are shown in Figure 1.2, where three regions are indicated. In the immediate area surrounding the ion (region I, "primary" region), some water molecules are oriented by the ionic charge, and removed from the network "structure" of bulk water to form a hydration sphere around the ion. In region III, the water structure is undisturbed because of the large distance from the ion, and the water response to the electric field of the ion is described by its bulk dielectric constant. Although the solvent is still polarized by the electrostatic field between Regions I and III, the hydrogen-bonded network differs from that in bulk water. This region is referred as the "secondary" or "structure-breaking" region, where the water has a perturbed structure. These structural changes in the primary, secondary, and tertiary regions are called hydration effects, reflecting ion-water interactions.

When an ion is transferred from an ideal gas into the solvent, the Gibbs free energy of solvation $\Delta_{solv}G^{o}$ can be expressed as:

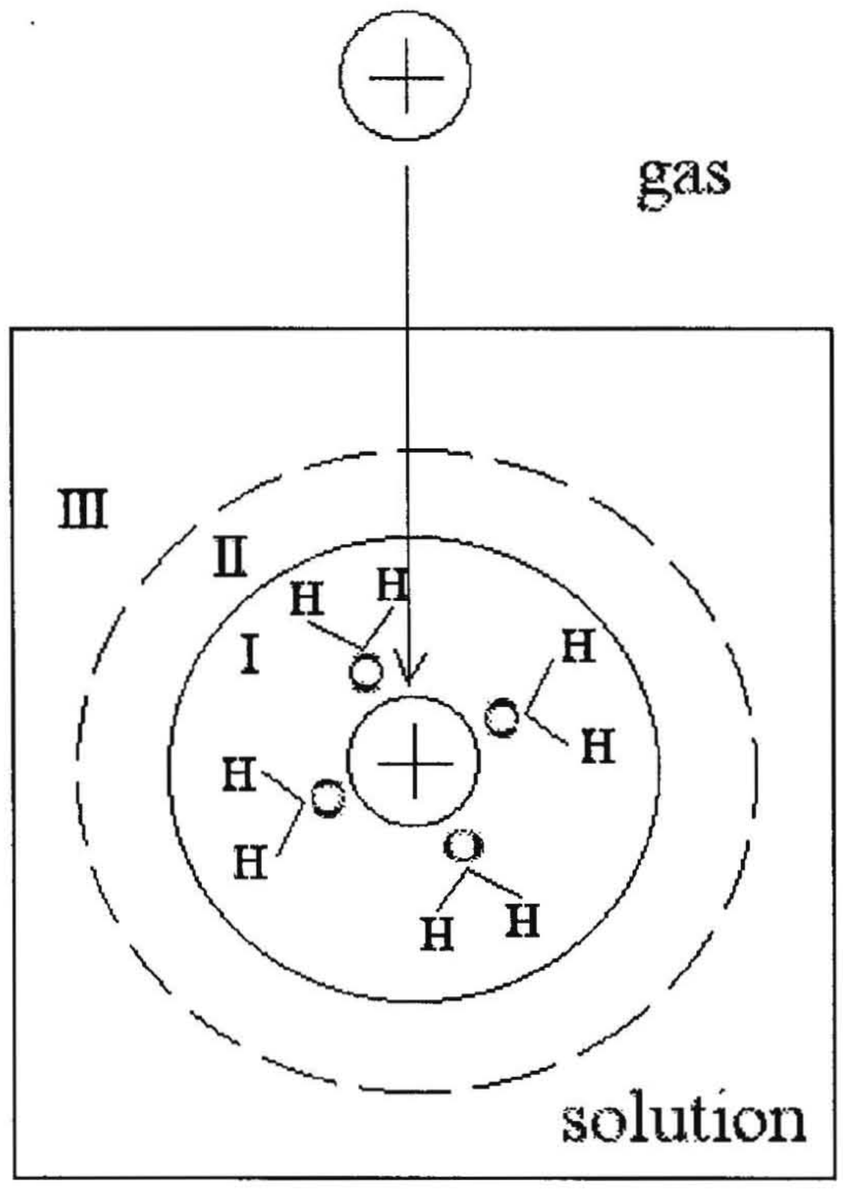

Figure 1.2 Schematic diagram of the solvation process and the formation of three regions. Region I ("primary" region): solvent sheath near the ion; Region II ("secondary" region): in-between region; Region III ("tertiary" region): bulk water.

$$\Delta_{solv}G^o = G^o_{aq} - G^o_{intr} - \Delta_{solv}G^o_{ss} \qquad (1.38)$$

where G^o_{aq} is the standard Gibbs free energy of the aqueous species; G^o_{intr} is the intrinsic gas phase Gibbs free energy of the ion at 1 bar in an ideal gas; and $\Delta_{solv}G^o_{ss}$ is the change in the Gibbs free energy arising from the difference in standard states between the gas phase and solution (the reference state of the gas phase is the ideal gas at 1 bar, but that of the solute in a dilute solution is the hypothetical 1 molal solution which obeys Henry's law).

The Gibbs free energy of solvation, $\Delta_{solv}G^o$, may be described by the expression:

$$\Delta_{solv}G^o = \Delta_{solv}G^o_{pol} + \Delta_{solv}G^o_{hydr} \qquad (1.39)$$

where $\Delta_{solv}G^o_{pol}$ is due to the long-range polarization of water caused by the charge distribution within the ion; and $\Delta_{solv}G^o_{hydr}$ comes from the short-range hydration effect because of the hydrogen-bonded "structure" of water.

A nonstructural treatment suggested by Born (1920) assumed that the ion was a rigid metallic sphere, and the solvent was a structureless continuum. When an ion is transferred into the solvent from the gas phase, it is stabilized by the induced charge formed on the surface of the cavity in which it resides, as described by the well-known Born equation, which will be discussed in Section 1.3.2. The polarization term $\Delta_{solv}G^o_{pol}$ for complex ions is then given by the following equation:

$$\Delta_{solv}G^{o}_{pol} = \Delta_{solv}G^{o}_{Born} + \Delta_{solv}G^{o}_{dipole} + \Delta_{solv}G^{o}_{quadrupole} \qquad (1.40)$$

which is a Taylor expansion in terms of solute multipolar interactions with the solvent.

Other contributions to the Gibbs free energy arising from electrostatic interactions were analyzed by Bockris and Reddy (1998). One of these contributions is the Gibbs free energy from ion-dipole interactions in the primary region, $\Delta_{solv}G^{o}_{dipole}$, which is related to the ion charge, the distance between the ion and the solvent dipole center, and the angle to the joint line of the ion and the dipole. At positions very close to the ion, the water molecule is viewed as a quadrupole, where two positive charges are on two hydrogen atoms, and two negative charges on two lone pairs of the oxygen atom.

In Equation (1.39), $\Delta_{solv}G^{o}_{hydr}$ represents the effect of perturbations in the solvent near the solute, which may include hydrogen-bonding between the solute and the solvent molecules. In this short-range region, the effects from the size and structure of solvent cannot be ignored. Since $\Delta_{solv}G^{o}_{hydr}$ cannot be treated at a molecular level in a continuum model, this term is often represented by an empirical function.

Standard partial molar volumes and heat capacities can be derived from the expressions for Gibbs free energy of the aqueous species G^{o}_{aq} through thermodynamic relationships. The resulting expressions contain similar contributions as those in Equations (1.38) and (1.39).

1.3.2 Born Equation

Generally, when an ion dissolves in the water, the first term $\Delta_{solv}G^{o}_{Born}$ in Equation (1.40) is dominant and all other terms can be ignored for the calculation of $\Delta_{solv}G^{o}$. The Born model assumes that, when a rigid charged sphere is placed in a structureless continuum, the ion-solvent interactions are solely electrostatic resulting from the charge on the ion. Hence, the Gibbs free energy $\Delta_{solv}G^{o}_{Born}$ is the work of transferring an ion from a vacuum into the solvent, expressed as the work of discharging the ion in a vacuum and the work of charging the ion in the solvent. The following expression is the Born equation:

$$\Delta_{solv}G^{o}_{Born} = -\frac{N_A(Ze)^2}{8\pi\varepsilon_o r_e}\left(1-\frac{1}{\varepsilon_r}\right) \tag{1.41}$$

where Z is the charge the ion has; e is the charge on an electron; N_A is Avogadro's number; ε_o is the permittivity of free space; ε_r is the solvent dielectric constant (or the relative permittivity); and r_e is the radius of the ion. The coefficient $\eta = e^2N_A/8\pi\varepsilon_o$ has the value of 6.95×10^{-5} J·m·mol^{-1}.

According to Equation (1.41), $\Delta_{solv}G^{o}_{Born}$ is always negative, and the magnitude increases with smaller radius, higher charge, and solvents with higher dielectric constant.

It is useful to derive the enthalpy, entropy, volume, and heat capacity changes associated with ion-solvent interactions from the expression for $\Delta_{solv}G^{o}_{Born}$.

$$\Delta_{solv}H^{o}_{Born} = -T^{2}\left(\frac{\partial}{\partial T}\frac{\Delta_{solv}G^{o}_{Born}}{T}\right)_{p} \tag{1.42}$$

$$\Delta_{solv}S^{o}_{Born} = -\left(\frac{\partial_{solv}\Delta G^{o}_{Born}}{\partial T}\right)_{p} \tag{1.43}$$

$$\Delta_{solv}C^{o}_{p,Born} = \left(\frac{\partial\Delta_{solv}H^{o}_{Born}}{\partial T}\right)_{p} \tag{1.44}$$

$$\Delta_{solv}V^{o}_{Born} = \left(\frac{\partial\Delta_{solv}G^{o}_{Born}}{\partial p}\right)_{T} \tag{1.45}$$

Therefore:

$$\Delta_{solv}C^{o}_{p,Born} = -\frac{N_{A}(Ze)^{2}}{8\pi\varepsilon_{o}r_{e}}\left[\left(\frac{2T}{\varepsilon_{r}^{3}}\right)\left(\frac{\partial\varepsilon_{r}}{\partial T}\right)^{2}_{p} - \frac{T}{\varepsilon_{r}^{2}}\left(\frac{\partial^{2}\varepsilon_{r}}{\partial T^{2}}\right)_{p}\right] \tag{1.46}$$

$$\Delta_{solv}V^{o}_{Born} = -\frac{N_{A}(Ze)^{2}}{8\pi\varepsilon_{o}r_{e}}\left(\frac{1}{\varepsilon_{r}^{2}}\right)\left(\frac{\partial\varepsilon_{r}}{\partial p}\right)_{T} \tag{1.47}$$

If the crystallographic radius r_x is used for r_e, the Born equation predicts enthalpies of ion-solvent interactions with the correct order of magnitude, but the values are much higher than the experimental results. This probably reflects the effects of dielectric saturation and molecular size which are not considered in the derivation. The effects can be crudely approximated by using an "effective" radius r_e that is larger than the crystallographic radius r_x. The Helgeson-Kirkham-Flowers (HKF) model has employed the Born equation for calculating $\Delta_{solv}G^o$, where the effective radius of ion r_e is used as an adjustable parameter. The details of HKF model will be discussed in the next section.

1.3.3 The Revised Helgeson-Kirkham-Flowers Model

Using the Born equation discussed above, Helgeson and co-workers (Helgeson and Kirkham, 1976; Helgeson *et al.*, 1981) developed an equation of state to represent experimental data (when they are available), and to predict standard partial molar properties. This equation of state, the Helgeson-Kirkham-Flowers (HKF) model, employs an *effective* ionic radius, where r_e is a simple linear function of crystallographic radius r_x and charge Z, $r_e = r_x + 0.94|Z|$ for cations and $r_e = r_x$ for anions. The revised HKF model (Tanger and Helgeson, 1988; Shock and Helgeson, 1988) also considered r_e to be a function of T and p.

In this model, the standard molar properties of aqueous ions Y^o are considered to have two contributions: an electrostatic term based on the Born equation ΔY^o_e, and a non-

electrostatic term ΔY_n^o determined empirically.

$$Y^o = \Delta Y_e^o + \Delta Y_n^o \qquad (1.48)$$

In comparison with Equations (1.38) and (1.39), ΔY_e^o stands for the long-range polarization term $\Delta_{solv} Y_{pol}^o$, and ΔY_n^o includes three terms: the intrinsic gas phase property of the solute Y_{intr}^o, the change arising from the difference in standard states between the gas phase and solution $\Delta_{solv} Y_{ss}^o$, and the short-range hydration effect $\Delta_{solv} Y_{hydr}^o$.

The electrostatic contribution ΔV_e^o to the standard partial molar volume V^o is given by a modified Born model:

$$\Delta V_e^o = -\omega_e Q + (1/\varepsilon_r - 1)(\partial \omega_e / \partial p)_T \qquad (1.49)$$

where ε_r is the solvent dielectric constant; ω_e stands for a temperature and pressure dependent Born coefficient,

$$\omega_e = \frac{N_A (Ze)^2}{8\pi \varepsilon_o r_e} \qquad (1.50)$$

and the Born function Q is given by:

$$Q = \left(\frac{1}{\varepsilon_r}\right)\left(\frac{\partial \ln \varepsilon_r}{\partial p}\right)_T \tag{1.51}$$

The non-electrostatic term ΔV_n° can be expressed as:

$$\Delta V_n^o = \sigma + \xi\left(\frac{1}{T - \Theta}\right) \tag{1.52}$$

where Θ is a solvent parameter equal to 228 K, which is based on the anomalous behavior at the pseudo-critical point of supercooled water (Angell, 1983); σ and ξ are temperature independent coefficients:

$$\sigma = a_1 + a_2\left(\frac{1}{\Psi + p}\right) \tag{1.53}$$

$$\xi = a_3 + a_4\left(\frac{1}{\Psi + p}\right) \tag{1.54}$$

where Ψ is a solvent parameter equal to 2600 bars; and a_1, a_2, a_3, and a_4 are temperature- and pressure- independent but species-dependant parameters. Therefore, the expression for the standard partial molar volume can be summarized as:

$$V^o = a_1 + a_2\left(\frac{1}{\Psi + p}\right) + \left[a_3 + a_4\left(\frac{1}{\Psi + p}\right)\right]\left(\frac{1}{T - \Theta}\right) - \omega_e Q + \left(\frac{1}{\varepsilon_r} - 1\right)\left(\frac{\partial \omega_e}{\partial p}\right)_T \quad (1.55)$$

Similarly, the standard partial molar heat capacity can also be given by Equation (1.48). The electrostatic contribution $\Delta C^o_{p,e}$ can be expressed by a modified Born model:

$$\Delta C^o_{p,e} = \omega_e T X + 2TY\left(\frac{\partial \omega_e}{\partial T}\right)_p - T\left(\frac{1}{\varepsilon_r} - 1\right)\left(\frac{\partial^2 \omega_e}{\partial T^2}\right)_p \quad (1.56)$$

where:

$$X = \varepsilon_r{}^{-1}\left[\left(\frac{\partial^2 \ln \varepsilon_r}{\partial T^2}\right)_p - \left(\frac{\partial \ln \varepsilon_r}{\partial T}\right)_p^2\right] \quad (1.57)$$

and

$$Y = \varepsilon_r{}^{-1}\left(\frac{\partial \ln \varepsilon_r}{\partial T}\right)_p \quad (1.58)$$

The non-electrostatic contribution $\Delta C^o_{p,n}$ can be represented by a temperature dependent function similar to that used for V^o. The pressure dependence of $\Delta C^o_{p,n}$ can be derived from the V^o expression based on the thermodynamic identity $(\partial C_p/\partial p)_T = -T(\partial^2 V/\partial T^2)_p$:

$$C^{o}_{p,n} = c_1 + c_2\left(\frac{1}{T-\Theta}\right)^2 - 2T\left(\frac{1}{T-\Theta}\right)^3\left[a_3(p-p_r) + a_4 \ln\left(\frac{\Psi+p}{\Psi+p_r}\right)\right] \qquad (1.59)$$

Here c_1 and c_2 are temperature- and pressure- independent but species-dependant parameters; Θ is again a parameter with the value of 228K; p_r is the reference pressure (1 bar); and a_3 and a_4 are determined by the V^o fits in Equation (1.55).

Standard partial molar volumes and heat capacities of aqueous ions and electrolytes typically exhibit an inverted U-shape as a function of temperature [Figure 1.3 (i)]. This is consistent with the singular temperatures of water at 228 K and 647 K (critical temperature) where second-derivative thermodynamic parameters approach $+\infty$. The parameters in the revised HKF model have been selected so that the electrostatic contribution dominates at high temperatures where the Born model is most satisfactory, and the nonelectrostatic contribution to V^o and C_p^o dominates at low temperatures. The revised HKF model has been used widely for the extrapolation of low temperature standard partial molar properties of aqueous ions and electrolytes to elevated temperatures and pressures.

The revised HKF model has also been used by Shock and Helgeson (1990) for the prediction of the standard partial molar properties of *neutral* aqueous organic species up to 1273 K and 500 MPa. It was fitted to the available experimental data for neutral aqueous organic species at elevated temperatures and pressures, as shown in Figure 1.3 (ii). The fitted parameters were then used to develop correlations with other low

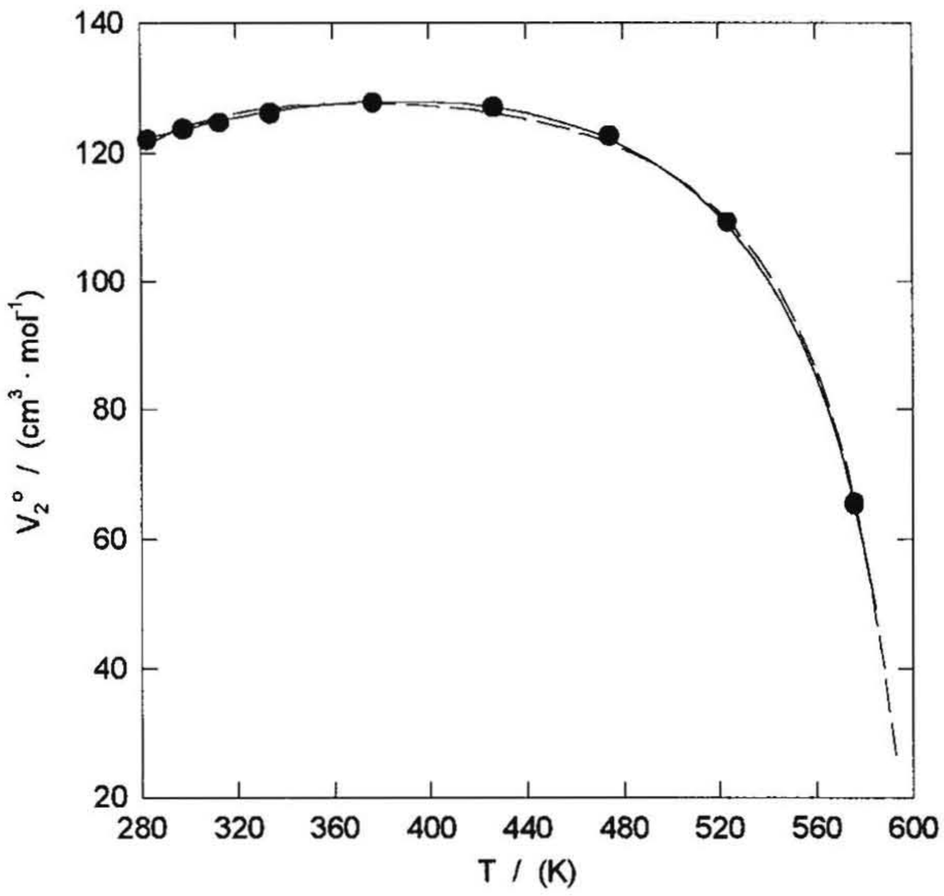

(i)

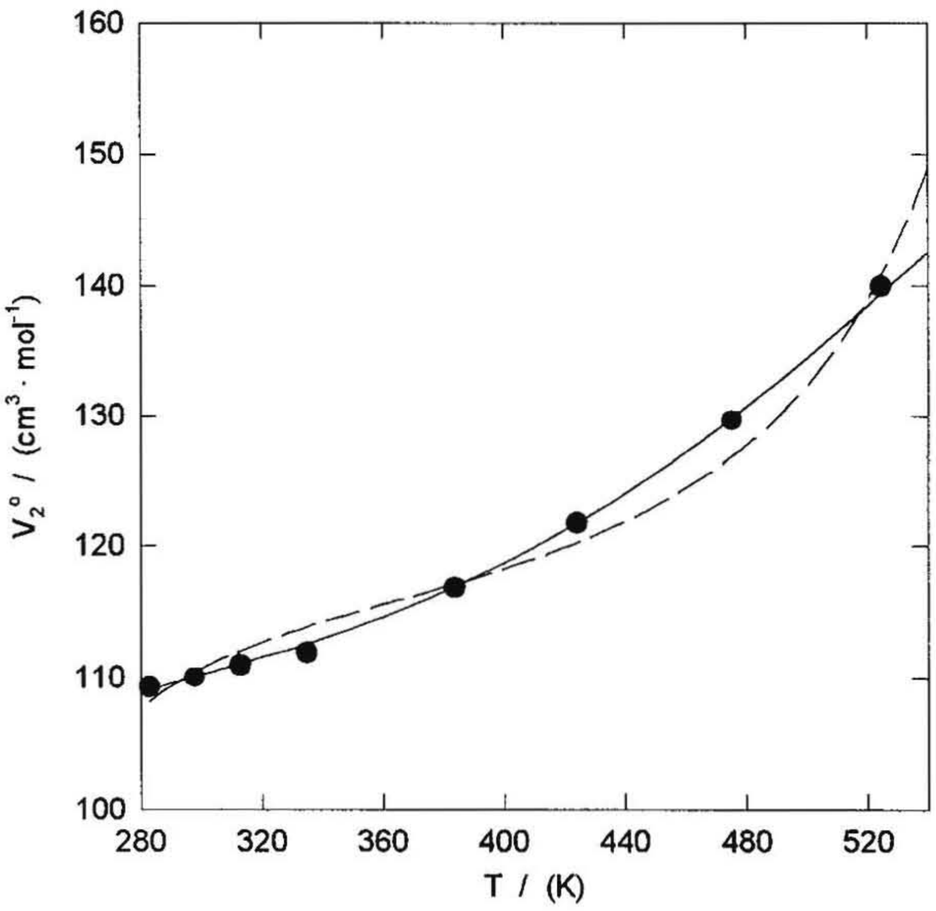

(ii)

Figure 1.3 Standard partial molar volumes V_2° at 20 MPa plotted against temperature (Hawrylak, 1999). (i) methyldiethanolammonium chloride; (ii) methyldiethanolamine. Symbols are values obtained from isothermal fits, and lines are fitted values: ——— , "density" model; – – –, revised HKF model.

temperature thermodynamic constants. In contrast to the positive ω_e for aqueous ions and electrolytes, ω_e can be either positive or negative for neutral species. According to Equation (1.50), when ω_e is negative, then Z_e, the effective charge, is an imaginary number. Clearly, the expression for the electrostatic contribution has no physical meaning, and the validity of the revised HKF model for neutral species is questionable. The predictive capability stated in the paper is also limited by the rather sparse experimental data available at the time the correlations were derived.

1.3.4 The "Density" Model

Franck (1956, 1961) observed that the ionization constants K of many aqueous species at elevated temperatures and pressures act as linear functions of density of water ρ_1^*, when log K is plotted against log ρ_1^* over a very wide range. Based on this observation, Marshall and Franck (1981) developed the "density" model to represent the ionization constant K of water at temperatures up to 1273 K and at pressures up to 1000 MPa. This has been used for representing K of general ionization reactions by Mesmer *et al.* (1988):

$$\log K = \left(a + \frac{b}{T} + \frac{c}{T^2} + \frac{d}{T^3} \right) + k \log \rho_1^* \tag{1.60}$$

$$k = \left(e + \frac{f}{T} + \frac{g}{T^2} \right) \tag{1.61}$$

where a, b, c, d, e, f, and g are adjustable parameters; and ρ_1^* is the density of water.

Other thermodynamic quantities can be derived from above equations. The Gibbs free energy of ionization $\Delta_r G°$ is related to K by:

$$\Delta_r G° = - RT \ln K \qquad (1.62)$$

Therefore:

$$\Delta G^o = -2.303RT\left[\left(a + \frac{b}{T} + \frac{c}{T^2} + \frac{d}{T^3}\right) + \left(e + \frac{f}{T} + \frac{g}{T^2}\right)\log \rho_1^*\right] \qquad (1.63)$$

The enthalpy of ionization $\Delta_r H°$ was obtained by:

$$\left(\frac{\partial}{\partial T}\frac{\Delta_r G^o}{T}\right)_p = -\frac{\Delta_r H^o}{T^2} \qquad (1.64)$$

Subsequently:

$$\Delta_r H^o = -2.303R\left(b + \frac{2c}{T} + \frac{3d}{T^2} + \left(f + \frac{2g}{T}\right)\log \rho_1^*\right) - RT^2 k\alpha_1^* \qquad (1.65)$$

where $\alpha_1^* = -(1/\rho_1^*)(\partial\rho_1^*/\partial T)_p$ is the thermal expansion coefficient of water; and k has been

given in Equation (1.61).

Similarly, the entropy of ionization $\Delta_r S°$, the standard partial molar heat capacity of ionization $\Delta_r C_p^o$, and the standard partial molar volume of ionization $\Delta_r V°$ are related to $\Delta_r G°$ by the following expressions:

$$\left(\frac{\partial \Delta_r G^o}{\partial T}\right)_p = -\Delta_r S^o \tag{1.66}$$

$$\left(\frac{\partial \Delta_r H^o}{\partial T}\right)_p = \Delta_r C_p^o \tag{1.67}$$

$$\left(\frac{\partial \Delta_r G^o}{\partial p}\right)_T = \Delta_r V^o \tag{1.68}$$

Therefore:

$$\Delta_r S^o = 2.303R\left(a - \frac{c}{T^2} - \frac{2d}{T^3} + \left(e - \frac{g}{T^2}\right)\log\rho_1^*\right) - RTk\alpha_1^* \tag{1.69}$$

$$\Delta_r C_p^o = -2.303R\left[-\frac{2c}{T^2} - \frac{6d}{T^3} - \left(\frac{2g}{T^2}\right)\log\rho_1^*\right] - R\alpha_1^*\left(2eT - \frac{2g}{T}\right) - RT^2 k\left(\frac{\partial \alpha_1^*}{\partial T}\right)_p \tag{1.70}$$

$$\Delta_r V^\circ = -RTk\beta_1^* \qquad (1.71)$$

where β_1^* is the compressibility coefficient of water, $(1/\rho_1^*)(\partial\rho_1^*/\partial p)_T$. Equation (1.60) can be further simplified over a restricted region, and the simplified form has fewer parameters (Anderson *et al.*, 1991).

1.3.5 A Hybrid Model

A hybrid model that combines the revised HKF model with the "density" model was developed by Tremaine *et al.* (1997). The equations of state are:

$$V^o = v_1 + v_2 / T^{1/2} + v_3 / (T-\Theta) + v_4 / T^{3/2} - qR\beta_1^* \qquad (1.72)$$

$$C_p^o = c_1 + c_2 / (T-\Theta)^2 + c_3 / T^3 - qRT(\partial\alpha_1^* / \partial T)_p \qquad (1.73)$$

The terms α_1^* and β_1^* are the thermal expansion coefficient and compressibility coefficient of water, as defined in Section 1.3.4. The constant $\Theta = 228$ K, is related to the anomalous behavior of supercooled water, as discussed in Section 1.3.3. The v_i, c_i, and q are adjustable parameters, where q is common for the two equations. The equations are structured so that the terms containing density derivatives dominate at high temperatures.

1.4 Thermodynamics of Concentrated Solutions

1.4.1 Standard State (Raoult's Law)

For mixtures of nonelectrolytes at concentrations that span the entire mole fraction range (from $x_2 = 0$ to $x_2 = 1$), ideal behaviour is generally selected to obey Raoult's law; and the standard state of each component is defined to be the pure substance at p = 1 bar. The chemical potential of component 2, μ_2, at temperature T and pressure p can be expressed as:

$$\mu_2(T, p) = \mu_2^*(T, p) + RT \ln a_2(T, p)$$

$$= \mu_2^*(T, p) + RT \ln [\gamma_{R,2}(T, p) \cdot x_2] \qquad (1.74)$$

where $\mu_2^*(T, p)$ is the chemical potential of the pure solvent at p = 1 bar, which is the standard state defined in terms of Raoult's law; $a_2(T, p)$ is the activity of component 2; $\gamma_{R,2}(T,p)$ is the activity coefficient of component 2 in terms of Raoult's law; and x_2 is the mole fraction of component 2. At the standard state, when $x_2 \rightarrow 1$, the activity coefficient $\gamma_{R,2}(T,p)$ approaches unity.

Therefore, in an ideal solution, the properties of all the components obey Raoult's law over the entire range of the composition at all temperatures and pressures. In a binary system, this becomes:

$$Y_m^{id} = (1 - x_2)Y_{m,1}^* + x_2 Y_{m,2}^* \qquad (1.75)$$

where $Y^*_{m,1}$ and $Y^*_{m,2}$ are the molar properties of pure components 1 and 2, respectively; and x_2 is the mole fraction of component 2.

1.4.2 Excess and Reduced Excess Molar Properties

The excess molar property $Y^E_{m,2}$ is defined as the difference of the actual property Y_m at given T, p, and composition from that of an ideal solution at the same conditions:

$$Y^E_{m,2} = Y_m - Y^{id}_m = Y_m - (1 - x_2)Y^*_{m,1} - x_2 Y^*_{m,2} \tag{1.76}$$

The activity coefficient $\gamma_{R,i}$, which is defined relative to Raoult's law, has been discussed above. $\gamma_{R,i}$ is related to the excess chemical potential by the following expression:

$$\ln\gamma_{R,i} = \frac{\mu_i - \mu_i^{id}}{RT} = \frac{\mu_i^E}{RT} = \frac{1}{RT}\left(\frac{\partial G^E}{\partial n_i}\right)_{T,p,n_{j\neq i}} \tag{1.77}$$

A simple expression for the excess Gibbs free energy proposed by Margules (1895) is referred as the Margules equation:

$$G^E_m/(RT) = w\cdot x_1\cdot x_2 = w\cdot x_2\cdot(1 - x_2) \tag{1.78}$$

where w is an interaction parameter constant at a given T and p. The activity coefficients

follow Equations (1.77) and (1.78):

$$\ln\gamma_{R,1} = w \cdot x_2^2 \tag{1.79}$$

$$\ln\gamma_{R,2} = w \cdot x_1^2 \tag{1.80}$$

Through thermodynamic relationships, V_m^E and $C_{p,m}^E$ can be derived from Equation (1.78):

$$V_m^E = x_1 \cdot x_2 \cdot R \cdot T(\partial w/\partial p)_T \tag{1.81}$$

$$C_{p,m}^E = -x_1 \cdot x_2 \cdot R \cdot T[2(\partial w/\partial T)_p + T(\partial^2 w/\partial T^2)_p] \tag{1.82}$$

The well-known Redlich-Kister equation, often used to fit the excess molar property data, is an expanded Margules equation:

$$Y_m^E = x_2(1-x_2)\sum_{i=0}^{p} A_i(2x_2 - 1)^i \tag{1.83}$$

where A_i are interaction parameters determined by least squares fits. Desnoyers and Perron (1997) have suggested that if more than four parameters are needed to fit Y_m^E data, specific interactions or systematic experimental errors may be present.

In order to increase the flexibility of Equation (1.83), Van Ness and Abbott (1982)

suggested a modified Redlich-Kister equation :

$$Y_m^E = \left[\frac{x_2(1-x_2)}{1+\sum_{n=1}^{p} D_n(2x_2-1)^n}\right]\sum_{m=0}^{q} C_m(2x_2-1)^m \qquad (1.84)$$

where D_n and C_m are adjustable interaction coefficients.

Because plotted excess properties approach zero at $x_2 = 0$ and $x_2 = 1$, they mask the limiting solute-solvent and solvent-solvent interactions. The quantity $Y_m^E/\{x_2(1-x_2)\}$, known as the reduced excess molar property, was proposed by Davis (1993) and Desnoyers and Perron (1997) as a means to identify the behavior associated with specific solute-solvent and solute-solute interactions. In binary systems, this quantity is directly related to the apparent molar properties (Perron *et al.*, 1992) by the equations:

$$Y_m^E / \{x_2(1-x_2)\} = (Y_{\phi,2} - Y_2^*) / x_1 = (Y_{\phi,1} - Y_1^*) / x_2 \qquad (1.85)$$

The extrapolation of this equation to $x_2 = 0$ and $x_2 = 1$ leads to the limiting of the excess properties: $(Y_2^o - Y_2^*)$ and $(Y_1^o - Y_1^*)$, respectively. As mentioned before, Y_2^o and Y_1^o are the standard partial molar properties. Therefore, Equation (1.85) provides important information for the interactions over the whole mole faction range, especially at very small and very large mole fractions.

1.4.3 Lumry's Model

Lumry *et al.* (1982) proposed a qualitative model for interpreting the effects of the hydrophobic hydration and the properties of aqueous solutions. This model considered two contributions. The first is the random hydrogen-bonding connectivity of water, which is a major effect, and the second is a geometric-reaction process associated with the specific fluctuation behavior of liquid water.

It is remarkable that the difference in the thermodynamic properties of water increases with increasing the order of differentiation with respect to temperature or pressure. For example, the difference in $\Delta_r V° = (\partial \Delta_r G°/\partial p)_T$ will be more evident than that in $\Delta_r G°$. This implies that a second contribution other than hydrogen-bonding effects must be present (Lumry *et al.*, 1982).

The geometric relaxation model assumes *clusters* exist in the random network of the hydrogen bonds of water. These clusters have a geometry that allows other molecules to enter into well-structured H-bonded units (mainly "short-bond" and "long-bond" forms). The cluster fluctuation processes between "short-bond" and "long-bond" forms, is called "geometric relaxation". In the short-bond form, five water molecules are rigidly H-bonded, resulting in a low enthalpy and low entropy. In this form much local free volume is available for a solute. The long-bond form has larger H-bond lengths, causing the tetrahedral constraint to diminish and the H-bonds to break. As a result, the entropy increases, and the local free volume decreases. This model also explains the enthalpy-entropy compensation effect in terms of a characteristic temperature at which the enthalpy

needed for the H-bond fluctuations in clusters would be exactly cancelled by the increase in entropy (for argon in water, this temperature is 295 K).

When Lumry's model is applied to the reduced excess molar properties $Y_m^E/\{x_2(1-x_2)\}$, the composition is typically subdivided into three regions (Pagé *et al.*, 1993) in which different effects are predominant: (i) at low mole fractions, the cosolvent occupies "holes" in the open structure of water and disrupts the cooperative fluctuations of liquid water (typically at $x_2 \leq 0.1$); (ii) the cosolvent eliminates the extensive hydrogen-bonding connectivity between water molecules (typically at mole fractions $0.1 < x_2 \leq 0.3$); (iii) water-cosolvent interactions are gradually replaced by cosolvent-cosolvent interactions (typically at $x_2 \geq 0.3$).

1.5 Literature on AMP Decomposition

The hydrothermal stability of AMP at elevated temperatures was investigated by Féron and Lambert (1992) through laboratory and loop tests. AMP could not be tested in an autoclave at 300°C because it would be completely destroyed before reaching that temperature in the autoclave. This implies a high thermal decomposition rate of AMP. An alternative technique, using a flow system to shorten the residence time, was performed in their study. By analyzing one of the decomposition products (ammonia), Féron and Lambert were able to infer a mechanism for the hydrolysis of AMP.

$$NH_2C(CH_3)_2CH_2OH + H_2O \rightarrow NH_3 + (CH_3)_2C(OH)CH_2OH \qquad (1.86)$$

$$(CH_3)_2C(OH)CH_2OH + H_2O \rightarrow CH_4 + CH_3COOH + CH_3OH \qquad (1.87)$$

$$CH_3OH + H_2O \rightarrow CO_2 + 3H_2 \qquad (1.88)$$

$$CH_3COOH \rightarrow CO_2 + CH_4 \qquad (1.89)$$

The loop tests were conducted under conditions close to a pressurized water reactor (PWR) secondary circuit, to verify the results above under power station conditions. During this run, the vapor temperature was set to be 282 ± 1°C. Three chemical conditions were employed in the experimental run: (1) a period with only ammonia; (2) a period with AMP addition and low oxygen content (< 5 $\mu g \cdot kg^{-1}$); (3) a period with AMP addition (the same concentration) but higher oxygen content (> 10 $\mu g \cdot kg^{-1}$) for the purpose of examining the effect of oxygen. It turned out that, in the boiler, 22 % of AMP decomposed in the second period, and 1 % more of AMP decomposed in the third period. In the whole secondary circuit, the decomposition percentage was 33 % and 42 % in the second and third periods, respectively. The study is consistent with the thermal decomposition mechanism proposed as Equation (1.86).

1.6 Objectives

1.6.1 Standard State Properties of Dilute Solutions

The goals of this research were to obtain thermodynamic data for dilute aqueous AMP and $AMPH^+Cl^-$ solutions at elevated temperatures, to model them with appropriate models, and to identify solvation effects. The specific objectives were as follows:

I. Measurement of the apparent molar volumes $V_{\phi,2}$ for dilute solutions of AMP and its salt at temperatures up to 556 K.

II. Measurement of the apparent molar heat capacities $C_{p,\phi,2}$ for dilute solutions of AMP and its salt near room temperature.

III. Calculation of the standard partial molar volumes V_2^o and the standard partial molar heat capacities $C_{p,2}^o$ based on the results from Steps (I) and (II).

IV. Application of appropriate equations of state to fit V_2^o and $C_{p,2}^o$ as functions of temperature.

V. Comparison of different models for fitting the experimental data of V_2^o and $C_{p,2}^o$: the revised HKF model, the "density" model, and a hybrid model from this laboratory.

VI. Investigation of solvation effects in V_2^o and $C_{p,2}^o$.

In order to model or predict the equilibrium constant at hydrothermal conditions, the standard partial molar volumes and heat capacities at elevated temperatures are needed. They were obtained from apparent molar properties in this study. The apparent

molar volumes $V_{\phi,2}$ for aqueous solution of AMP and its salt were determined with two platinum vibrating tube densimeters at temperatures from 283 to 556 K. Standard partial molar volumes V_2^o were derived isothermally by the extrapolation of apparent molar volumes. The measurements were not made at higher temperatures because decomposition of aqueous $AMPH^+Cl^-$ occurred at 556 K. At temperatures above 373 K, the pressure must be higher than 0.1 MPa to keep the aqueous solutions in liquid state. In this study, the pressures 20 MPa and 10 MPa were used for the pressure-dependent investigations. The apparent molar heat capacities $C_{p,\phi,2}$ of AMP and $AMPH^+Cl^-$ solutions were measured with a Picker microcalorimeter at temperatures from 283 to 328 K, and subsequently the standard partial molar heat capacities were derived from the isothermal fits. Three models were used to represent the temperature dependence of V_2^o, and to predict high temperature $C_{p,2}^o$ values from low temperature data through thermodynamic relationships.

1.6.2 Properties of Concentrated Solutions

The goal of this part of the thesis was to measure the properties for the system (AMP + H_2O) over a wide range of mole fractions, and subsequently to calculate the excess properties and reduced excess properties. Molecular interactions and temperature dependence were investigated. The specific objectives were:

I Measurement of the heat capacities for the system (AMP + H_2O) over the whole mole fraction range up to the normal boiling temperature of water.

II. Measurement of the densities for the system (AMP + H_2O) over the whole mole fraction range up to 353 K.

III. Calculation of the excess molar heat capacities $C^E_{p,m}$ and the excess molar volumes V^E_m based on Steps (I) and (II).

IV. Application of a modified Redlich-Kister equation for fitting the excess molar properties, and examining molecular interactions through reduced excess molar properties.

The heat capacities and densities for (AMP + H_2O) were measured over the whole mole fraction range with a CSC 4100 differential scanning calorimeter and a DMA 5000 densimeter. The excess molar properties were derived, and were represented, by a modified Redlich-Kister equation. Lumry's model was employed to interpret the molecular interactions and the structure changes based on the reduced excess molar properties.

Chapter 2: Experimental

2.1 Picker Flow Microcalorimeter

Specific heat capacity measurements of dilute solutions from $283.15 \leq T \leq 328.15$ K at 0.1 MPa were made with a Sodev Picker flow microcalorimeter (Picker *et al.*, 1971). The methods were described by Xiao and Tremaine (1996).

The Picker flow microcalorimeter is shown schematically in Figure 2.1. The specific heat capacity c_p of a liquid in each cell can be expressed as:

$$c_p = \frac{W}{f_m \Delta T} \tag{2.1}$$

Here W is the applied power; f_m is the mass flow rate of the liquid through the cell; and ΔT is the temperature increment due to the power and the flow rate.

Because the mass flow rate is the product of volumetric flow rate and density, if volumetric flow rates in two cells are the same (as in this study), and their densities are known, the ratio of mass flow rates for the two fluids can be obtained. The instrument maintains the same value of ΔT in both cells by applying the energy W_o to both fluids (a sample solution and water) in the two cells, and an extra energy ΔW to the sample solution. The relative heat capacity of the solution to water can then be expressed as:

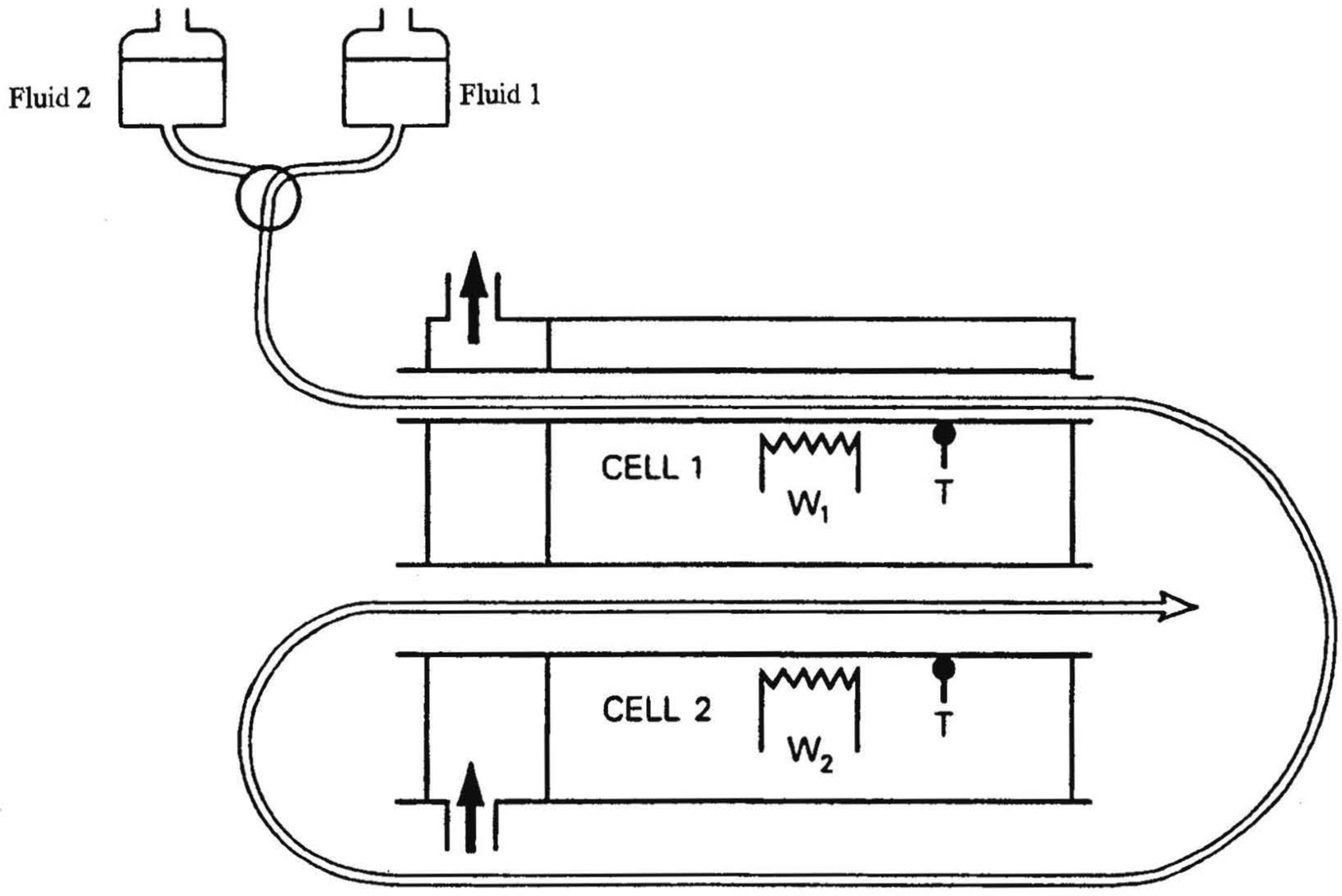

Figure 2.1 Schematic of Picker flow microcalorimeter.

$$\frac{c_{p,sol}}{c^*_{p,1}} = \left(1 + \frac{\Delta W}{W_o}\right)\left(\frac{\rho^*_1}{\rho_{sol}}\right) \qquad (2.2)$$

Here $c_{p,sol}$ and $c^*_{p,1}$ are the specific heat capacities of the solution and water, respectively; and ρ_{sol} and ρ^*_1 are the densities of the solution and water, respectively.

In the Picker calorimeter, two symmetrical cells connected by a long tube ("delay line") allow two fluids to flow, sequentially through each cell. Fluid 1 is allowed to flow into the system and passes through cell 1 and cell 2. Then the two-position six-port valve is changed to allow fluid 2 to flow into cell 1. As fluid 2 displaces the original fluid 1 into cell 2, there will be a time when cell 1 contains fluid 2, and cell 2 contains fluid 1. A constant power W_o is supplied to both cells by two zener diodes, and a bias DC voltage applied to the sample cell provides extra power ΔW in order to obtain same ΔT in the two cells. This power difference ΔW allows the relative heat capacities of the two fluids to be measured, *if* the relative densities of the two fluids are known and the volumetric flow rates in the two cells are the same, as required by Equation (2.2). In this study, water is fluid 1, and the sample under investigation is fluid 2.

Desnoyers *et al.* (1976) discovered that a small but significant systematic error arises from small heat losses, whose effect can be eliminated by a calibration of two fluids with known specific heat capacities (standard NaCl solution and water). The heat leak correction factor ff is calculated from the expression:

$$ff = \frac{(c_p\rho)_{std} - (c^*_{p,1}\rho^*_1)}{(c_p\rho)_{\exp} - (c^*_{p,1}\rho^*_1)} \tag{2.3}$$

where $(c_p\rho)_{exp}$ is the product of the experimental specific heat capacity and experimental density of standard NaCl solution; and $(c_p\rho)_{std}$ is that of the properties calculated from the literature values (Archer, 1992).

Equation (2.2) then can be revised as:

$$\frac{c_{p,sol}}{c^*_{p,1}} = \left(1 + ff\,\frac{\Delta W}{W_o}\right)\left(\frac{\rho^*_1}{\rho_{sol}}\right) \tag{2.4}$$

2.2 Differential Scanning Calorimeter

A CSC 4100 heat-flux differential scanning calorimeter (DSC) was used to determine the heat capacities of AMP from 278 to 368 K over the whole mole fraction range. The system is a "passive" design which monitors heat flow into and out of the sample chambers using extremely sensitive detectors, so that only a small amount of sample is needed. The DSC contains four wells, each with a thermo-electric device (TED) at its base to measure the heat flux to or from a common heat sink, whose temperature is monitored by an RTD. As shown in Figure 2.2, matched cells containing measured amounts of sample or a reference material can be placed in the wells. A 1000 ohm

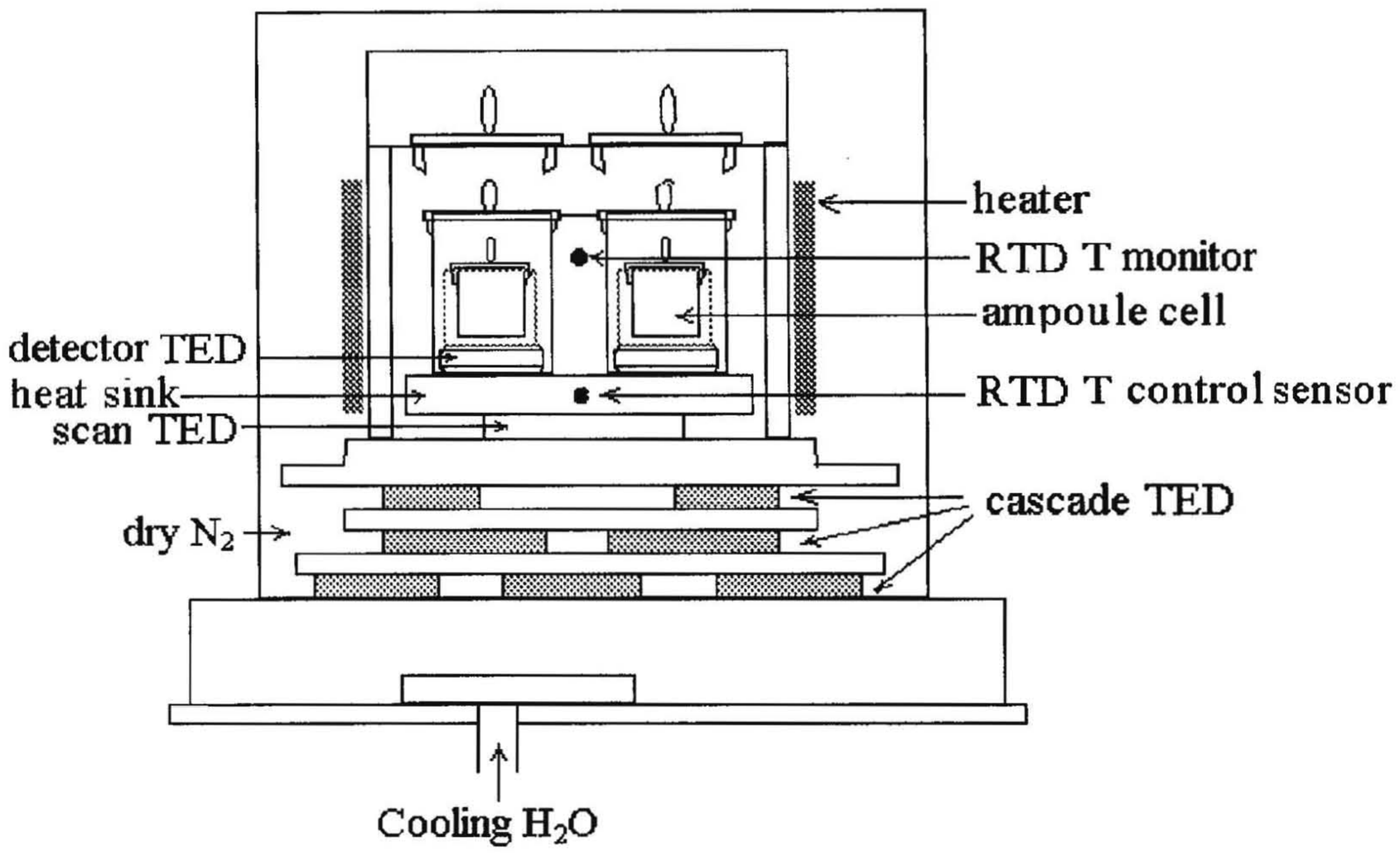

Figure 2.2 Schematic of CSC 4100 differential scanning calorimeter.

platinum RTD (referred as "RTD T monitor" in Figure 2.2) is used to monitor the temperature for the system, hence the temperature of the samples. An adiabatic shield reduces the heat exchange between the heat sink and atmosphere by an order of magnitude. The temperature is controlled by the heater, which provides energy to increase the temperature, and the cascade TED which removes heat. Cooling water is pumped through the system to remove heat from the cascade TED. A dry nitrogen purge prevents the formation of condensation inside the measuring unit. The raw data were stored as differential sensor voltages and converted to heat capacities, using calibration constants.

2.3 Vibrating Tube Densimeters

2.3.1 Sodev Flow Densimeter

Kratky *et al.* (1969) reported that the density of a fluid can be obtained by measuring the resonant vibrational frequency of tubes containing that fluid. Several flow vibrating tube densimeters have been designed for fast measurements using this principle (Picker *et al.*, 1974; Xiao and Tremaine, 1996; Anton Paar GmbH, 1998). In this study the densities of all solutions at low molalities and temperatures ($T < 373$ K) relative to water were measured by a commercial Sodev 03D flow vibrating tube densimeter.

The principle of the vibrating tube is based on the properties of a mechanical oscillator. The fluid is placed inside a vibrating tube, and the resonant frequency (or the resonant period τ) of this vibrating tube is a function of the density ρ of that fluid.

$$\rho = A + K \cdot \tau^2 \tag{2.5}$$

where A and K are constants of the system, determined by two reference fluids with known densities:

$$K = \frac{\rho_2 - \rho_1}{\tau_2^2 - \tau_1^2} \tag{2.6}$$

Therefore, the density of an aqueous solution relative to water can be calculated by:

$$\rho_{sol} = \rho_1^* + K(\tau_{sol}^2 - \tau_1^2) \tag{2.7}$$

where ρ_1^* and ρ_{sol} are the densities of water and the sample solution; and τ_1 and τ_{sol} are the corresponding vibration resonant periods.

This densimeter was coupled to the Picker flow microcalorimeter in-line to provide the densities required in the heat capacity calculations.

2.3.2 High-Temperature Densimeter

High temperature measurements were performed by a platinum vibrating-tube densimeter developed by Xiao and Tremaine (1996), and up-graded by Clarke (2000). This densimeter is based on the design of Albert and Wood (1984), which was modified by Corti *et al.* (1990).

The principle is very similar to that of the low-temperature densimeter as described in Section 2.3.1. The core unit of the densimeter is an metal-alloy U-tube (90 % platinum + 10 % iridium), a permanent horseshoe magnet, and two Inconel rods in a cylindrical brass block, as shown in Figure 2.3. The top of the U-tube is silver soldered into two holes in the brass block. The two rods are glued to the U-tube with insulating cement, so that they lie within the poles of a permanent horseshoe magnet that rests between the two arms of the U-tube. An alternating current through one rod interacts with the permanent magnetic field to drive the U-tube to vibrate. The current induced in the other rod is used to sense the vibration. These two Inconel rods, attached (not in contact) to the U-tube with ceramic adhesive, are connected through fine silver wires to a feedback amplifier, which maintains the tube at its resonant frequency. The resonant frequency is recorded by a frequency meter for the density calculation, as shown in Equation (2.7).

The whole flow system is shown in Figure 2.3. The sample injection system contains a HPLC pump (17) to deliver water at a constant volumetric flow rate. A sample is injected by a syringe into the loop (16), sealed by changing the position of the nearest valve, pre-pressurized by pump (18), and stored there. Water from the pump (17) is allowed to flow into the system as a reference. After the values of resonant periods of water, τ_1, are stable, the graphic values of τ_1 (about twenty-five points) are recorded. Then the position of another two-position six-port valve close to pump (17) is changed, so that the water from the pump will enter the loop (16) to push the original sample into the

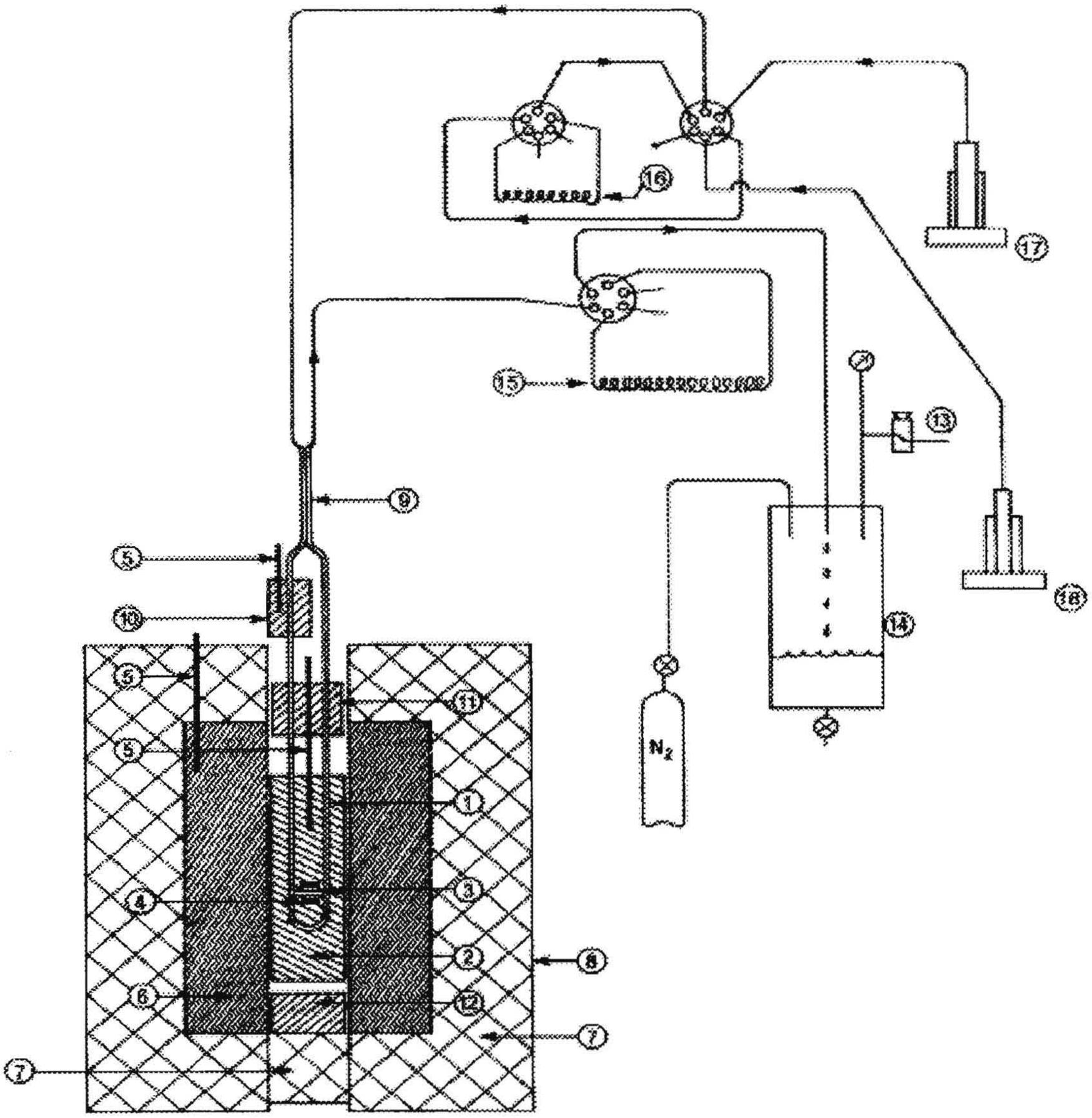

Figure 2.3 Schematic of the high-temperature vibrating tube densimeter. 1, platinum U-shaped vibrating tube; 2, densimeter cell body; 3, Inconel rods for sensing and driver current; 4, permanent magnet; 5, RTD; 6, cylindrical brass block (oven); 7, thermal insulator; 8, stainless steel container; 9, heat exchanger; 10, aluminum preheater; 11, aluminum heat shield; 12, brass heat shield; 13, back-pressure regulator; 14, stainless steel reservoir; 15, sampling loop; 16, injection loop; 17, water deliver pump; 18, pre-pressurizing pump. (reproduced from Clarke, 2000)

measuring unit.

A small aluminum cylinder that acts as a preheater was placed right after the injection system. This cylinder brings the temperature of the solution or water to nearly the measuring temperature, so that the temperature fluctuation is reduced. The preheater is heated by a Chromalox heater, and controlled to ± 0.2 K by a temperature controller.

The brass cylinder was heated by two strands of insulated heating wire (nickel + chromium), which was wrapped around the brass block in a symmetrical counter-current configuration. The large thermal mass of this brass cylinder and the thermal insulated cotton around it were arranged for the thermal stability. The temperature of the brass block (oven) was measured by a 100 Ω platinum RTD near the edge of the brass block, and controlled by a temperature controller. The temperature of the densimeter itself was measured by another 100 Ω platinum RTD located in the middle of the U-tube, and monitored by a Hewlett-Packard multimeter. The RTD was calibrated by the measurements of the ice point of water and the freezing points of tin and lead (standard reference materials from NIST), and the accuracy was estimated to be ± 0.02 K (Xiao, 1997). The pressure was measured by a pressure transducer and a process indicator in-line. When water or the sample flowed through the U-tube, the periods were recorded by a universal counter as the tube vibrated at its natural frequency. The system temperature and pressure were recorded as well.

The sampling loop (15) with the third two-position six-port valve allows sampling after high-temperature measurements for the decomposition analysis. The high pressure

of the flow system was obtained and maintained by a nitrogen cylinder and a back-pressure regulator. The electronic circuit design and details of the equipment construction were described by Xiao (1997).

2.3.3 DMA 5000 Densimeter

A DMA 5000 vibrating tube densimeter was employed for the density measurements of the system (AMP + H_2O) over the whole mole fraction range. It is the first commercial oscillating densimeter suitable for high viscosity liquids and a wide range temperature with high accuracy. It was used here because of the high viscosities of concentrated AMP solutions.

In the DMA 5000 vibrating tube densimeter, a U-shaped borosilicate glass tube containing a sample is electro-magnetically driven into harmonic oscillation, whose resonant period is measured using the same principles as those of the Sodev and high-temperature vibrating tube densimeters discussed in Sections 2.3.1 and 2.3.2. The only difference is that, in this instrument, there is a proprietary reference oscillator which allows the calibration constant K to be determined by the manufacturer and verified daily by one measurement at 293 K, instead of using two reference fluids to determine the calibration constant daily. The sample viscosity can cause the damping of the U-tube's oscillation, and move the oscillation nodes slightly. The densimeter measures oscillations at several frequencies and in two modes (H & D Fitzgerald Ltd., 2000), hence provides automatic viscosity correction. The internal software of the densimeter assumes that

$$\rho = A \cdot \tau^2 \cdot (1 + D \cdot damping + E \cdot damping^2) - B + C \cdot \tau^4 \qquad (2.8)$$

where A, D, E, B, and C are constants; τ is the oscillation period; and *damping* is the damping factor (H & D Fitzgerald Ltd., 2000).

The densimeter provides three options to correct for the influence of viscosity: "Density (not viscosity correct.)", "Density (viscosity < 700 MPa·s)", and "Density (viscosity > 500 MPa·s)". The details of the correction method are not published by the manufacturer. An assessment of the DMA 5000 densimeter by H & D Fitzgerald Ltd. (2000) found that the viscosity influence on the density is fairly stable for viscosity > 500 MPa·s. For samples 0.690 g·ml < ρ < 1.620 g·ml and viscosities up to 600 MPa·s, the following form is preferred:

$$\rho = A + B \cdot \tau^2 + C \cdot damping \qquad (2.9)$$

and for viscosities below 30 MPa·s, another form is used:

$$\rho = A + B \cdot \tau^2 + C / damping \qquad (2.10)$$

Two built-in Pt 100 temperature sensors were used to measure temperature with a precision of ± 0.002 K (H & D Fitzgerald Ltd., 2000).

Chapter 3: Thermodynamics of Dilute Aqueous 2-Amino-2-Methyl-1-Propanol (AMP) and 2-Amino-2-Methyl-1-Propanol Hydrochloride ($AMPH^+Cl^-$): Apparent Molar Volumes and Heat Capacities

3.1 Introduction

In this chapter, apparent molar volumes for both aqueous AMP and $AMPH^+Cl^-$ were reported at two pressures, and up to the decomposition temperature of aqueous $AMPH^+Cl^-$, 556 K. Apparent molar heat capacities were reported at low temperatures (283.15 K ≤ T ≤ 373 K). Linear equations were fitted to these results, and extrapolation of the fitted lines to infinite dilution led to values for the standard partial molar properties. The temperature and pressure dependences of the resulting standard partial molar properties were then represented by each of the three models presented in Sections 1.3.3, 1.3.4, and 1.3.5. The success of these models was evaluated. The effects of hydration and AMP ionization are discussed.

3.2 Experimental Methods

3.2.1 Materials

2-Amino-2-methyl-1-propanol (AMP) was obtained from three sources. (i) The first sample, purchased from ACROS Organics (99 %), was heavily contaminated with impurity; (ii) This sample was purified, and the purified product was used as the second sample; (iii) The third sample was obtained from Fluka [≥ 99.0 % (Gas Chromatography

Grade)].

Sample (i) of AMP (ACROS) was used as received to prepare a stock solution for the measurements on Sodev Picker calorimeter and densimeter at low temperatures (283 K ≤ T ≤ 328 K). This stock solution of AMP was standardized by titration of the ionizable amine groups with 0.1 mol·kg^{-1} hydrochloric acid. A stock solution of 2-amino-2-methyl-1-propanol hydrochloride ($AMPH^+Cl^-$) was then prepared by adding an excess weighed amount of standard HCl to the standard AMP solutions. These stock solutions of AMP and $AMPH^+Cl^-$ were used for the preparation of a series of more dilute solutions by mass.

Several months after the measurements using these dilute solutions were made, the purity of AMP from the opened source bottle was shown by titration with HCl to be no more than 93.5 mole per cent. The major impurity is water, as observed in our fractional distillation. Although the stock solutions were standardized by titration for the $-NH_2$ group before those measurements were made, unknown impurities other than water in the original AMP may affect the results. Therefore, the measurements of AMP and $AMPH^+Cl^-$ solutions should be repeated under the same conditions to verify the previous data.

Table 3.1 lists the physical properties of pure AMP used here for the purity determination. A fractional crystallization process was performed in an attempt to purify the material, but the result was not satisfactory due to the difficulty of the solid-liquid separation because of the low melting point of AMP (Table 3.1).

Table 3.1 Physical properties of AMP from the literature.

Sources	melting point	boiling point at 760mm	density at 20°C relative to water at 4°C	refractive index (at 20°C, sodium D line)
Budavari *et al.* (1989) (Merck Index)	30-31°C	165°C	0.934	1.449
Perrin and Armarego (1988)	31°C	164-166°C	0.935	-------
Lide (1990)	25-26°C	165.5°C	0.934	1.449

Double distillation of AMP (ACROS) under an inert atmosphere maintained by nitrogen was performed, and the stable fraction at 165.4°C was collected (the second distillation was a fractional distillation). The product had purity higher than 99 mole per cent, tested by titration and gas chromatography-mass spectrometry (GC-MS). The index of refraction for the AMP after double distillation was 1.4484 ± 0.0005 at 20.0°C (consistent with literature as shown in Table 3.1), and 1.4423 ± 0.0002 at 34.4°C.

The product after double distillation of the above AMP was used for comparison with commercial product to estimate purity analysis by physical property measurements. No thermodynamic properties were measured using this sample.

The third sample, AMP from Fluka, was used as received to prepare a series of dilute solutions after its purity was confirmed by titration and GC-MS. A small amount of NaOH was added to suppress hydrolysis, and the concentrations are listed in Tables A.1.3, A.1.4, and A.1.7 in the Appendices. Solid $AMPH^+Cl^-$ was obtained from Fluka [≥ 99.0 % (T)], and dried at 386 K for 48 h. This sample ($AMPH^+Cl^-$) was titrated by a standard solution of 0.1 $mol \cdot kg^{-1}$ $AgNO_3$ (Fisher, certified A.C.S., ≥ 99.7 %) using potassium chromate as the indicator, which showed the purity to be 100 ± 0.5 mole per cent. The $AgNO_3$ solution was standardized by titration against a 0.1 $mol \cdot kg^{-1}$ standard NaCl solution. A series of $AMPH^+Cl^-$ solutions were prepared with excess HCl. The concentrations are listed in Table A.1.8 and in Tables A.1.5 and A.1.6. These solutions were used to repeat the measurements of the apparent molar properties of both aqueous AMP and $AMPH^+Cl^-$ at 298.15 K with the Sodev Picker calorimeter and densimeter.

Also, these high purity solutions have been used for all the density measurements with the high-temperature densimeter.

All the AMP solutions were handled with care to minimize the time of exposure to the surroundings so as to avoid CO_2 contamination. Sample solutions made with materials from Fluka were handled and stored in a glove bag with dry nitrogen. Solutions of hydrochloric acid were prepared by diluting a 15 mol·kg^{-1} stock solution (Fisher A.C.S. certified reagent grade) and standardized by titration against TRIS [tris(hydroxymethyl)aminomethane; Aldrich, certified A.C.S]. The sodium hydroxide solutions were prepared from a 50 per cent, carbonate-free solution (Fisher) by dilution, and standardized by titration against a standard solution of potassium hydrogen phthalate (Baker, 99.97 %). Sodium chloride (ACP Chemicals Inc., Certified A.C.S., 99.99 per cent) was used for the low temperature (< 100°C) measurements, and sodium chloride (Alfa, 99.99 per cent) for high temperature measurements. All the standard sodium chloride solutions were prepared after drying the salt for 24 h at 393 K. Nanopure water (resistivity > 17 MΩ·cm) was used for preparing all the solutions after being boiled for 20 to 30 minutes, and this nanopure water was also used as a reference fluid. All the solutions above were prepared by mass.

3.2.2 Experiments on the Picker Flow Microcalorimeter

The Picker flow microcalorimeter has been discussed in Section 2.1. In this study, the densities and the heat capacities of the NaCl standard solution relative to water were

measured daily, the heat leak correction factor *ff* was then calculated according to Equation (2.3), using specific heat capacities and densities for the standard NaCl solution from Archer (1992). Values for $c^*_{p,1}$ and ρ^*_1 for water were taken from Hill (1990). The heat loss factors (± 0.005) were 1.038 at T = 283.15 K, 1.029 at T = 298.15 K, 1.028 at T = 303.15 K, 1.000 at T = 328.15 K, and 1.029 at T = 328.15 K for the original measurements on AMP sample (i). In the measurement with AMP sample (iii) (Fluka) at 298.15 K, the heat loss factor was 1.025. The heat loss factors for the measurements with $AMPH^+Cl^-$ [made from AMP sample (i)] were 1.040 at T = 283.15 K, 1.056 at T = 283.15 K, 1.029 at T = 298.15 K, 1.016 at T = 303.15 K, and 1.002 at T = 328.15 K. In the measurement with $AMPH^+Cl^-$ (Fluka) at 298.15 K, the heat loss factor was 1.027.

The temperature in the calorimeter was controlled to ± 0.01 K by a Sodev CT-L circulating pump and temperature control unit, and monitored by a thermistor which was calibrated with a Hewlett-Packard 2804A quartz-crystal thermometer (Xiao, 1997).

3.2.3 Experiments on the Sodev Flow Densimeter

The principle of this equipment has been discussed in Section 2.3.1. The characteristic constant K was calculated from Equation (2.6), from daily measurements on the two reference fluids, a standard NaCl solution and water. The literature densities of the standard NaCl solution and water were taken from Archer (1992) and Hill (1990). A second Sodev CT-L temperature control unit was used to control the temperature of the Sodev densimeter independently from that used with the Picker calorimeter.

3.2.4 Measurements on the High-Temperature Densimeter

Measurements of apparent molar volumes vs T and p were made on the high-temperature densimeter described in Section 2.3.2. Experimental temperatures and pressures were set and allowed to stabilize overnight before measurements. An HPLC pump was used to deliver water at a constant volumetric flow rate of 0.05 ml/min. For each sample, about 22 cm^3 solution was injected manually by a syringe into a 15 cm^3 injection loop, so that the loop was rinsed by the excess solution which was then discarded. A preheater and the brass oven brought the fluid inside the U-tube to the desired temperature, and the system pressure was provided and maintained by a high pressure nitrogen cylinder (6000 psi) and a back-pressure regulator (Tescom). Cooling water was circulated around the outlet end of the densimeter measuring unit to remove heat. For each run, the resonant periods of water and the solution under investigation were recorded in turn. The density of the solution relative to water was then calculated from Equation (2.7). At the end of each day's measurements, the calibration constant K was obtained again by measuring the resonant periods of a standard NaCl solution and water, with the literature values given in Section 3.2.3.

3.2.5 Hydrothermal Stability of AMP

In this study, the highest temperature used in the density measurements of AMP and $AMPH^+Cl^-$ solutions at 19.6 MPa was 555.6 K. The effluent solutions were collected for analysis using a sampling loop downstream from the densimeter. While these samples

were collected, a very strong pungent odor was noticed, which the original solutions did not have. The amount of the ammonia produced was analyzed by a Beckman 121MB Amino Acid Analyzer to determine the percentage decomposition according to the mechanism proposed by Féron and Lambert (1992). Each sample was analyzed by ion chromatography in a dilute acid solution with trace amount of ninhydrin acting as a colorimetric indicator, and was detected by a UV-visible detector. For AMP and $AMPH^+Cl^-$ solutions, each analysis included an original solution (standard) and the corresponding effluent, both of which were diluted to the optimum concentration for the ion chromatograph. The results are shown in Table 3.2. AMP was analyzed twice. Because no peak for ammonia was detected the first time, possibly because of the rather low concentration, a second set of AMP solutions (standard and effluent) with higher concentrations was prepared for the analysis.

As shown in Table 3.2, the $AMPH^+Cl^-$ solution had a high percentage of decomposition at T = 555.6 K and p = 19.6 MPa. This result is reflected in the behavior of the experimental $V_{\phi,2}$ data for the $AMPH^+Cl^-$ solution at this condition, which will be discussed below in Section 3.3.1.

Table 3.2 Thermal decomposition for AMP and $AMPH^+Cl^-$ solutions after measurements of densities with the high-temperature vibrating tube densimeter at T = 555.6 K and p = 19.6 MPa.

species	experimental concentration ($mol \cdot kg^{-1}$)	concentration used for analysis ($mmol \cdot kg^{-1}$)	ammonia detected ($nano\text{-}moles \cdot ml^{-1}$)	decomposition percentage (%)
AMP 1 (standard)	1.2314	0.2784	(no peak)	-------
AMP 1 (effluent)	1.2314	0.2731	(no peak)	-------
$AMPH^+Cl^-$ (standard)	1.8292	0.3386	(no peak)	-------
$AMPH^+Cl^-$ (effluent)	1.8292	0.3355	92.6	27.6
AMP 2 (standard)	1.5605	2.203	~1.0	-------
AMP 2 (effluent)	1.5605	2.532	~8.0	~0.28

3.3 Results

3.3.1 Apparent Molar Properties

Apparent molar volumes $V_{\phi,2}$ and heat capacities $C_{p,\phi,2}$ were calculated from the experimental densities and specific heat capacities by Equations (1.10) and (1.11), given in Section 1.2.1. In this study the density and specific heat capacity of water ρ_1^* and $c_{p,1}^*$ were taken from Hill (1990).

A small amount of excess HCl was added to all the $AMPH^+Cl^-$ solutions (Section 3.2.1), in order to suppress the formation of neutral AMP. The effect of the excess HCl in $AMPH^+Cl^-$ solutions was subtracted, by applying Young's rule (Section 1.2.2) using the expression:

$$Y_{\phi,2}[AMPH^+Cl^-(aq)] = \{Y_\phi^{exp} \cdot (m_2 + m_3) - Y_{\phi,3}[HCl(aq)] \cdot m_3\} / m_2 \qquad (3.1)$$

Here the subscripts "2" and "3" denote $AMPH^+Cl^-$ and HCl, respectively. In these very dilute solutions, $V_{\phi,3}[HCl(aq)] \approx V_3^o[HCl(aq)]$, and values for the latter were taken from Hershey *et al.* (1984) for the calculations at 283 K ≤ T ≤ 328 K, and from SUPCRT software (Johnson *et al.*, 1992) for those at higher temperatures. Similarly, $C_{p,\phi,3}[HCl(aq)] \approx C_{p,3}^o[HCl(aq)]$, and values for the latter were taken from Tremaine *et al.* (1986) for temperatures 283 K ≤ T ≤ 328 K, and from SUPCRT software (Johnson *et al.*, 1992) for higher temperatures.

The degree of formation of neutral AMP in the solutions of $AMPH^+Cl^-$ was

calculated from the ionization constants reported by Balakrishnan (1988), and found to be negligible, undoubtedly because excess HCl was added to all the $AMPH^+Cl^-$ solutions used in this study.

The effects of excess NaOH in the AMP solutions were subtracted from the apparent molar properties, using Young's rule:

$$Y_{\phi,2}[AMP(aq)] = \{Y_{\phi}^{exp} \cdot (m_2 + m_3) - Y_{\phi,3}[NaOH(aq)] \cdot m_3\} / m_2 \qquad (3.2)$$

Because of the small concentrations of NaOH, we assume that $V_{\phi,3}[NaOH(aq)] \approx V_3^o[NaOH(aq)]$, and $C_{p,\phi,3}[NaOH(aq)] \approx C_{p,3}^o[NaOH(aq)]$. The data for $V_3^o[NaOH(aq)]$ and $C_{p,3}^o[NaOH(aq)]$ were taken from Hovey *et al.* (1988) for low temperatures, and the values of $V_3^o[NaOH(aq)]$ were obtained from Simonson *et al.* (1989) for the high temperature calculations.

In AMP solutions, the following equilibrium exists:

$$\begin{array}{lccc} AMP(aq) + H_2O(l) & \rightleftharpoons & AMPH^+(aq) + OH^-(aq) & (3.3) \\ m_2 \cdot (1 - \alpha) & & m_2 \cdot \alpha \quad m_2 \cdot \alpha & \end{array}$$

where m_2 is the initial molality of AMP. The degree of the dissociation α can be calculated by the expression:

$$\alpha = \{- (m_3 + K) + [(m_3 + K)^2 + 4Km_2]^{0.5}\} / (2m_2) \qquad (3.4)$$

Here m_3 is the molality of NaOH added ($m_3 = 0$ when no NaOH was added); and the equilibrium constant K for Equation (3.3) was calculated from the equilibrium constant of water K_w, and the K_a of the reaction $AMPH^+(aq) \rightleftharpoons AMP(aq) + H^+(aq)$. The values of K_w were obtained from Lide (1990) for low temperatures, and from SUPCRT (Johnson *et al.*, 1992) for high temperatures. The values of K_a were obtained from Balakrishnan (1988).

The contributions to apparent molar properties from $AMPH^+$ and OH^- can be subtracted by applying Young's rule:

$$V_{\phi,2}[AMP(aq)] = \{V_\phi^{exp} - \alpha \cdot V_\phi[AMPH^+(aq)] - \alpha \cdot V_\phi[OH^-(aq)] + \alpha \cdot V_\phi[(H_2O(l)]\} / (1 - \alpha) \qquad (3.5)$$

Here,

$$V_\phi[AMPH^+(aq)] + V_\phi[OH^-(aq)] = V_\phi[AMPH^+Cl^-(aq)] + V_\phi[(NaOH(aq)] - V_\phi[NaCl(aq)] \qquad (3.6)$$

Because of the small value of α, the apparent molar volumes of $AMPH^+Cl^-(aq)$, NaOH(aq), NaCl(aq), and $H_2O(l)$ were considered to have the same values as the corresponding standard partial molar volumes. Values for $V^o[AMPH^+Cl^-(aq)]$ were

obtained from this study; the sources of V^{o}[(NaOH(aq)] were given above; values for V^{o}[NaCl(aq)] were taken from Hovey *et al.* (1988) for the temperatures from 283 K ≤ T ≤ 328 K, and from Archer (1992) for high temperatures; and values for V^{o}[(H_2O(l)] were calculated from the NIST compilations (Harvey *et al.*, 1996).

Besides the Young's rule correction, the calculations for $C_{p,\phi,2}$[AMP(aq)] should include a term for the chemical relaxation correction, C_p^{rel}, as discussed in Section 1.2.3. $C_{p,\phi,2}$[AMP(aq)] can then be expressed as:

$$C_{p,\phi,2}[AMP(aq)] = \{C_{p,\phi}^{exp} - \alpha \cdot C_{p,\phi}[AMPH^{+}(aq)] - \alpha \cdot C_{p,\phi}[OH^{-}(aq)] + \alpha \cdot C_{p,\phi}[(H_2O(l)] - C_p^{rel}\} / (1 - \alpha) \qquad (3.7)$$

where

$$C_{p,\phi}[AMPH^{+}(aq)] + C_{p,\phi}[OH^{-}(aq)] = C_{p,\phi}[AMPH^{+}Cl^{-}(aq)] + C_{p,\phi}[(NaOH(aq)] - C_{p,\phi}[NaCl(aq)] \qquad (3.8)$$

and

$$C_p^{rel} = (\Delta_r H)^2 \alpha(1 - \alpha) / [RT^2(2 - \alpha)] \qquad (3.9)$$

Here $\Delta_r H$ is the partial molar enthalpy of the dissociation reaction [Equation (3.3)].

In these calculations, $C_{p,\phi}[AMPH^+Cl^-(aq)]$, $C_{p,\phi}[(NaOH(aq)]$, $C_{p,\phi}[NaCl(aq)]$, $C_{p,\phi}[(H_2O(l)]$, and $\Delta_r H$ were assumed to be approximately equal to $C_p^o[AMPH^+Cl^-(aq)]$, $C_p^o[(NaOH(aq)]$, $C_p^o[NaCl(aq)]$, $C_p^o[(H_2O(l)]$, and $\Delta_r H^o$, respectively, because of the small values of α.

The values of $C_p^o[AMPH^+Cl^-(aq)]$ were obtained from this study; the source of $C_p^o[(NaOH(aq)]$ was given above; $C_p^o[NaCl(aq)]$ were taken from Hovey *et al.* (1988); and $C_p^o[(H_2O(l)]$ were obtained from NIST compilations (Harvey *et al.*, 1996).

The value of $\Delta_r H^o$ for Equation (3.3) was calculated by the following method:

$$AMP(aq) + H^+(aq) \rightleftharpoons AMPH^+(aq) \qquad (\Delta_r H_1^o) \qquad (3.10)$$

$$H_2O(l) \rightleftharpoons H^+(aq) + OH^-(aq) \qquad (\Delta_r H_2^o) \qquad (3.11)$$

The sum of Equations (3.10) and (3.11) lead to Equation (3.3). Therefore, $\Delta_r H^o$ of the Equation (3.3) can be calculated: $\Delta_r H^o = \Delta_r H_1^o + \Delta_r H_2^o$. The value of $\Delta_r H_1^o$ was taken from Balakrishnan (1988), and that of $\Delta_r H_2^o$ was from SUPCRT software (Johnson *et al.*, 1992).

Tables A.1.1 and A.1.2 present apparent molar volumes and heat capacities of aqueous AMP from ACROS at low temperatures (283 K ≤ T ≤ 328 K), while those of aqueous AMP from Fluka are presented in Tables A.1.3 and A.1.4. Apparent molar volumes and heat capacities of the aqueous $AMPH^+Cl^-$ solutions at low temperatures are listed in Tables A.1.5 and A.1.6. In these tables the values of $(\rho - \rho_1^*)$, $[1-c_p.\rho/(c_{p,1}^* \cdot \rho_1^*)]$, and

C_p^{rel} are also listed, where ρ_1^*, ρ, $c_{p,1}^*$, and c_p are the densities and specific heat capacities of water and solution, respectively; and C_p^{rel} is the chemical relaxation contribution. Tables A.1.7 and A.1.8 present the apparent molar volumes of aqueous AMP and aqueous $AMPH^+Cl^-$ solutions at high temperatures (T > 373 K).

The experimental apparent molar volumes and heat capacities are plotted in Figures 3.1-3.8. The new data from the highly purified Fluka compound agree well with older measurements which were made using the ACROS AMP, whose purity was suspect, confirming that the initial data are valid.

The properties above 555.6 K were not measured because of the thermal decomposition discussed in Section 3.2.5. Since at 555.6 K the decomposition of AMP solution was only 0.28 %, the measured properties are considered to be valid and are tabulated in Table A.1.7. For the $AMPH^+Cl^-$ solutions, significant decomposition occurred at 555.6 K (27.6 %), and the behavior of the experimental data is also anomalous, as shown in Figure 3.9. The apparent molar volumes at this temperature decrease rapidly with increasing ionic strength, while those at other temperatures are almost independent of ionic strength. The data for $AMPH^+Cl^-$ solutions at 555.6 K and 19.6 MPa were not tabulated because of the severe decomposition.

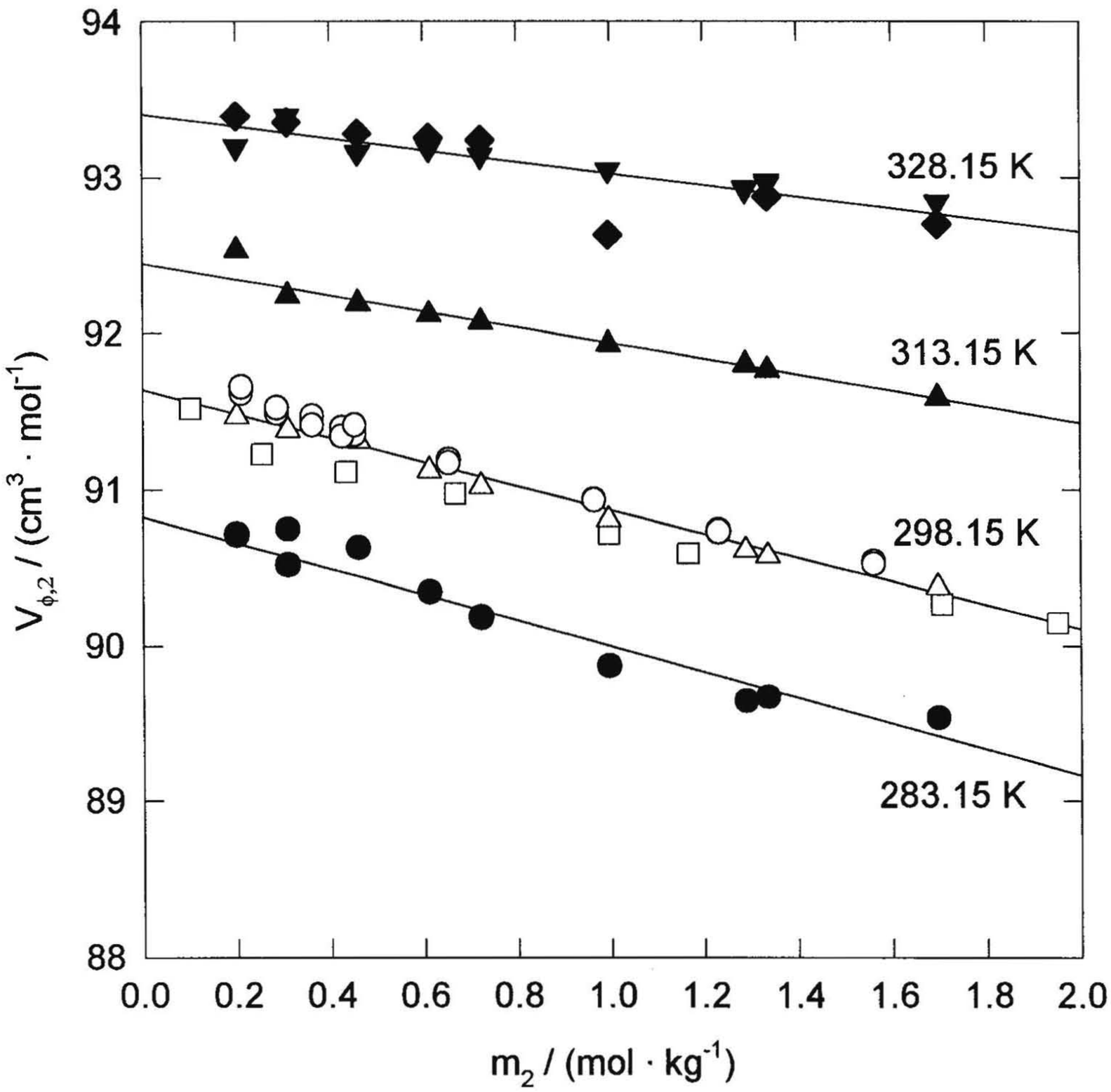

Figure 3.1 The apparent molar volumes $V_{\phi,2}$ of AMP solutions at 0.1 MPa from 283.15 to 328.15 K plotted as a function of molality. Solid symbols and △, experimental results with AMP (ACROS); ○, experimental results with AMP (Fluka); □, literature results from Roux *et al.*(1980). Lines, isothermal least squares fits to Equation (3.12).

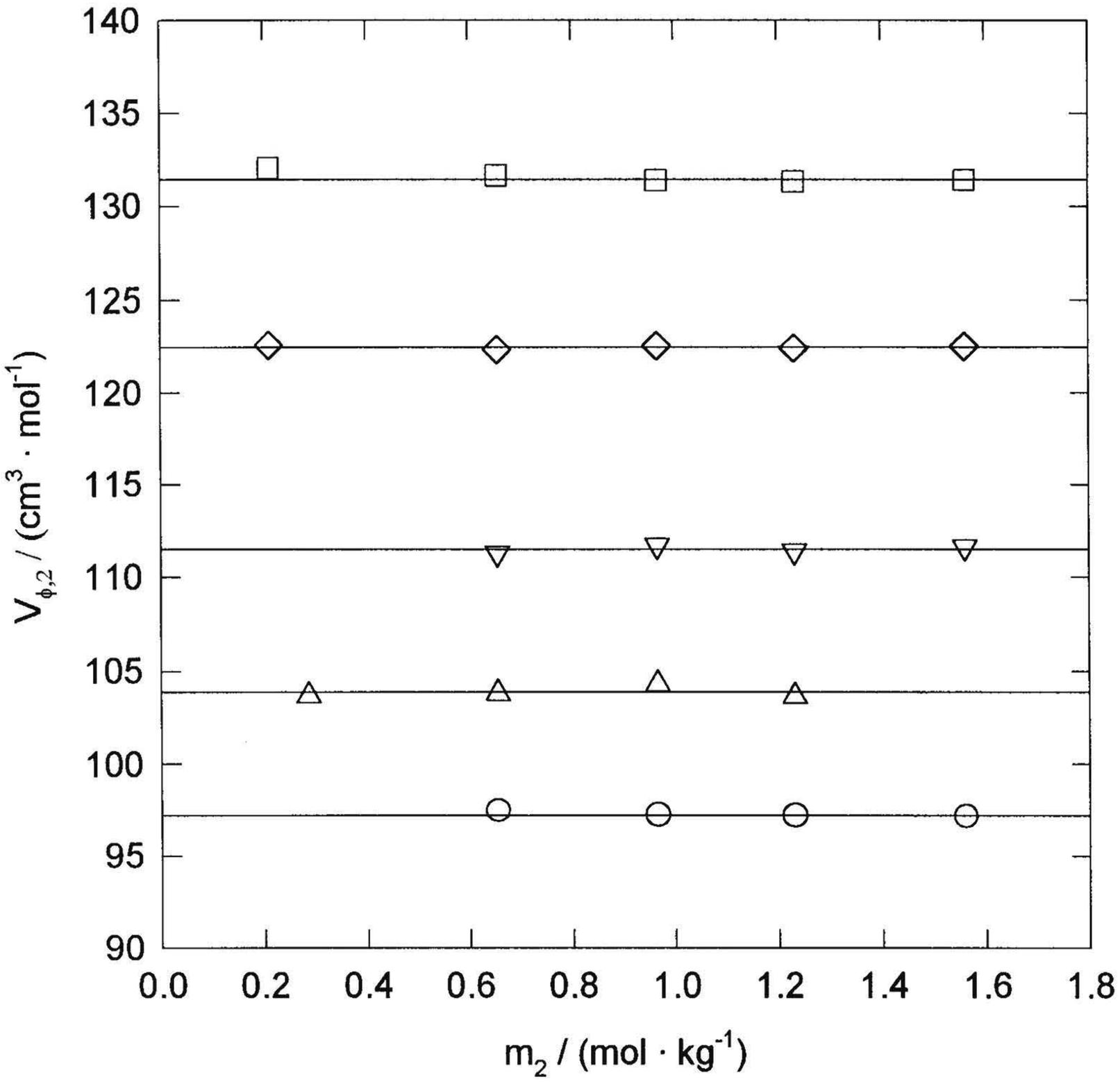

Figure 3.2 The apparent molar volumes $V_{\phi,2}$ of AMP (Fluka) solutions at 20 MPa plotted as a function of molality. ○, 378.79 K, 20.36 MPa; △, 429.97 K, 19.47 MPa; ▽, 480.37 K, 19.62 MPa; ◇, 530.32 K, 19.61 MPa; □, 555.59 K, 19.63 MPa. Lines, isothermal least squares fits to Equation (3.12).

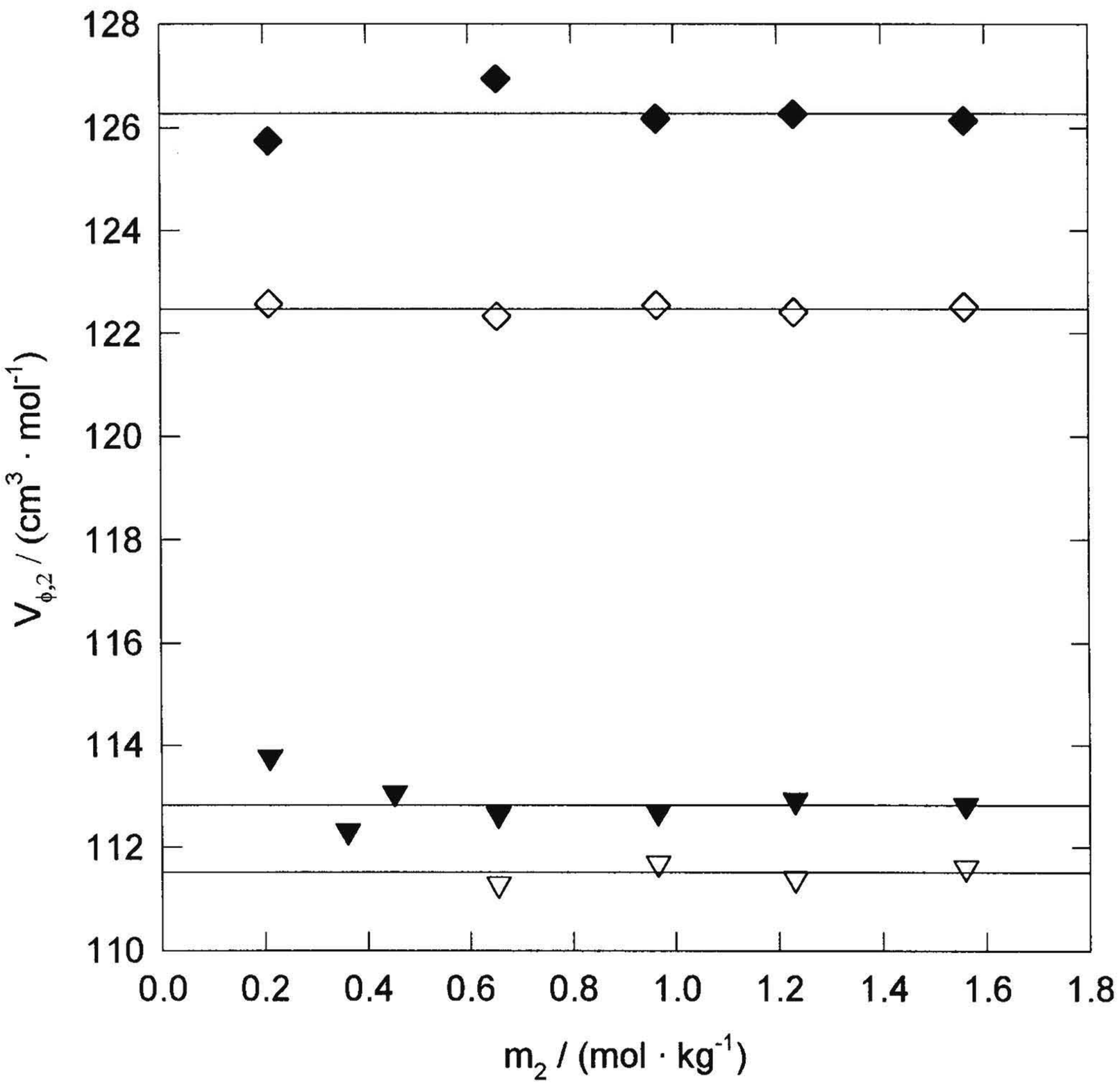

Figure 3.3 Pressure effects on the apparent molar volumes $V_{\phi,2}$ of AMP (Fluka) solutions as a function of molality. ∇, 480.37 K, 19.62 MPa; ▼ 480.89 K, 10.21 MPa; ◇, 530.32 K, 19.61 MPa; ◆, 530.88 K, 10.33 MPa. Lines, isothermal least squares fits to Equation (3.12).

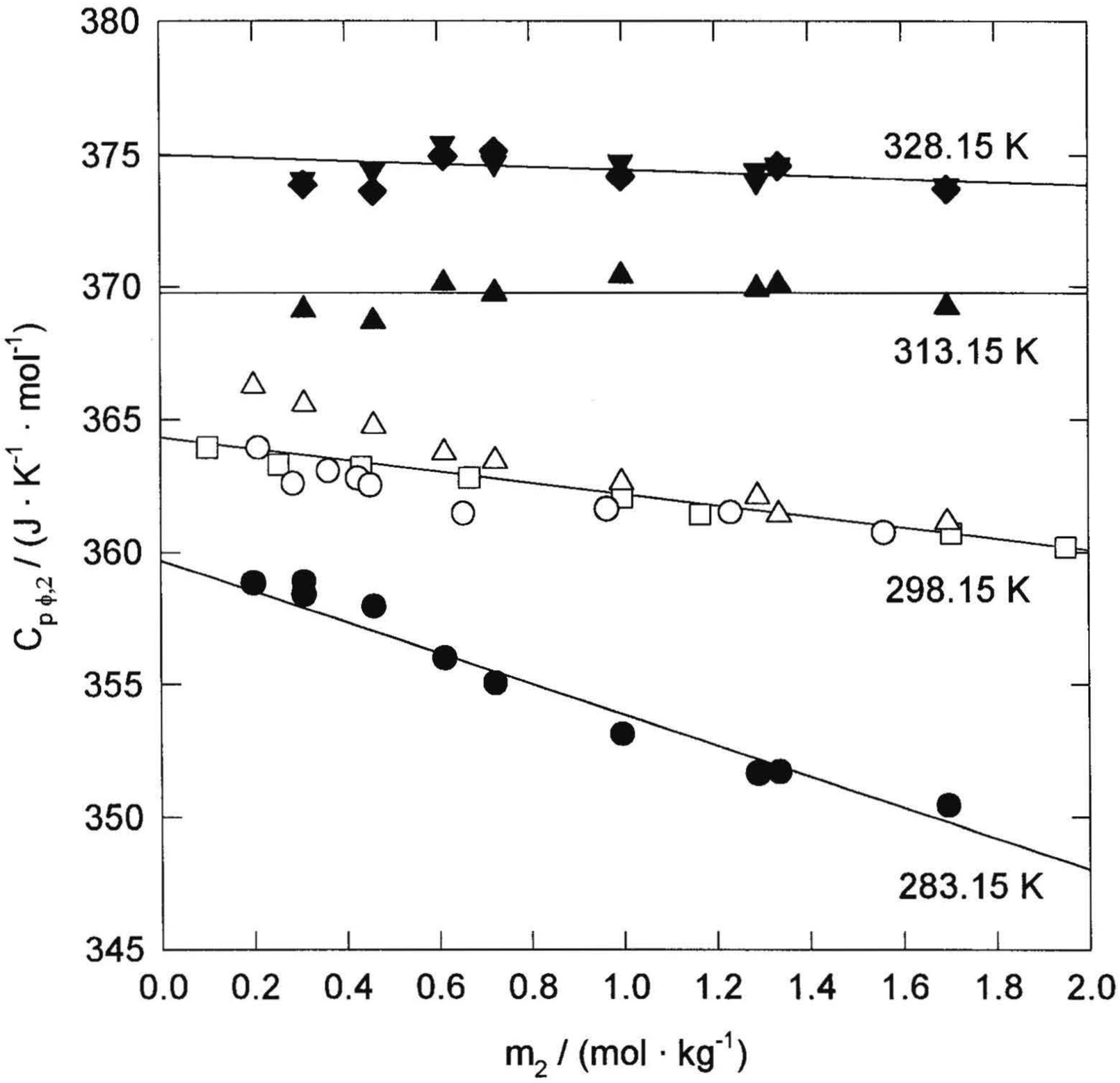

Figure 3.4 The apparent molar heat capacities $C_{p,\phi,2}$ of AMP solutions at 0.1 MPa from 283.15 to 328.15 K plotted as a function of molality. Solid symbols and △, experimental results with AMP (ACROS); ○, experimental results with AMP (Fluka); □, literature results from Roux *et al.* (1980). Lines, isothermal least squares fits to Equation (3.13).

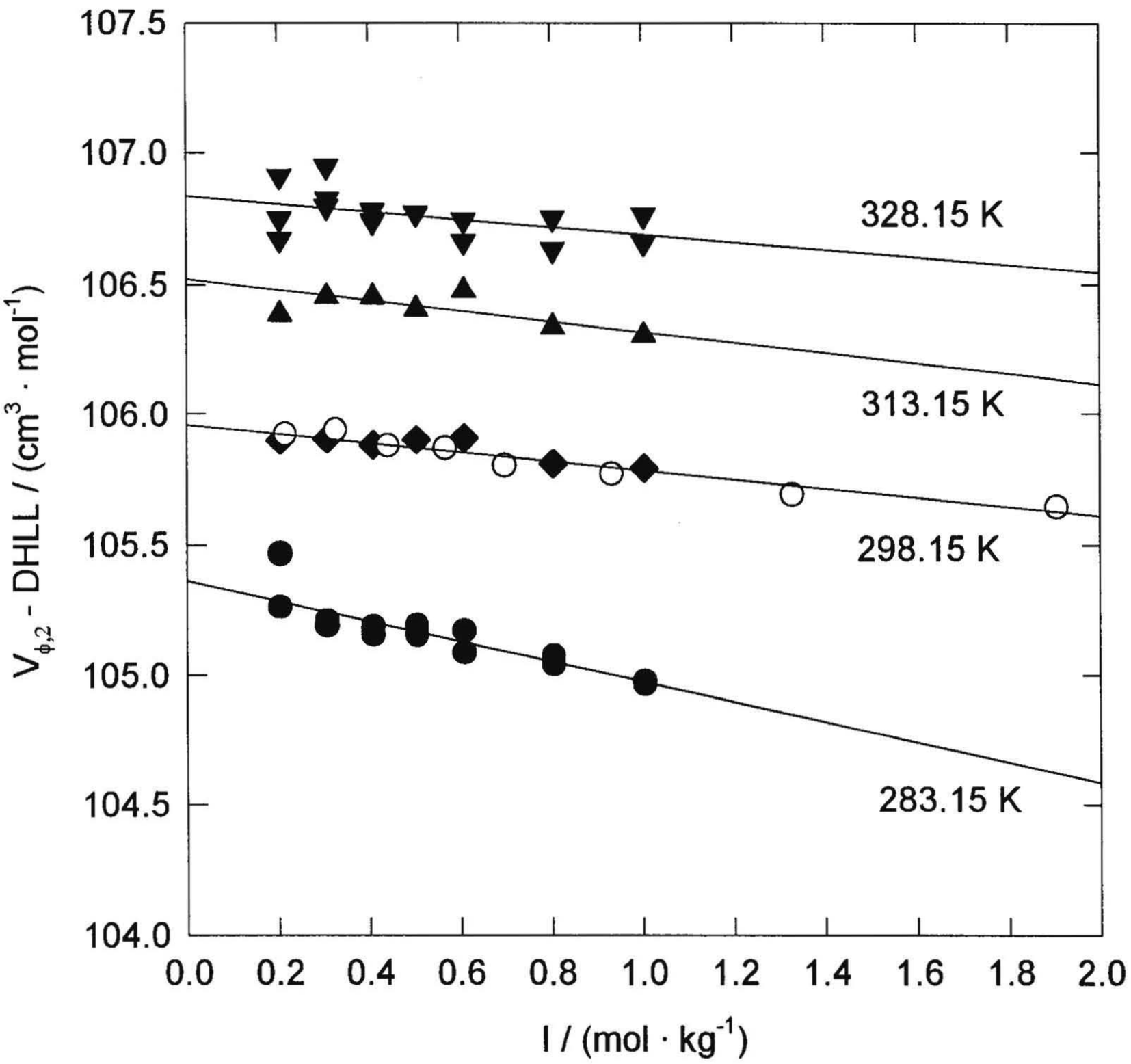

Figure 3.5 The apparent molar volumes $V_{\phi,2}$ of $AMPH^+Cl^-$ solutions at 0.1 MPa from 283.15 to 328.15 K plotted as a function of ionic strength after subtracting the Debye-Hückel limiting law term [Equation (3.16)]. Solid symbols, experimental results with $AMPH^+Cl^-$ [made from AMP(ACROS)]; ○, experimental results with $AMPH^+Cl^-$ (Fluka). Lines, isothermal least squares fits to Equation (3.14).

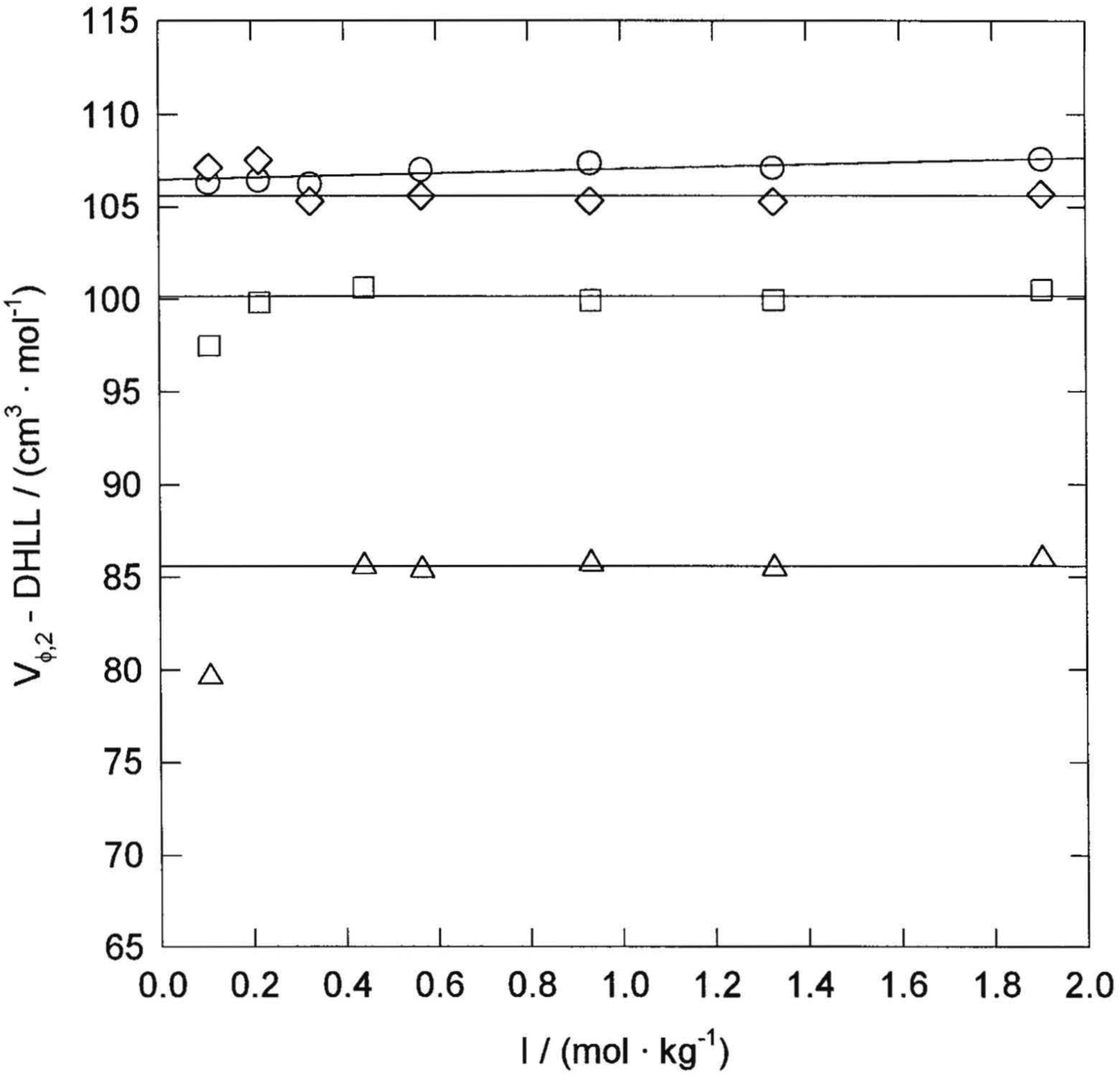

Figure 3.6 The apparent molar volumes $V_{\phi,2}$ of $AMPH^+Cl^-$ (Fluka) solutions at 20 MPa plotted as a function of ionic strength after subtracting the Debye-Hückel limiting law term. ○, 378.75 K, 20.36 MPa; ◇, 434.69 K, 20.31 MPa; □, 480.37 K, 19.62 MPa; △, 530.32 K, 19.61 MPa. Lines, isothermal least squares fits to Equation (3.14).

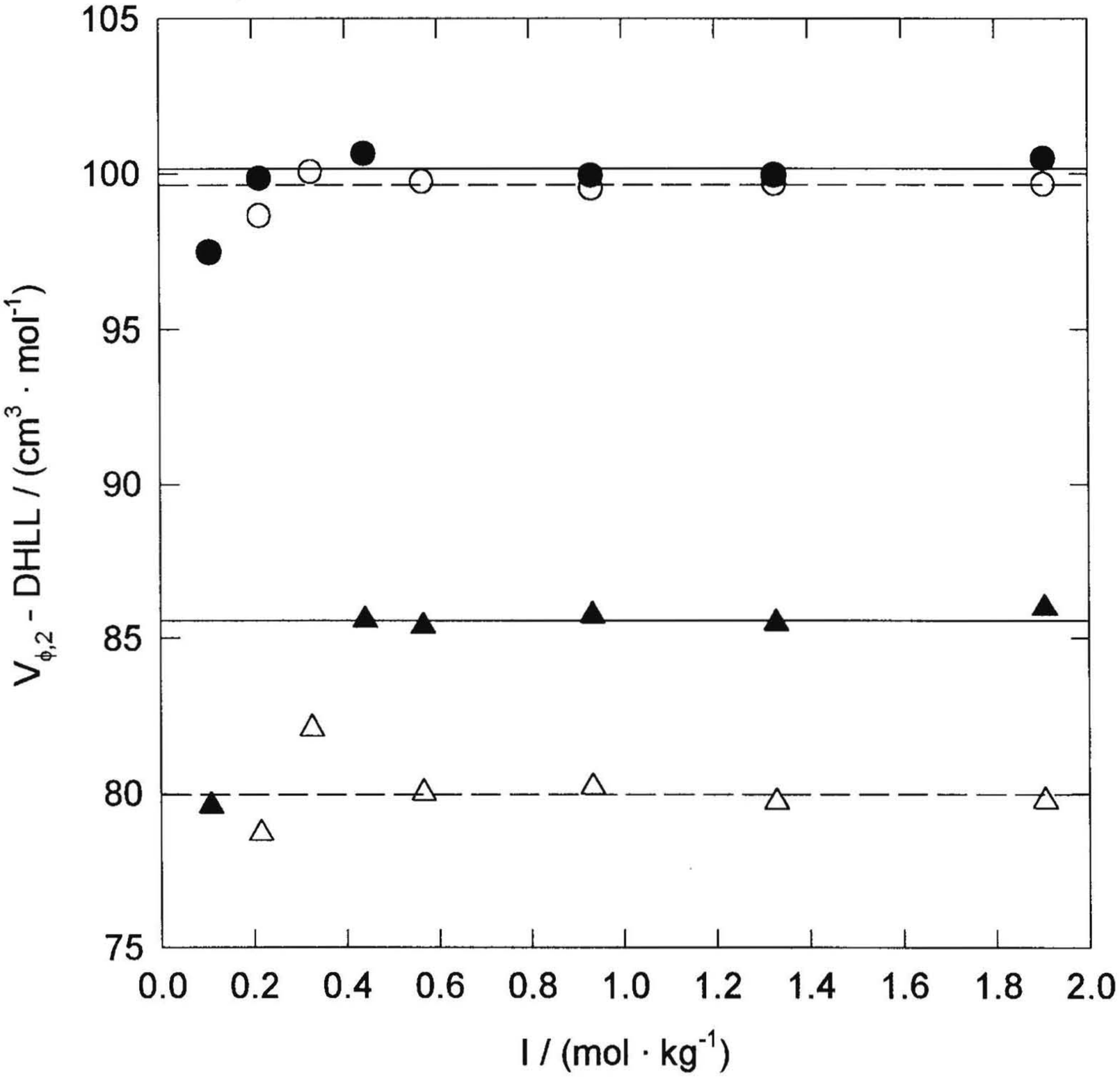

Figure 3.7 Pressure effects on the apparent molar volumes $V_{\phi,2}$ of $AMPH^+Cl^-$ (Fluka) solutions as a function of ionic strength after subtracting the Debye-Hückel limiting law term. ▲, 530.32 K, 19.61 MPa; △, 530.88 K, 10.33 MPa; ●, 480.37 K, 19.62 MPa; ○, 480.89 K, 10.21 MPa. Lines, isothermal least squares fits to Equation (3.14).

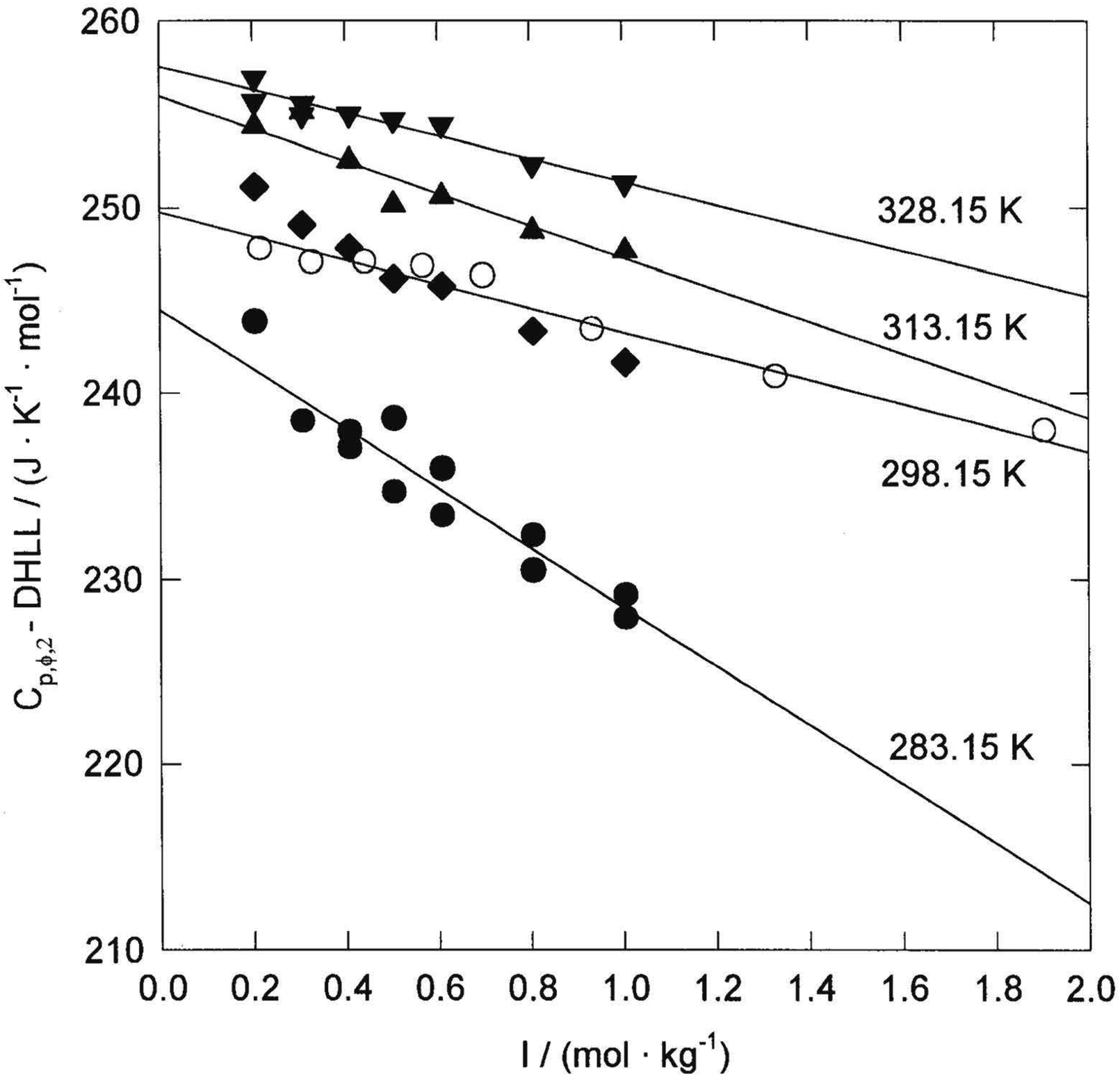

Figure 3.8 The apparent molar heat capacities $C_{p,\phi,2}$ of $AMPH^+Cl^-$ solutions at 0.1 MPa from 283.15 to 328.15 K plotted as a function of ionic strength after subtracting the Debye-Hückel limiting law term. Solid symbols, experimental results with $AMPH^+Cl^-$ [made from AMP(ACROS)]; ○, experimental results with $AMPH^+Cl^-$ (Fluka). Lines, isothermal least squares fits to Equation (3.15).

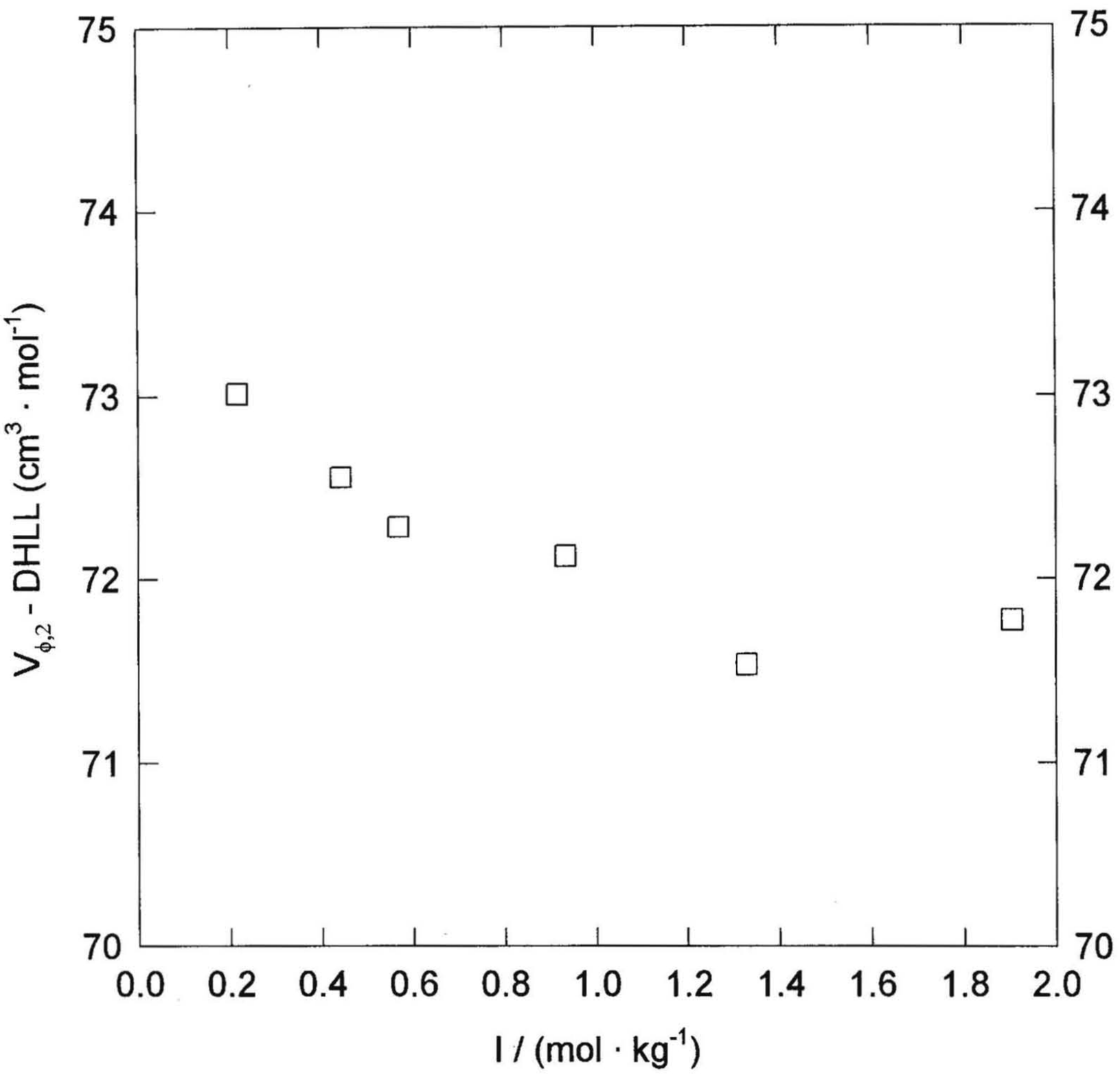

Figure 3.9 Decomposition effects: the apparent molar volumes $V_{\phi,2}$ of $AMPH^+Cl^-$ solutions at 555.59 K and 19.63 MPa plotted as a function of ionic strength after subtracting the Debye-Hückel limiting law term.

3.3.2 Standard Partial Molar Properties

Standard partial molar properties can be derived by the extrapolation of apparent molar properties to infinite dilution. For AMP solutions, linear functions were fitted to the experimental apparent molar properties at each temperature:

$$V_{\phi,2} = V_2^o + B_V m \tag{3.12}$$

$$C_{p,\phi,2} = C_{p,2}^o + B_C m \tag{3.13}$$

where $V_{\phi,2}$ and $C_{p,\phi,2}$ are the apparent molar volume and heat capacity, respectively; V_2^o and $C_{p,2}^o$ are the standard partial molar volume and heat capacity, respectively; B_V and B_C are fitted parameters; and m is the molalilty. The weighting factor used in these fits was set to equal to the molality of the AMP solutions, because Xiao and Tremaine (1997) pointed out that uncertainties are inversely proportional to the molality of the solutions.

The apparent molar properties for $AMPH^+Cl^-$ solutions can be related to standard partial molar properties by the extended Debye-Hückel equations (Guggenheim's form):

$$V_{\phi,2} = V^o + 1.5\frac{\omega A_V}{I}\left[I - 2I^{1/2} + 2\ln(1 + I^{1/2})\right] + C_V I \tag{3.14}$$

$$C_{p,\phi,2} = C^{o}_{p,2} + 1.5\frac{\omega A_C}{I}\left[I - 2I^{1/2} + 2\ln(1 + I^{1/2})\right] + C_C I \qquad (3.15)$$

Here I is the ionic strength: $I = 1/2 \cdot \sum m_i Z_i^2$; A_V and A_C are the Debye-Hückel limiting slopes which can be obtained from the compilation of Archer and Wang (1990); ω is the valence factor; and C_V and C_C are fitted parameters. In these isothermal fits, the weighting factors were assigned to be equal to the ionic strength, according to Xiao and Tremaine (1997).

The fitted parameters for $V_{\phi,2}$ and $C_{p,\phi,2}$ of AMP and $AMPH^+Cl^-$ solutions at low temperatures are given in Tables 3.3 and 3.4. The fitted parameters for $V_{\phi,2}$ of AMP and $AMPH^+Cl^-$ solutions at high temperatures are listed in Tables 3.5 and 3.6. It is noteworthy that, at high temperatures, the apparent molar volumes of aqueous AMP and $AMPH^+Cl^-$ are nearly independent of the molality or ionic strength. As shown in Tables 3.5 and 3.6, except for aqueous $AMPH^+Cl^-$ at T = 378.75 K, all other isothermal fits can be represented by a constant, equal to V_2^o or $C^o_{p,2}$.

Experimental apparent molar volumes and heat capacities are shown in Figures 3.1-3.8 along with the fitted lines. The Debye-Hückel limiting law term, DHLL, has the following form:

$$DHLL = 1.5\frac{\omega A_V}{I}\left[I - 2I^{1/2} + 2\ln(1 + I^{1/2})\right] \qquad (3.16)$$

Table 3.3 Parameters for $V_{\phi,2}$ of AMP and $AMPH^+Cl^-$ solutions at low temperatures from isothermal fits of Equations (3.12) and (3.14), respectively.

Parameter	T = 283.15 K	T = 298.15 K	T = 313.15 K	T = 328.15 K
		AMP		
V_2^o / ($cm^3 \cdot mol^{-1}$)	90.83 ± 0.09	91.64 ± 0.03	92.45 ± 0.03	93.41 ± 0.08
B_V / ($cm^3 \cdot kg \cdot mol^{-2}$)	-0.8315 ± 0.0797	-0.7639 ± 0.0280	-0.5083 ± 0.0279	-0.3799 ± 0.0639
s[a]	0.10	0.07	0.03	0.11
		$AMPH^+Cl^-$		
V_2^o / ($cm^3 \cdot mol^{-1}$)	105.37 ± 0.03	105.96 ± 0.01	106.52 ± 0.05	106.83 ± 0.04
C_V / ($cm^3 \cdot kg \cdot mol^{-2}$)	-0.3895 ± 0.0447	-0.1752 ± 0.0133	-0.2031 ± 0.0703	-0.1446 ± 0.0626
s[a]	0.03	0.02	0.04	0.05

[a] Standard deviation of the regression.

Table 3.4 Parameters for $C_{p,\phi,2}$ of AMP and $AMPH^+Cl^-$ solutions from isothermal fits of Equations (3.13) and (3.15), respectively.

Parameter	T = 283.15 K	T = 298.15 K	T = 313.15 K	T = 328.15 K
		AMP		
$C^o_{p,2}$ / ($J \cdot K^{-1} \cdot mol^{-1}$)	359.7 ± 0.5	364.3 ± 0.3	369.8 ± 0.2	375.0 ± 0.3
B_C / ($J \cdot kg \cdot K^{-1} \cdot mol^{-2}$)	-5.825 ± 0.439	-2.107 ± 0.242	0	-0.568 ± 0.261
s[a]	0.58	0.57	0.50	0.43
		$AMPH^+Cl^-$		
$C^o_{p,2}$ / ($J \cdot K^{-1} \cdot mol^{-1}$)	244.5 ± 1.2	249.8 ± 0.5	256.0 ± 1.0	257.6 ± 0.4
C_C / ($J \cdot kg \cdot K^{-1} \cdot mol^{-2}$)	-15.991 ± 1.569	-6.480 ± 0.461	-8.685 ± 1.336	-6.197 ± 0.531
s[a]	1.02	0.79	0.68	0.31

[a] Standard deviation of the regression.

Table 3.5 Parameters for $V_{\phi,2}$ of AMP solutions at high temperatures from isothermal fits of Equation (3.12).

Parameter	T = 378.79 K p = 20.36 MPa	T = 429.97 K p = 19.47 MPa	T = 480.37 K p = 19.62 MPa
V_2^o / ($cm^3 \cdot mol^{-1}$)	97.20 ± 0.06	103.88 ± 0.17	111.52 ± 0.09
B_V / ($cm^3 \cdot kg \cdot mol^{-2}$)	0	0	0
s[a]	0.13	0.30	0.18

Parameter	T = 530.32 K p = 19.61 MPa	T = 555.59K p = 19.63 MPa
V_2^o / ($cm^3 \cdot mol^{-1}$)	122.48 ± 0.04	131.45 ± 0.08
B_V / ($cm^3 \cdot kg \cdot mol^{-2}$)	0	0
s[a]	0.08	0.18

Parameter	T = 480.89 K p = 10.21 MPa	T = 530.88 K p = 10.33 MPa
V_2^o / ($cm^3 \cdot mol^{-1}$)	112.82 ± 0.10	126.28 ± 0.15
B_V / ($cm^3 \cdot kg \cdot mol^{-2}$)	0	0
s[a]	0.24	0.31

[a] Standard deviation of the regression.

Table 3.6 Parameters for $V_{\phi,2}$ of $AMPH^+Cl^-$ solutions at high temperatures from isothermal fits of Equation (3.14).

Parameter	T = 378.75 K p = 20.36 MPa	T = 434.69 K p = 20.31 MPa	T = 480.37 K p = 19.62 MPa
V_2^o / ($cm^3 \cdot mol^{-1}$)	106.46 ± 0.22	105.58 ± 0.20	100.15 ± 0.22
C_V / ($cm^3 \cdot kg \cdot mol^{-2}$)	0.5901 ± 0.1610	0	0
s[a]	0.20	0.47	0.49
Parameter	T = 530.32 K p = 19.61 MPa	T = 480.89 K p = 10.21 MPa	T = 530.88 K p = 10.33 MPa
V_2^o / ($cm^3 \cdot mol^{-1}$)	85.58 ± 0.40	99.62 ± 0.10	79.96 ± 0.28
C_V / ($cm^3 \cdot kg \cdot mol^{-2}$)	0	0	0
s[a]	0.92	0.24	0.63

[a] Standard deviation of the regression.

Therefore, in Equations (3.14) and (3.15), ($V_{\phi,2}$ - DHLL) and ($C_{p,\phi,2}$ - DHLL) are linear functions of ionic strength (Figures 3.5- 3.8), and the extrapolation to infinite dilution leads to the corresponding standard partial molar properties.

3.3.3 Uncertainty Estimation

The heat capacities at 283.15 K ≤ T ≤ 328.15 K were measured by a Sodev Picker flow microcalorimeter. This Picker flow microcalorimeter has the sensitivity of 5×10^{-5} $J\cdot K^{-1}\cdot cm^{-3}$, and a precision in relative specific heat capacity of ± 0.3 % up to limit of sensitivity, as indicated by the manufacturer. The statistical uncertainty of the relative specific heat capacity is 0.5 per cent (Picker *et al.*, 1971; Desnoyers *et al.*, 1976). The major source of error arises from heat loss. In this study, the heat loss correction factor *ff* was introduced to the calculations (Section 2.1), which can be determined by a calibration with a standard NaCl solution and water. The systematic error is usually ignored because it is smaller than the overall uncertainties (Picker *et al.*, 1971).

The statistical uncertainty associated with the density measurements by our Sodev and high-temperature flow densimeters came from the random errors related to the calibration constant determination, the periods measurements for water and the solutions, and so on. Xiao and Tremaine (1997) suggested that the statistical uncertainty of density $\delta\rho$ could be estimated by:

$$\delta\rho = \{(\rho - \rho_1^*)^2(\delta K / K)^2 + 8[K\tau(\delta\tau)]^2 + [\beta_1^*\rho_1^*(\delta p)]^2 + [\alpha_1^*\rho_1^*(\delta T)]^2\}^{1/2} \quad (3.17)$$

where δK and δτ are the standard deviations of calibration constant and vibrational period, respectively; and β_1^* and α_1^* are the compressibility coefficient of water and thermal expansion coefficient of water, respectively (Section 1.3.4).

Because the density measured is relative, δT and δp are only related to the *differences* of temperature and pressure between the measurement on solution and that on water. Under the conditions in this study, it was estimated that $\delta T < 0.02$ K, $\delta p < 0.01$ MPa, and $\delta K/K \approx 0.002$ (Xiao and Tremaine, 1997). The error limits of densities δρ were determined (Xiao and Tremaine, 1997) to be 0.02 ~ 0.17 kg·m^{-3} for 0.1 molal solutions and 0.12 ~ 0.28 kg·m^{-3} for 1.0 molal solutions. Subsequently, the statistical errors of apparent molar volumes $\delta V_{\phi,2}$ are 0.40 ~ 1.70 cm^3·mol^{-1} for 0.1 molal solutions and 0.18 ~ 0.25 cm^3·mol^{-1} for 1.0 molal solutions. These data also implied that the errors are inversely proportional to the molality of solution. Therefore, the weighting factors in the fits were set to be proportional to the molalities (or ionic strength for electrolytes) in this study.

The systematic error associated with the density measurements is mainly from the uncertainties in the calibration constant and the non-linearity of the densimeter, which was suggested to be a minor contribution to the uncertainties (Xiao and Tremaine, 1997).

Functions were fitted to the apparent molar properties at each temperature by

weighted least squares for extrapolation to obtain standard molar properties; and three models for the temperature dependence were fitted to these standard partial molar properties. In conclusion, uncertainties in $C^{o}_{p,2}$ and V^{o}_{2} were calculated from the standard deviation from isothermal fits (95 % confidence limit), and the overall uncertainty in the experimental measurements of $C_{p,\phi,2}$ and $V_{\phi,2}$, respectively.

3.3.4 Comparison with Literature Data

Xu *et al.* (1991) measured the densities of aqueous AMP solutions over the temperatures from 293 K ≤ T ≤ 364 K. In their study, the lowest concentration, also the only concentration that overlaps with this study was 1.015 $mol \cdot kg^{-1}$. At 328.65 K, their study showed the density of 0.9830 $g \cdot cm^{-3}$ for their 1.015 $mol \cdot kg^{-1}$ AMP solution. In this study, at 328.15 K the density of 0.996412 $mol \cdot kg^{-1}$ AMP solution was measured twice giving 0.9839 $g \cdot cm^{-3}$ and 0.9835 $g \cdot cm^{-3}$.

Roux *et al.* (1980) investigated the apparent molar volumes and heat capacities for (AMP + H_2O) systems at 298 K, which have been plotted in Figures 3.1 and 3.4 along with data from this study. Their results are in excellent agreement with results from this study using the AMP materials from ACROS and Fluka.

No density or heat capacity data at high temperatures were found in the literature search for comparison.

3.4 "Equations of State" for Aqueous AMP and $AMPH^+Cl^-$

3.4.1 The Revised HKF Model

The standard partial molar properties V_2^o and $C_{p,2}^o$ of both AMP and $AMPH^+Cl^-$ solutions were represented by the revised Helgeson-Kirkham-Flowers (HKF) model (Section 1.3.3). After optimization, three parameters were selected in this work for the fits of standard partial molar volume, V_2^o:

$$V_2^o = v_1 + v_3 / (T - \Theta) - \omega_e Q \tag{3.18}$$

where V_2^o is the standard partial molar volume; $\Theta = 228$ K was selected based on the anomalous behavior of supercooled water (Angell, 1983); v_1, v_3, and ω_e are fitted parameters (ω_e denotes Born coefficient); and Q is the Born function defined by:

$$Q = \left(\frac{1}{\varepsilon_r}\right)\left(\frac{\partial \ln \varepsilon_r}{\partial p}\right)_T \tag{3.19}$$

where ε_r is the dielectric constant of water.

The standard partial molar heat capacity $C_{p,2}^o$ has the following expression:

$$C_{p,2}^o = c_1 + c_2\left(\frac{1}{T-\Theta}\right)^2 - 2T\left(\frac{1}{T-\Theta}\right)^3 \cdot v_3\left(p - p_r\right) + \omega_e TX \tag{3.20}$$

where c_1 and c_2 are fitted parameters; Θ is again a constant with the value of 228K; p_r is the reference pressure (0.1 MPa); v_3 and ω_e were determined by the V_2^o fits in Equation (3.18); and X is defined by:

$$X = \varepsilon_r{}^{-1}\left[\left(\frac{\partial^2 \ln \varepsilon_r}{\partial T^2}\right)_p - \left(\frac{\partial \ln \varepsilon_r}{\partial T}\right)_p^2\right] \tag{3.21}$$

The parameters in the revised HKF model for fitting V_2^o and $C_{p,2}^o$ of aqueous AMP and $AMPH^+Cl^-$ are listed in Table 3.7.

Table 3.7 Revised HKF model parameters in the fits of V_2^o and $C_{p,2}^o$ of aqueous AMP and $AMPH^+Cl^-$ in Equations (3.18) and (3.20).

	V_2^o / ($cm^3 \cdot mol^{-1}$)	
Parameter	AMP	$AMPH^+Cl^-$
v_1 / ($cm^3 \cdot mol^{-1}$)	100.04 ± 2.22	114.75 ± 1.01
v_3 / ($K \cdot cm^3 \cdot mol^{-1}$)	-718.02 ± 175.12	-450.62 ± 79.32
$\omega_e \cdot 10^{-5}$ / ($MPa \cdot cm^3 \cdot mol^{-1}$)	-3.3850 ± 0.3042	3.6984 ± 0.1381
s[a]	1.93	0.87
	$C_{p,2}^o$ / ($J \cdot K^{-1} \cdot mol^{-1}$)	
Parameter	AMP	$AMPH^+Cl^-$
c_1 / ($J \cdot K^{-1} \cdot mol^{-1}$)	340.62 ± 1.60	305.69 ± 2.50
$c_2 \cdot 10^{-4}$ / ($J \cdot K \cdot mol^{-1}$)	-1.3897 ± 0.7561	-11.307 ± 1.185
s[a]	1.32	2.06

[a] Standard deviation of the regression.

3.4.2 The "Density" Model

The "density" model of Mesmer *et al.* (1988) has been used to represent and predict solute properties up to high temperatures (Section 1.3.4).

The following equation for log K was used in this study,

$$\log K = (vT + a + b / T + c / T^2) + e \cdot \log \rho_1^* - (a_0 + b_0 / T^2) \cdot p / (2.303RT) \qquad (3.22)$$

This yields the following expressions for V_2^o and $C_{p,2}^o$,

$$V_2^o = a_0 + b_0 / T^2 - eRT\beta_1^* \qquad (3.23)$$

$$C_{p,2}^o = 2.303R(2vT + 2c / T^2) - 2eRT\alpha_1^* - eRT^2(\partial\alpha_1^* / \partial T)_p - 6pb_0 / T^3 \qquad (3.24)$$

where $\beta_1^* = (1/\rho_1^*)(\partial\rho_1^*/\partial p)_T$ is the compressibility coefficient of water; $\alpha_1^* = -(1/\rho_1^*)(\partial\rho_1^*/\partial T)_p$ is the thermal expansion coefficient of water; T and p are temperature in K and pressure in MPa, respectively; and a_0, b_0, e, v, a, b, and c are adjustable parameters. After Equation (3.23) was fitted to the V_2^o data, the values of the parameters b_0 and e were taken and used as constants for the $C_{p,2}^o$ fits in Equation (3.24).

The parameters in the "density" model for the fits of V_2^o and $C_{p,2}^o$ for aqueous AMP and $AMPH^+Cl^-$ are listed in Table 3.8.

Table 3.8 "Density" model parameters for the fits of V_2^o and $C_{p,2}^o$ of aqueous AMP and $AMPH^+Cl^-$ in Equations (3.23) and (3.24).

	V_2^o / ($cm^3 \cdot mol^{-1}$)	
Parameter	AMP	$AMPH^+Cl^-$
a_0 / ($cm^3 \cdot mol^{-1}$)	103.45 ± 2.20	123.70 ± 1.79
$b_0 \cdot 10^{-5}$ / ($K^2 \cdot cm^3 \cdot mol^{-1}$)	-14.937 ± 2.041	-9.8630 ± 1.5708
e	-4.1283 ± 0.2733	6.0071 ± 0.2645
s[a]	1.33	0.93
	$C_{p,2}^o$ / ($J \cdot K^{-1} \cdot mol^{-1}$)	
Parameter	AMP	$AMPH^+Cl^-$
v / (K^{-1})	0.0226 ± 0.0006	0.0190 ± 0.0004
$c \cdot 10^{-5}$ / (K^2)	1.6246 ± 0.1784	1.9779 ± 0.1050
s[a]	2.43	1.43

[a] Standard deviation of the regression.

3.4.3 A Hybrid Model

The "hybrid" equations of state were discussed in Section 1.3.5. In this study, the following equations were used:

$$V^o = v_1 + v_2 / T^{1/2} + v_3 / (T - \Theta) - qR\beta_1^* \qquad (3.25)$$

$$C_p^o = c_1 + c_2 / (T - \Theta)^2 - qRT(\partial\alpha_1^* / \partial T)_p \qquad (3.26)$$

The terms α_1^* and β_1^* again denote the thermal expansion coefficient and compressibility coefficient of water, respectively; Θ = 228 K; and v_i, c_i, and q are fitted parameters. After Equation (3.25) was fitted to V_2^o data, the value of q was taken and used as a constant for $C_{p,2}^o$ fits in Equation (3.26).

The parameters (hybrid model) for the fits of V_2^o and $C_{p,2}^o$ of aqueous AMP and $AMPH^+Cl^-$ are listed in Table 3.9.

Table 3.9 Hybrid model parameters for the fits of V_2^o and $C_{p,2}^o$ of aqueous AMP and $AMPH^+Cl^-$ in Equations (3.25) and (3.26).

	V_2^o / ($cm^3 \cdot mol^{-1}$)	
Parameter	AMP	$AMPH^+Cl^-$
v_1 / ($cm^3 \cdot mol^{-1}$)	157.75 ± 7.81	174.08 ± 13.53
$v_2 \cdot 10^{-3}$ / ($K^{1/2} \cdot cm^3 \cdot mol^{-1}$)	-1.3754 ± 0.1625	-1.0663 ± 0.2820
v_3 / ($K \cdot cm^3 \cdot mol^{-1}$)	354.06 ± 144.42	603.47 ± 251.65
$q \cdot 10^{-3}$ / (K)	-2.1785 ± 0.1253	4.0220 ± 0.2173
s[a]	0.45	0.79
	$C_{p,2}^o$ / ($J \cdot K^{-1} \cdot mol^{-1}$)	
Parameter	AMP	$AMPH^+Cl^-$
c_1 / ($J \cdot K^{-1} \cdot mol^{-1}$)	354.35 ± 2.27	309.58 ± 2.21
$c_2 \cdot 10^{-5}$ / ($J \cdot K \cdot mol^{-1}$)	-1.9681 ± 0.1076	1.8726 ± 0.1047
s[a]	1.87	1.82

[a] Standard deviation of the regression.

3.5 Discussion on Standard Partial Molar Properties at Elevated Temperatures and Pressures

Standard partial molar properties of aqueous AMP and $AMPH^+Cl^-$ as functions of temperature are shown in Figures 3.10-3.13, along with the fits based on the three models described above. At temperatures below 373 K, the pressure effects on the standard partial molar properties are very small and within the uncertainties in this study, so the low-temperature V_2^o data (< 373 K), which were determined at 0.1 MPa, were used for the fits at 20 MPa. This is the same approximation adopted by Hnědkovský *et al.* (1995). All three models predict that at elevated temperatures, standard partial molar properties will approach positive infinity for the neutral amine, AMP, and negative infinity for the amine salt, $AMPH^+Cl^-$.

Because of the divergence of the compressibility of water near the critical point of water, standard partial molar properties including volume and heat capacity must also diverge, and the direction of the divergence depends on the nature of solute-water interactions. Typically, in the neighborhood of the critical point, electrolytes will approach negative infinity, and nonelectrolytes will go to positive infinity (Hawrylak, 1999; Tremaine *et al.*, 1997; Shvedov and Tremaine, 1997). One such example is illustrated in Figure 1.3 (Hawrylak, 1999). Some polar nonelectrolytes exhibit anomalous properties. For example, the V_2^o and $C_{p,2}^o$ of boric acid both go to *negative* infinity near the solvent critical point (Hnědkovský *et al.*, 1995).

At the vicinity of the critical point, ions and very hydrophilic molecules attract

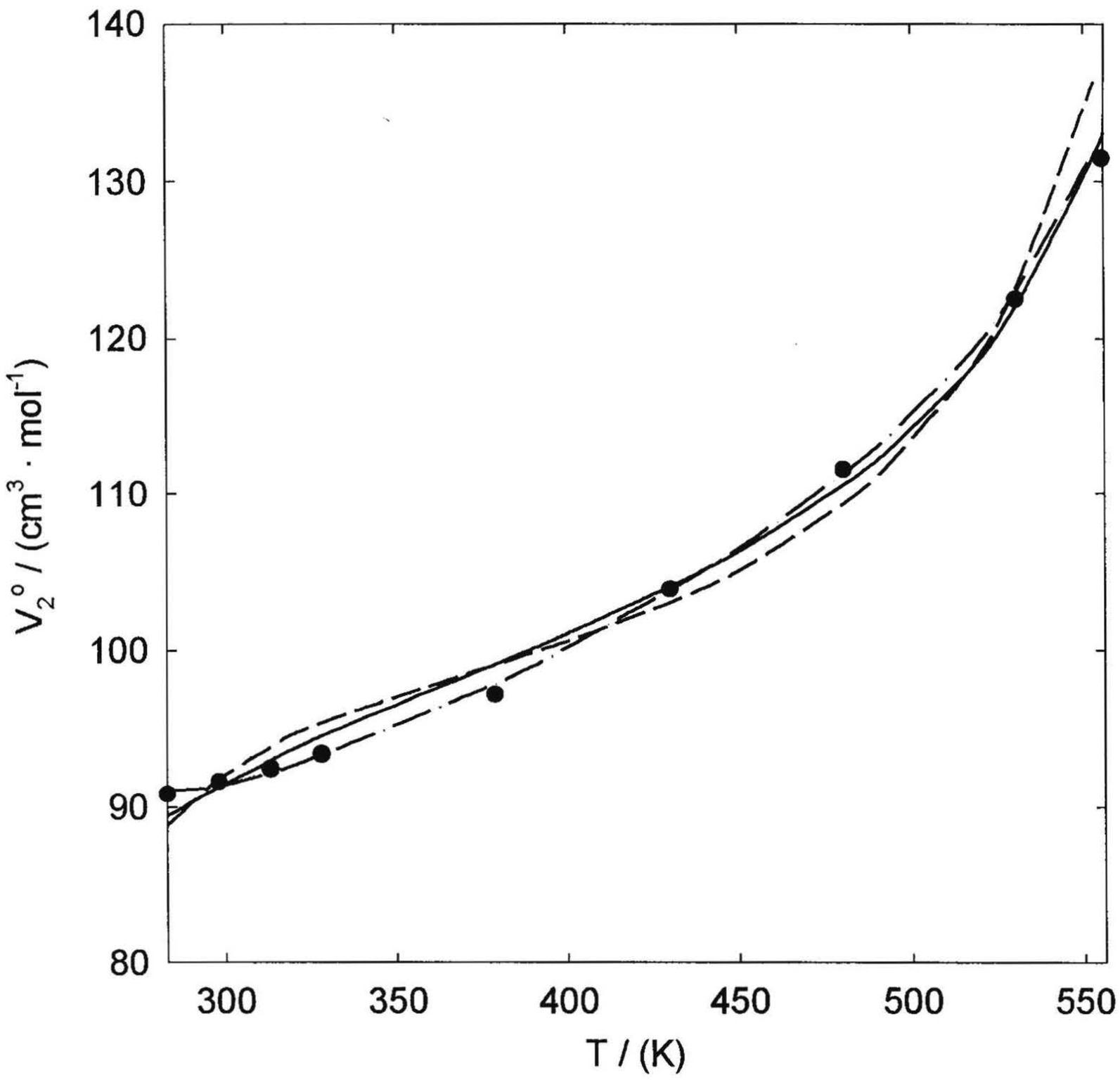

Figure 3.10 Standard partial molar volumes V_2^o of AMP at 20 MPa plotted as a function of temperature. Symbols are results from isothermal least squares fits to Equation (3.12). Lines are values calculated from the fits on three models: ——— , "density" model; – – –, revised HKF model; –·–·–, hybrid model.

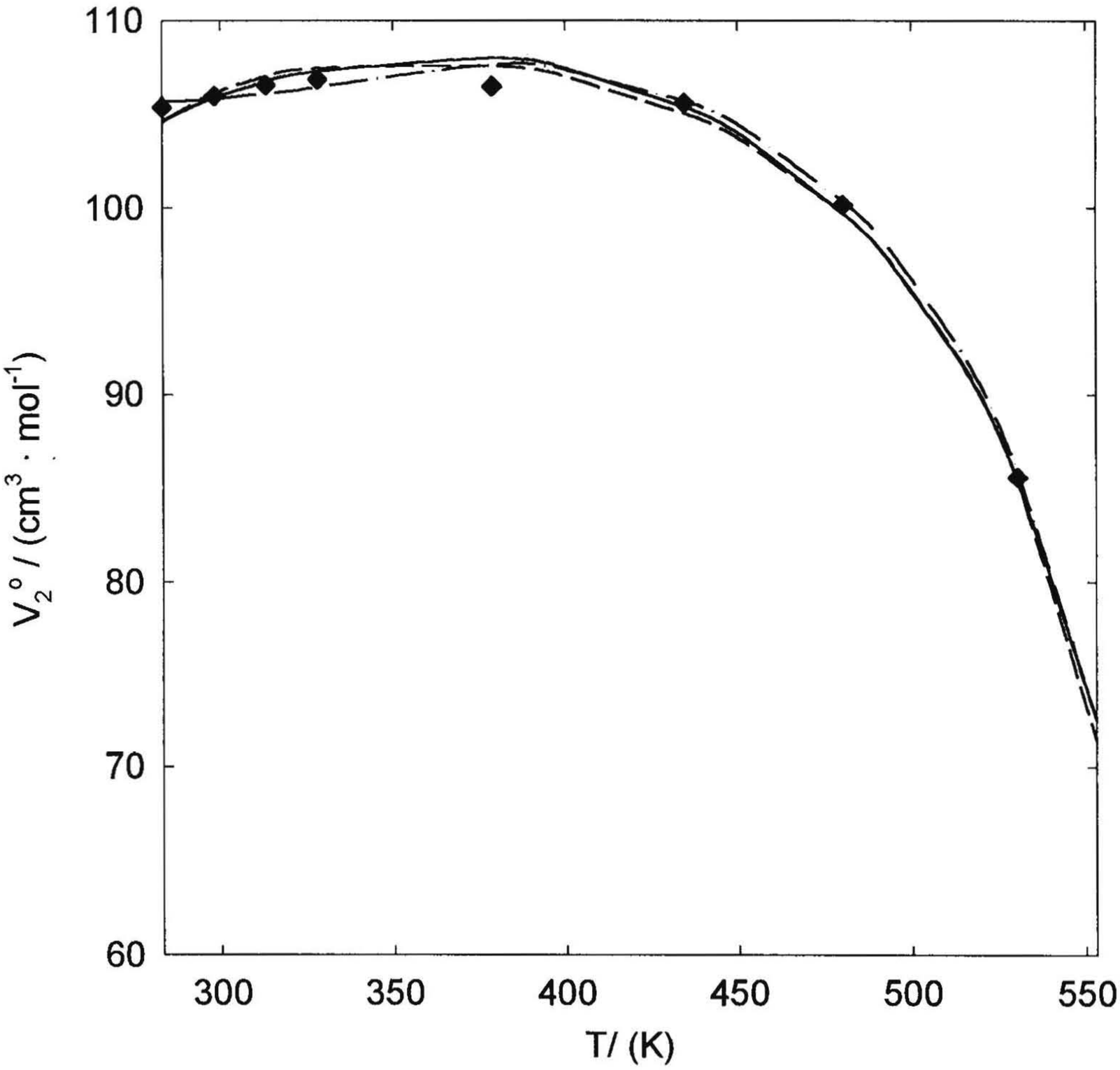

Figure 3.11 Standard partial molar volumes V_2^o of $AMPH^+Cl^-$ at 20 MPa plotted as a function of temperature. Symbols are results from isothermal least squares fits to Equation (3.14). Lines are values calculated from the fits on three models: ——— , "density" model; – – –, revised HKF model; –·–·–, hybrid model.

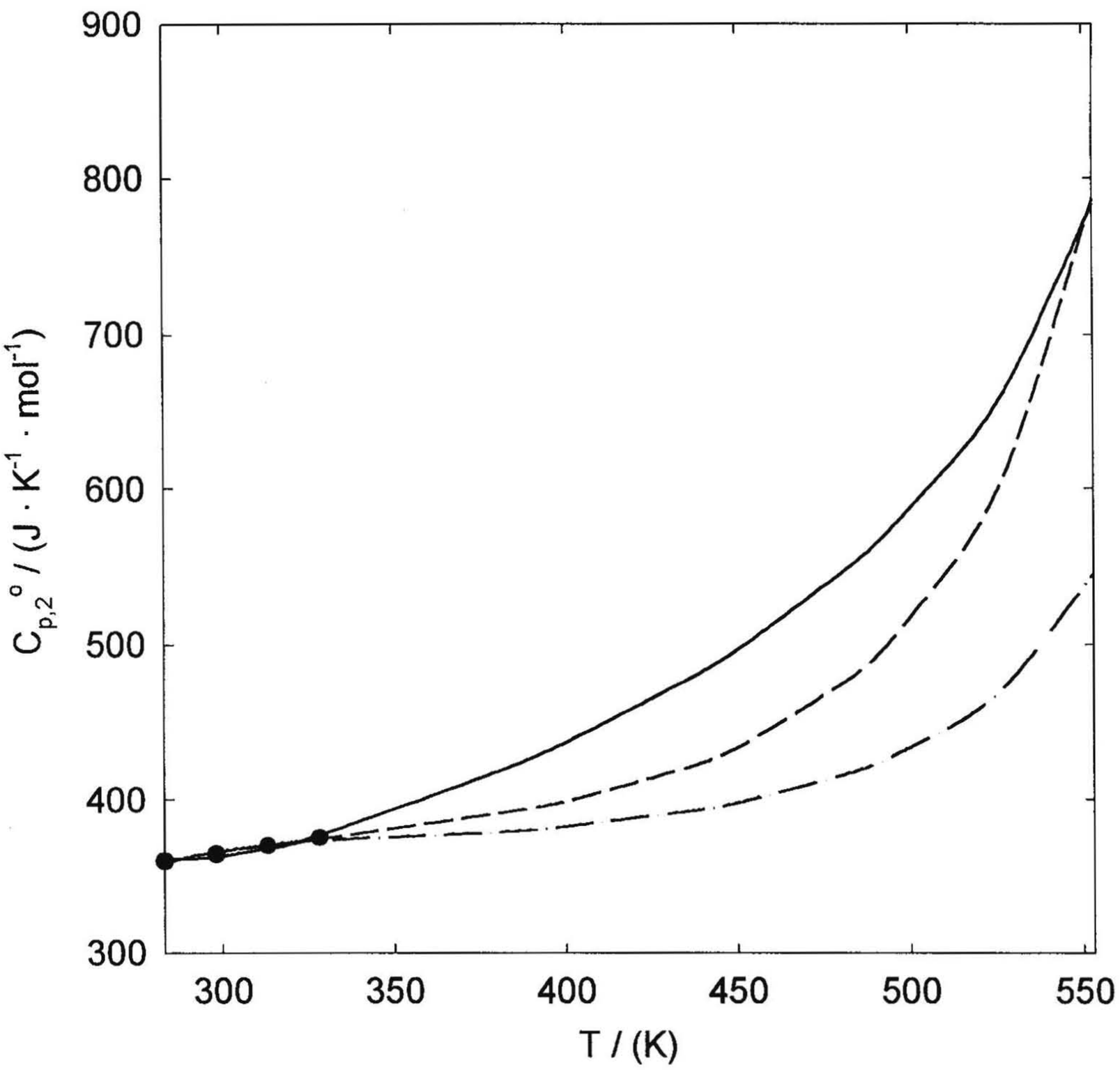

Figure 3.12 Standard partial molar heat capacities $C_{p,2}^{o}$ of AMP at 20 MPa plotted as a function of temperature. Symbols are results from isothermal least squares fits to Equation (3.13). Lines are values calculated from the fits on three models: ——— , "density" model; – – –, revised HKF model; –·–·–, hybrid model.

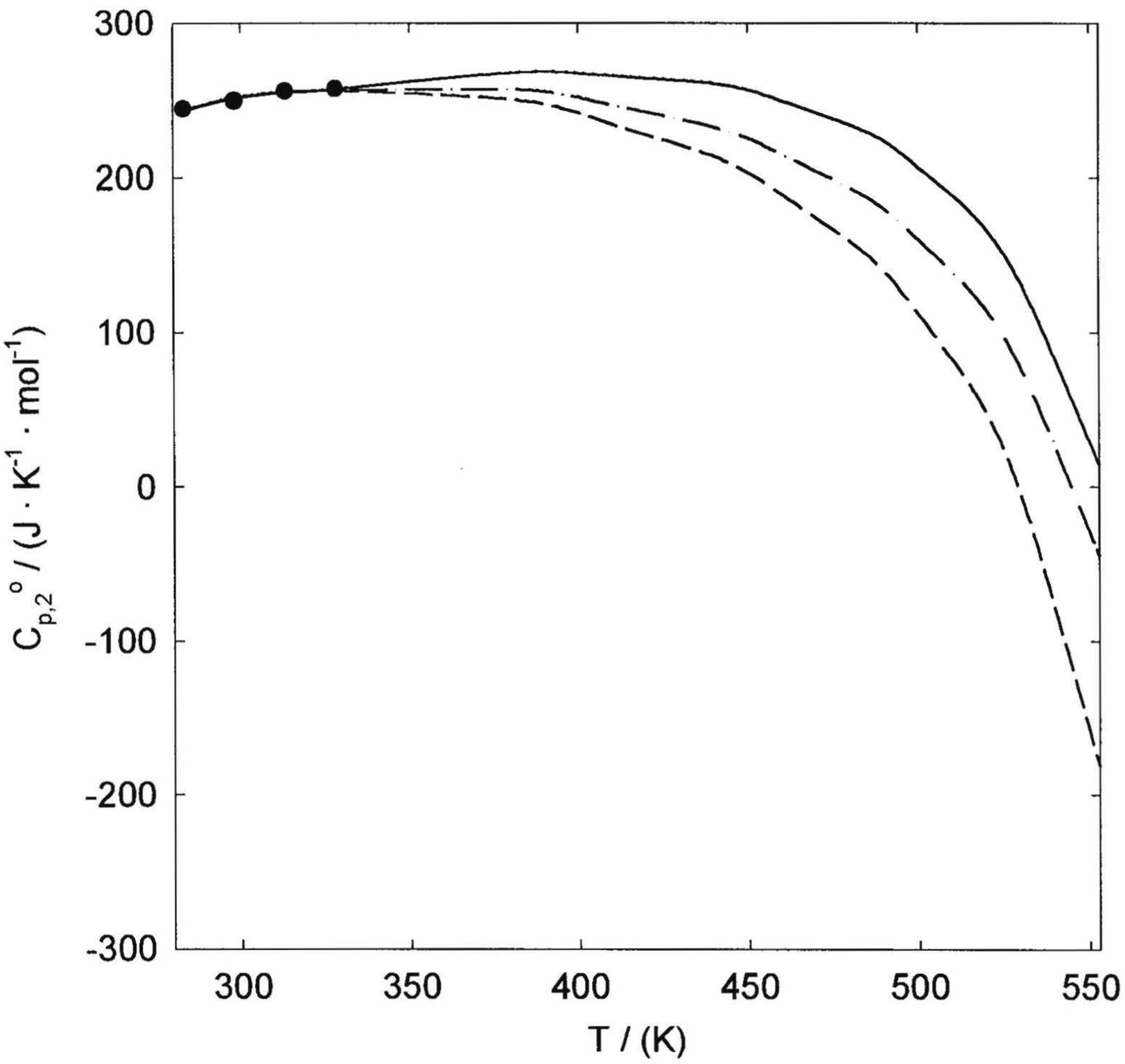

Figure 3.13 Standard partial molar heat capacities $C_{p,2}^{o}$ of $AMPH^{+}Cl^{-}$ at 20 MPa plotted as a function of temperature. Symbols are results from isothermal least squares fits to Equation (3.15). Lines are values calculated from the fits on three models: ——, "density" model; – – –, revised HKF model; –·–·–, hybrid model.

the solvent molecules, resulting a negative divergence of V_2^o. For nonpolar neutral species, the repulsive force between the hydrophobic solute and water leads to positive divergences of the standard partial molar volumes. In the cases of polar neutral species, such as boric acid, the attractive interactions between the polar and highly hydrogen-bonding solute and water are strong enough to result in net attraction, so that both V_2^o and $C_{p,2}^o$ approach -∞ as the temperature is raised to the critical temperature (Hnědkovský *et al.*, 1995).

The effects of pressure on the standard partial molar volumes were investigated, and are shown in Tables 3.5 and 3.6 for aqueous AMP and $AMPH^+Cl^-$, respectively. A clearer illustration lies in Figures 3.3 and 3.7 for aqueous AMP and $AMPH^+Cl^-$, respectively.

Figure 3.3 indicates an increasing apparent molar volume of aqueous AMP as pressure decreases. This is not surprising, since at lower pressure the compressibility of water is higher, and the neutral solute has a stronger ability to expand the solvent, resulting a higher standard partial molar volume. Figure 3.7 shows a decreasing apparent molar volume of aqueous $AMPH^+Cl^-$ as the pressure decreases. Again this arises because the compressibility of water is higher at lower pressure, so that the attractive forces between the solute and solvent molecules will be enhanced.

The standard partial molar properties ($C_{p,2}^o$ and V_2^o) of aqueous $AMPH^+Cl^-$ at 20 MPa exhibit a maximum near the temperature of 373 K, and then decrease toward -∞ as the temperature increases.

3.6 Discussion on Equations of State

3.6.1 The Revised HKF Model

The revised HKF model has been used for the fits and predictions of the properties of AMP and $AMPH^+Cl^-$. This model is viewed commonly to have strong extrapolating power for aqueous ions and electrolytes. The contributions to standard partial molar properties Y^o have been discussed in Section 1.3.3. The tables of fitted parameters (Tables 3.7-3.9) show that for the properties of aqueous $AMPH^+Cl^-$, the revised HKF model has almost the same performance in V_2^o fits as the other two models, but the largest standard deviation in the $C_{p,2}^o$ fits among the three models (however, one more parameter was used in the hybrid model).

As discussed in Section 1.3.3, the application of this model on AMP has no theoretical basis. The fitted results of V_2^o agree well with the V_2^o from isothermal fits of experimental $V_{\phi,2}$, as well as other models (while the fit with the revised HKF model has the largest standard deviation). However, there is a slightly inverted U-curve at low temperatures in the V_2^o fits, which is not presented in the V_2^o data from isothermal fits of experimental $V_{\phi,2}$. On the other hand, the revised HKF model gives the best fit and prediction for $C_{p,2}^o$ (the lowest standard deviation and fewest parameters). In Figure 3.12, the predicted heat capacity function from this model appears between values from other two models.

3.6.2 The "Density" Model

The "density" model has the advantage of simpler equations of state than models based on the Born Equation. Helgeson and Kirkham (1976) pointed out that the revised HKF and "density" models were similar in representing and predicting properties at high temperatures, because the Born function Q, as defined in Equation (1.51), was related to the "β_1^*T" term in the "density" model by a linear function. Moreover, Sedlbauer *et al.* (2000) considered that models based on the solvent density and compressibility presented the partial molar volumes better than those based on the solvent dielectric constant (for example, the revised HKF model).

The "density" model has been widely used for fitting and extrapolating of the thermodynamic properties of both neutral and ionic species (Mesmer *et al.*, 1998). In this study, the "density" model had the best performance in fitting $C_{p,2}^o$ of aqueous $AMPH^+Cl^-$ (the lowest standard deviation and fewest parameters), but displayed the largest standard deviation when fitted to the data for aqueous AMP among the three models (although only five parameters were used in this model). Of the two models only involving five parameters, the "density" model fit to the V_2^o data for aqueous $AMPH^+Cl^-$ was a little worse, but that for aqueous AMP was better.

3.6.3 The Hybrid Model

The hybrid model combines the low temperature part of the revised HKF model, which reflects the properties of water at supercooled condition, and the high

temperature term from "density" model, which is universal for both neutral and ionic species.

This model requires six parameters for fitting V_2^o and $C_{p,2}^o$ for both aqueous AMP and $AMPH^+Cl^-$ (in the other two models five parameters were the optimum). This additional one parameter was used in the low temperature term. The standard deviations in the fits of V_2^o were the lowest among the three models, and those in the extrapolations of $C_{p,2}^o$ were in the middle. A limitation of this model is that the equations of state are complicated.

3.7 AMP Ionization

The standard partial molar properties of AMP and $AMPH^+Cl^-$ are reported in Section 3.3.2. Provided properties of aqueous HCl are known, the standard partial molar properties of $AMPH^+$ on the conventional scale can be obtained since $V^o(H^+, aq) \equiv 0$ and $C_p^o(H^+, aq) \equiv 0$. These results are shown in Tables 3.10-3.11.

The standard partial molar volume change ($\Delta_r V^o$) and standard partial molar heat capacity change ($\Delta_r C_p^o$) of the AMP ionization were calculated. Here the ionization was considered as an "isocoulombic" reaction to leave out the strong effect of Cl^- (Tremaine *et al.*, 1997):

$$AMP(aq) + H^+(aq) \rightleftharpoons AMPH^+(aq) \qquad (3.27)$$

Table 3.10 Standard partial molar volumes of aqueous $AMPH^+$ $[(CH_3)_2C(CH_2OH)NH_3^+]$ on the conventional scale, $V°(H^+, aq) \equiv 0$. $V°(Cl^-, aq) = V°(HCl, aq)$, and the sources of latter are given in Section 3.3.1.

T / (K)	p / (MPa)	$V°$ / ($cm^3 \cdot mol^{-1}$)		
		$Cl^-(aq)$	$AMPH^+Cl^-(aq)$	$AMPH^+(aq)$
283.15	0.1	17.10	105.37	88.27
298.15	0.1	17.89	105.96	88.07
313.15	0.1	18.08	106.52	88.44
328.15	0.1	17.50	106.83	89.33
378.75	20.36	16.1	106.46	90.4
434.69	20.31	11.4	105.58	94.2
480.37	19.62	3.6	100.15	96.6
530.32	19.61	-15.9	85.58	101.5
480.89	10.21	2.1	99.62	97.5
530.88	10.33	-20.9	79.96	100.9

Table 3.11 Standard partial molar heat capacities of aqueous $AMPH^+$ on the conventional scale, $C_p^o(H^+, aq) \equiv 0$. $C_p^o(Cl^-, aq) = C_p^o(HCl, aq)$, and the sources of latter are given in Section 3.3.1.

T / (K)	p / (MPa)	C_p^o / ($J \cdot K^{-1} \cdot mol^{-1}$)		
		$Cl^-(aq)$	$AMPH^+Cl^-(aq)$	$AMPH^+(aq)$
283.15	0.1	-148.3	244.5	392.8
298.15	0.1	-126.6	249.8	376.4
313.15	0.1	-115.5	256.0	371.5
328.15	0.1	-111.7	257.6	369.3

The values of $V^o(AMPH^+, aq)$ and $C_p^o(AMPH^+, aq)$ were calculated and these are listed in Tables 3.10-3.11, where those of $V^o(AMP, aq)$ and $C_p^o(AMP, aq)$ were obtained from Section 3.3.2. The sources of properties of HCl (aq) were given in Section 3.3.1. The contributions to $\Delta_r V^o$ and $\Delta_r C_p^o$ for the AMP ionization are illustrated in Figures 3.14 and 3.15.

Figure 3.14 shows that the temperature-dependent values of $V^o(AMPH^+Cl^-, aq)$ and $V^o(HCl, aq)$ are remarkably similar, which can be explained by the large contribution of the Cl^-(Tremaine *et al.*, 1997). The behavior of $V^o(AMP, aq)$ and $V^o(AMPH^+Cl^-, aq)$ is quite different. The standard partial molar volume change of ionization, $\Delta_r V^o$, has very small values which are nearly constant with temperature. This implies that the large difference between $V^o(AMP, aq)$ and $V^o(AMPH^+Cl^-, aq)$ do come from the large effect of the Cl^-.

A similar calculation for the extrapolated values of $\Delta_r C_p^o$, based on the hybrid model, are consistent with the discussion above. Again, the temperature dependence of $C_p^o(AMPH^+Cl^-, aq)$ and $C_p^o(HCl, aq)$ is very similar. $C_p^o(AMP, aq)$ and $C_p^o(AMPH^+Cl^-, aq)$ approach very positive or negative values at high temperatures, respectively, but the values of $\Delta_r C_p^o$ are still nearly constant. Because $\Delta_r C_p^o$ is the difference between $C_p^o(AMPH^+, aq)$ and $C_p^o(AMP, aq)$, it does not contain a contribution from the chloride ion.

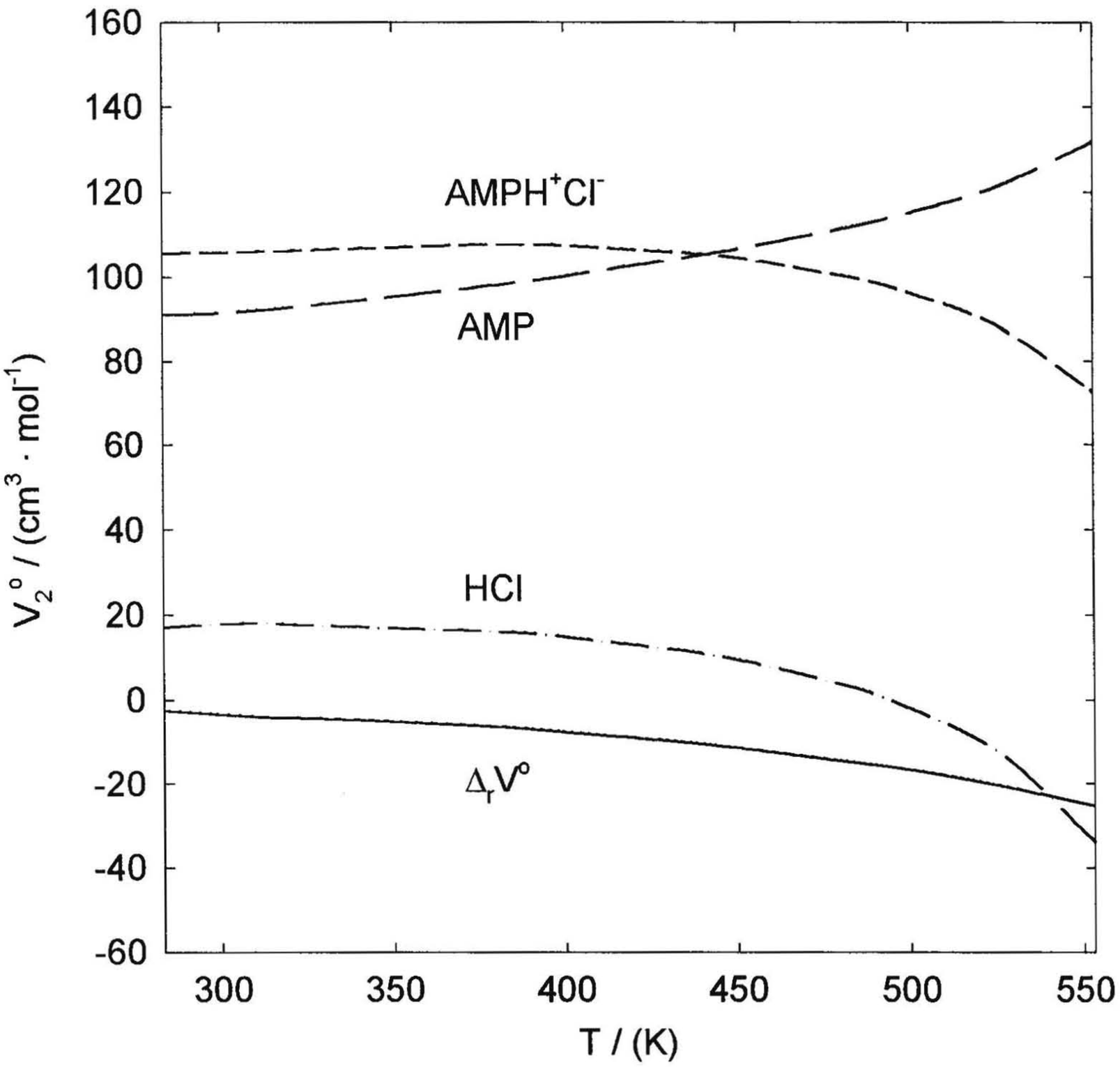

Figure 3.14 Contributions to the standard partial molar volume change $\Delta_r V^o$ for Equation (3.27). Lines were calculated from the fits on the hybrid model (Section 3.4.3): ——, $\Delta_r V^o$; –·–·–, V^o(HCl, aq); — — —, V^o(AMP, aq); – – –, V^o(AMPH$^+$Cl$^-$, aq).

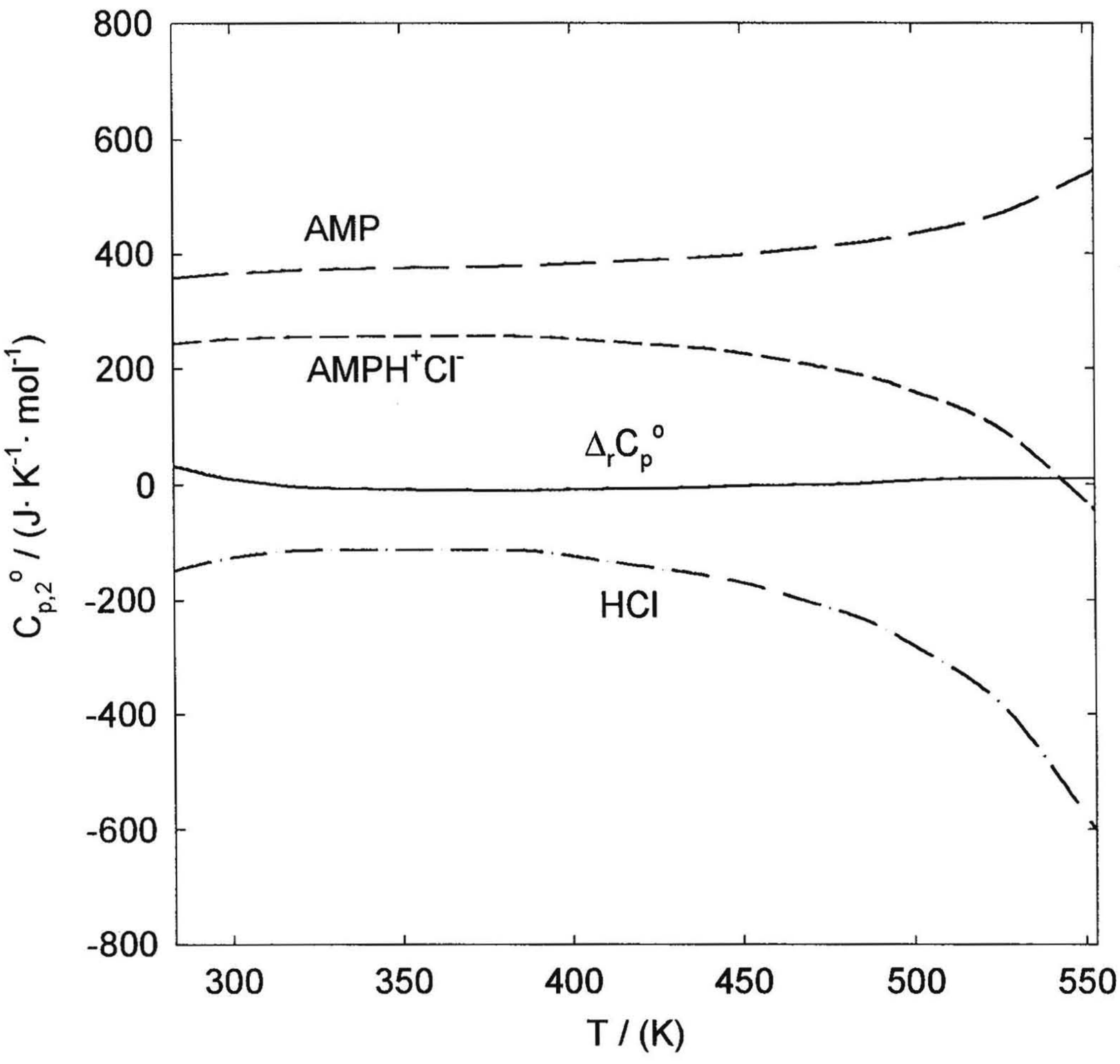

Figure 3.15 Contributions to the standard partial molar heat capacity change $\Delta_r C_p^o$ for Equation (3.27). Lines were calculated from the fits on the hybrid model (Section 3.4.3): ——, $\Delta_r C_p^o$; –·–·–, C_p^o(HCl, aq); — — —, C_p^o (AMP, aq); – – –, C_p^o(AMPH^{+}Cl^{-}, aq).

Chapter 4: Excess Molar Properties of [2-Amino-2-Methyl-1-Propanol + Water] Mixtures at Finite Concentrations from 278 to 368 K

4.1 Introduction

Values for the heat capacities of pure AMP have been reported in the literature (Maham *et al.*, 1997; Chiu *et al.*, 1999) as have some values for the apparent molar heat capacities and volumes of aqueous AMP (Roux *et al.*, 1980; Xu *et al.*, 1991). Most of these studies are over a limited range of temperature and composition. The objective of work in this chapter was to determine the excess molar heat capacities $C^E_{p,m}$ and the excess volumes V^E_m of aqueous AMP over the whole mole fraction range and as wide a temperature range as possible, up to the normal boiling point of water. A modified Redlich-Kister equation was fitted to the excess molar properties, and the molecular interactions were interpreted using Lumry's model, based on the reduced excess molar properties. The properties of another alkanolamine-water system, (methyldiethanolamine + H_2O), which were determined by Hawrylak (1999) and Hawrylak *et al.* (2000), are introduced for comparison.

4.2 Experimental Methods

4.2.1 Materials

AMP from Fluka [≥ 99.0 % (Gas Chromatography Grade)] was used as received. All the AMP solutions were prepared by mass, transferred and stored inside a glove bag

purged with nitrogen, because AMP is hygroscopic and sensitive to carbon dioxide. Nanopure water used in this study is the same as the water described in Section 3.2.1.

4.2.2 Experiments on Differential Scanning Calorimeter

The calibration factor of the differential scanning calorimeter (DSC, Section 2.2) in Watts/Volt can be obtained by applying a known power to a TED and measuring the resulting voltage. Although the DSC had been calibrated by the manufacturer, the calibration was verified periodically by measuring the enthalpy of fusion of water. During the period of this study, the enthalpy of fusion of water was measured to be always within 1 per cent of the literature value, 333.9 $J \cdot g^{-1}$, as given by the manufacturer (CSC, 1995).

Matched cells were placed in the wells, one of which was left empty to be a reference, while the other three contained 4.0×10^{-7} m^3 of (AMP + H_2O). As the temperature was scanned, the heat flux to or from each of four cells was measured and converted to heat capacities by using calibration constants. The results of same samples in three cells at each scan were averaged, and then the average from ascending and descending scans was used. The temperature of the heat sink was monitored by an RTD. A scan rate of 0.0167 $K \cdot s^{-1}$ over the whole temperature range was employed for all the samples.

Data were obtained by scanning over a temperature range of 268 K $\leq$ T $\leq$ 383 K, and the data at the range 278 K $\leq$ T $\leq$ 368 K were used for the analysis. The temperature range was selected based on the following experience. When the starting temperature was

below 268 K, the ice did not melt entirely when temperature was raised above 273 K, hence the heat capacity of ice contributed to the experimental data. On the other hand, when the end temperature was above 383 K, gasket corrosion became severe. The data at the two scanning temperature ends were discarded because of the fluctuations observed at the beginning and end of each run.

4.2.3 Vapor Corrections

In the CSC 4100 DSC measurements, the three sealed sample cells must be operated with a vapor space inside for the expansion of the liquid sample during the heating process. Since an equilibrium amount of vapor was produced upon heating, part of the experimental heat capacity came from the heat of vaporization. A correction was then required, especially when temperatures approach the boiling point of the volatile component in the solutions. Because of the high boiling point of AMP (Table 3.1), water was assumed to be the only volatile component. Therefore, the experimental heat capacity C_p^{exp} can be expressed as (Hawrylak, 1999):

$$C_p^{\exp} = [n_1(l) + n_2] \cdot C_{p,m}(mix) + n_1(g) \cdot C^*_{p,m,1}(g) + \Delta H_{vap,m,1}\left(\frac{\partial n_1(g)}{\partial T}\right)_V \qquad (4.1)$$

where subscripts 1 and 2 denote water and AMP, respectively; $C_{p,m}(mix)$ is the molar heat capacity of the (AMP + H_2O) mixture in the liquid state; and $\Delta H_{vap,m,1}$ is the enthalpy of

vaporization of water. With the assumption that the gas behaves ideally, the term $(\partial n_1(g)/\partial T)_V$ can be expressed as:

$$\left(\frac{\partial n_1(g)}{\partial T}\right)_V = \left(\frac{\partial (p_1 V_1(g)/RT)}{\partial T}\right)_V = \left[\frac{V_1(g)}{RT}\left(\frac{\partial p_1}{\partial T}\right)_V + \frac{p_1 V_1(g)}{R}\left(-\frac{1}{T^2}\right)\right] \tag{4.2}$$

The Clausius-Clapeyron equation expresses the temperature dependence of the vapor pressure as:

$$\left(\frac{\partial p_1}{\partial T}\right)_V = \frac{p_1 \Delta H_{vap,m,1}}{RT^2} \tag{4.3}$$

The vapor pressure of water in the solution was assumed to obey Raoult's Law: $p_1 = x_1 \cdot p_1^*$, so that the combination of Equations (4.2) and (4.3) gives:

$$\left(\frac{\partial n_1(g)}{\partial T}\right)_V = x_1\left[\frac{V_1(g)}{RT}\left(\frac{p_1^* \Delta H_{vap,m,1}}{RT^2}\right) - \frac{p_1^* V_1(g)}{RT^2}\right] \tag{4.4}$$

In this study, an approximately constant vapor space of 6.0×10^{-7} m^3 for (AMP + H_2O) mixtures was used.

The accuracy of our heat capacity measurements is 2 percent or better, as determined by comparing values of $C^*_{p,m,1}$ obtained from measurements on liquid water in this study with tabulated values of $C^*_{p,m,1}$(l) from the NIST compilations (Harvey *et al.*, 1996).

4.2.4 Experiments on DMA 5000 Densimeter

The operation of the DMA 5000 densimeter has been discussed in Section 2.3.3. To ensure that no bubbles had formed, each solution was equilibrated at 353 K, then scanned downward to 293 K in a series of temperature-programmed steps. After thermal equilibrium was obtained at each step, the instrument software automatically converted the resonant period of U-tube oscillation to densities by means of pre-determined calibration coefficients. Calibration was verified daily by comparing experimental results of degassed nanopure water and dry air with literature values (Bettin and Spieweck, 1990; DIN 51 757, 1994). The accuracy is 0.002 per cent or better. The densimeter also provides automatic correction of viscosity-related errors by measuring the damping of the U-tube's oscillation. The option "Density (Viscosity < 700 MPa·s)" was selected for this study, based on the viscosities of (AMP + H_2O) reported in the literature (Hsu and Li, 1997).

As is the case for all vibrating tube densimeters, samples must be maintained in the liquid state at the measuring temperatures. Pure AMP was therefore measured above 303 K (inclusive), based on the melting point shown in Table 3.1.

4.3 Results

4.3.1 Molar Heat Capacities and Volumes

The experimental molar heat capacities $C^*_{p,m,2}$ and volumes $V^*_{m,2}$ of pure AMP are tabulated in Tables A.2.1 and A.2.2. The $C^*_{p,m,2}$ results have been fitted as a function of temperature by the Maier-Kelley equation (Lewis and Randall, 1961):

$$C^*_{p,m,2} = p_1 + p_2 \cdot T + p_3 / T^2 \qquad (4.5)$$

The parameters p_1, p_2, p_3 and overall standard deviation s are given in Table 4.1. The experimental $C^*_{p,m,2}$ data and fit for AMP are shown in Figure 4.1, along with literature values from Chiu *et al.* (1999), Chueh and Swanson (1973), Missenard (1965), and Maham *et al.* (1997). While the values from this work and those from Maham *et al.* (1997) and Chiu *et al.* (1999) are in excellent agreement, the values from this work show more curvature, possibly because the purity was higher.

The molar volume results $V^*_{m,2}$ for pure AMP in Table A.2.2 were represented by a polynomial equation,

$$V^*_{m,2} = q_1 + q_2 \cdot T + q_3 \cdot T^2 \qquad (4.6)$$

to yield the parameters q_1, q_2, and q_3 listed in Table 4.1.

Table 4.1 Coefficients of Equations (4.5) and (4.6) for molar heat capacities $C^*_{p,m,2}$ and molar volumes $V^*_{m,2}$ of pure AMP, respectively.

parameter	Equation (4.5) for $C^*_{p,m,2}$ fit
p_1 / $(J \cdot K^{-1} \cdot mol^{-1})$	-238.8 ± 48.7
p_2 / $(J \cdot K^{-2} \cdot mol^{-1})$	1.141 ± 0.096
$p_3 \cdot 10^{-7}$ / $(J \cdot K \cdot mol^{-1})$	1.261 ± 0.183
s^a / $(J \cdot K^{-1} \cdot mol^{-1})$	1.04

parameter	Equation (4.6) for $V^*_{m,2}$ fit
q_1 / $(cm^3 \cdot mol^{-1})$	84.15 ± 0.46
$q_2 \cdot 10^3$ / $(cm^3 \cdot mol^{-1} \cdot K^{-1})$	-5.887 ± 2.801
$q_3 \cdot 10^4$ / $(cm^3 \cdot mol^{-1} \cdot K^{-2})$	1.516 ± 0.043
s^a / $(cm^3 \cdot mol^{-1})$	0.0031

[a] Standard deviation of the regression.

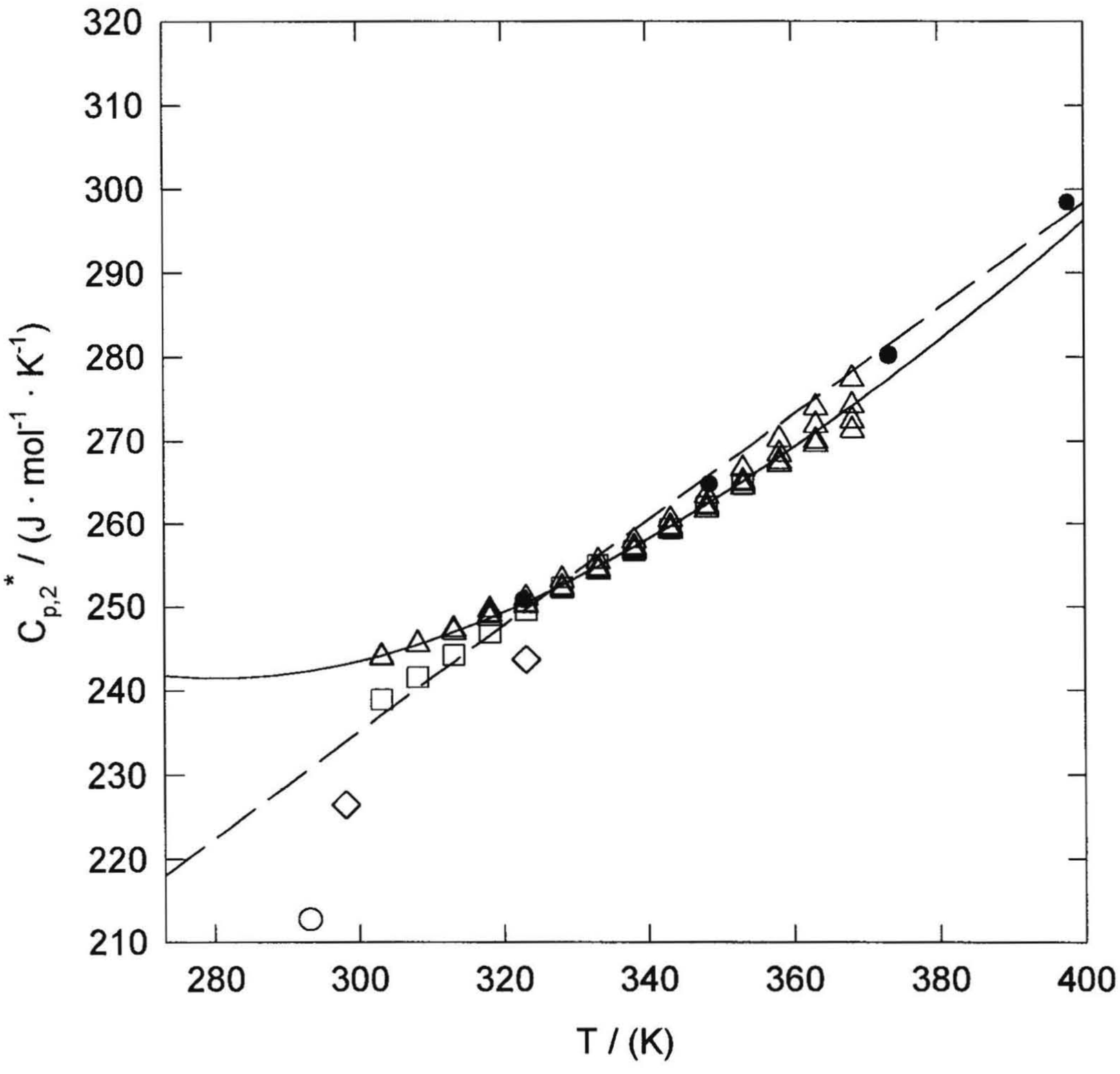

Figure 4.1 Molar heat capacities of pure AMP: □, Chiu *et al.* (1999); ○, Chueh and Swanson (1973); ◇, Missenard (1965); ●, Maham *et al.* (1997); Δ, experimental data in this study; ——, fitted values of Equation (4.5); — — —, fitted values from Maham *et al.* (1997).

4.3.2 Excess Molar Heat Capacities and Volumes

Excess molar properties were calculated from the experimental heat capacities and volumes, according to the usual expression for a binary system, according to Equation (4.7):

$$Y_m^E = Y_m\,(exp) - (1 - x_2)Y_{m,1}^* - x_2 Y_{m,2}^* \qquad (4.7)$$

where x_2 is the mole fraction of amine.

Values of $C_{p,m,1}^*$ for water were taken from the NIST compilations (Harvey *et al.*, 1996), and values of $C_{p,m,2}^*$ for AMP were calculated from the parameters in Table 4.1. The experimental values of $C_{p,m}$ and the resulting $C_{p,m}^E$ for the (AMP + H_2O) mixtures are listed in Table A.3.1. Values of $V_{m,1}^*$ for water from Bettin and Spieweck (1990) and values of $V_{m,2}^*$ for pure AMP calculated from the parameters in Table 4.1 were used to calculate V_m^E of the aqueous AMP solutions. Here the values of $V_{m,1}^*$ in Bettin and Spieweck (1990) were selected for excess property calculations, because they were used for the calibration by the manufacturer. These values agree with the values in the NIST compilations (Harvey *et al.*, 1996) well, as shown in Table 4.2. The experimental results of $(\rho - \rho_1^*)$ and V_m^E for the (AMP + H_2O) mixtures are listed in Table A.3.2. These values, along with the results of our measurements on dilute solutions with the Sodev Picker calorimeter and densimeter, are summarized in Table 4.3. The properties of another alkanolamine-water system, (methyldiethanolamine + H_2O) which was examined by

Table 4.2 Comparison of densities ρ_l^* of water from NIST compilations (Harvey *et al.*, 1996) and those from Bettin and Spieweck (1990).

T / K	$\rho_l^{*\,a}$ / g·cm^{-3}	$\rho_l^{*\,b}$ / g·cm^{-3}	$(\rho_l^{*\,a} - \rho_l^{*\,b})\cdot 10^6$ / g·cm^{-3}
293.15	0.998207	0.998203	4
298.15	0.997047	0.997043	4
303.15	0.995649	0.995645	4
308.15	0.994033	0.994029	4
313.15	0.992216	0.992212	4
318.15	0.990212	0.990208	4
323.15	0.988034	0.988030	4
328.15	0.985693	0.985688	5
333.15	0.983195	0.983191	4
338.15	0.980550	0.980546	4
343.15	0.977764	0.977759	5
348.15	0.974842	0.974838	4
353.15	0.971790	0.971785	5

[a] NIST compilations (Harvey *et al.*, 1996).
[b] Bettin and Spieweck (1990).

Table 4.3 Properties of (amine + water) mixtures and T = 298.15 K.

	$C^{o}_{p,2}$ / J·K^{-1}·mol^{-1}	$C^{*}_{p,2}$ / J·K^{-1}·mol^{-1}	$(C^{o}_{p,2} - C^{*}_{p,2})$ / J·K^{-1}·mol^{-1}	$C^{o}_{p,1}$ / J·K^{-1}·mol^{-1}	$C^{*}_{p,1}$ / J·K^{-1}·mol^{-1}	$(C^{o}_{p,1} - C^{*}_{p,1})$ / J·K^{-1}·mol^{-1}
MDEA	384.92 ± 0.56[a]	269.55 ± 2.70	115.37 ± 2.76	93.06 ± 0.23	75.33 ± 0.01[c]	17.73 ± 0.23
AMP	364.32 ± 0.57[b]	243.12 ± 2.43	121.20 ± 2.50	55.35 ± 1.56	75.33 ± 0.01[c]	-19.98 ± 1.56

	V^{o}_{2} / cm^{3}·mol^{-1}	V^{*}_{2} / cm^{3}·mol^{-1}	$(V^{o}_{2} - V^{*}_{2})$ / cm^{3}·mol^{-1}	V^{o}_{1} / cm^{3}·mol^{-1}	V^{*}_{1} / cm^{3}·mol^{-1}	$(V^{o}_{1} - V^{*}_{1})$ / cm^{3}·mol^{-1}
MDEA	109.92 ± 0.04[a]	114.92 ± 0.01[d]	- 5.00 ± 0.04	18.10 ± 0.01	18.07 ± 0.01[c]	0.028 ± 0.012[d]
AMP	91.64 ± 0.07[b]	95.87 ± 0.01	- 4.23 ± 0.07	15.10 ± 0.02	18.07 ± 0.01[c]	-2.97 ± 0.018

[a] Hawrylak (1999).
[b] Chapter 3 in this study.
[c] Harvey *et al.* (1996).
[d] Hawrylak *et al.* (2000).

Hawrylak (1999) and Hawrylak *et al.* (2000), were also listed and calculated in Table 4.3 for comparison and the investigation of molecular interactions.

The experimental excess properties have been treated with the modified Redlich-Kister equation proposed by Van Ness and Abbott (1982):

$$Y_m^E = \left[\frac{x_2(1-x_2)}{1+\sum_{n=1}^{p} D_n(2x_2-1)^n}\right]\sum_{m=0}^{q} C_m(2x_2-1)^m \qquad (4.8)$$

where Y_m^E is $C_{p,m}^E$ in $J \cdot K^{-1} \cdot mol^{-1}$ or V_m^E in $cm^3 \cdot mol^{-1}$; and D_n and C_m are adjustable interaction coefficients. Equation (4.8) was fitted by least squares regression to the experimental $C_{p,m}^E$ (AMP + H_2O) with a weighting factor of $1/(x_1 \cdot x_2)$, using two or three parameters. The values of parameters are listed in Table 4.4, and the experimental plots and least-squares curves are shown in Figure 4.2. Equation (4.8) was fitted to the experimental values of V_m^E (AMP + H_2O) using three parameters and the weighting factor $1/(x_1 \cdot x_2)$, and the values of the parameters are given in Table 4.5. The corresponding experimental plots and the least-squares fitted curves of V_m^E (AMP + H_2O) are shown in Figure 4.3.

The excess molar heat capacities $C_{p,m}^E$ and volumes V_m^E of (methyldiethanolamine + H_2O), i.e., (MDEA + H_2O) from Hawrylak (1999) and Hawrylak *et al.* (2000), are shown in Figures A.4.2 and A.4.3. The values for $C_{p,m}^E$

Table 4.4 Parameters from Equation (4.8) for the excess molar heat capacities of aqueous AMP.

Parameter					
	T= 278.15 K	T= 283.15 K	T= 288.15 K	T= 293.15 K	T= 298.15 K
C_0	-31.7704	-20.4440	-11.6381	-4.9620	--------
C_1	-65.9269	-57.7302	-48.0237	-41.7601	-36.4282
D_1	0.7856	0.8054	0.8251	0.8209	0.8236
s[a]	2.48	2.14	1.89	1.70	1.56
	T= 303.15 K	T= 308.15 K	T= 313.15 K	T= 318.15 K	T= 323.15 K
C_0	7.9495	12.4297	16.7014	20.3129	23.8968
C_1	-25.0915	-20.9790	-16.1032	-12.1803	-8.1931
D_1	0.8438	0.8307	0.8247	0.8154	0.8052
s[a]	2.04	1.49	1.43	1.41	1.42
	T= 328.15 K	T= 333.15 K	T= 338.15 K	T= 343.15 K	T= 348.15 K
C_0	27.7092	30.3525	33.0810	35.7011	38.2806
C_1	--------	--------	---------	---------	----------
D_1	0.8399	0.7962	0.7489	0.7011	0.6517
s[a]	1.45	1.34	1.39	1.49	1.56
	T= 353.15 K	T= 358.15 K	T= 363.15 K	T= 368.15 K	
C_0	40.9164	43.3871	45.4355	46.1005	
C_1	---------	---------	--------	--------	
D_1	0.6023	0.5549	0.5133	0.4915	
s[a]	1.68	1.83	1.86	1.82	

[a] Standard deviation of the regression, $J \cdot K^{-1} \cdot mol^{-1}$.

Table 4.5 Parameters from Equation (4.8) for the excess molar volumes of aqueous AMP.

parameter				
	T = 293.15 K	T = 298.15 K	T = 303.15 K	T = 308.15 K
C_0	-4.4530 ± 0.0197	-4.4166 ± 0.0181	-4.3796 ± 0.0155	-4.3478 ± 0.0139
C_1	2.2272 ± 0.0320	2.1814 ± 0.0267	2.0862 ± 0.0229	2.0067 ± 0.0206
D_2	-0.2758 ± 0.0113	-0.2462 ± 0.0102	-0.2333 ± 0.0089	-0.2197 ± 0.0082
s^a	0.0195	0.0179	0.0153	0.0137
	T = 313.15 K	T = 318.15 K	T = 323.15 K	T = 328.15 K
C_0	-4.3209 ± 0.0127	-4.2974 ± 0.0111	-4.2768 ± 0.0095	-4.2581 ± 0.0083
C_1	1.9314 ± 0.0188	1.8603 ± 0.0165	1.7913 ± 0.0140	1.7295 ± 0.0123
D_2	-0.2075 ± 0.0076	-0.1971 ± 0.0067	-0.1882 ± 0.0058	-0.1796 ± 0.0052
s^a	0.0125	0.011	0.0093	0.0082
	T = 333.15 K	T = 338.15 K	T = 343.15 K	T = 348.15 K
C_0	-4.2401 ± 0.0076	-4.2217 ± 0.0070	-4.2029 ± 0.0079	-4.1816 ± 0.0098
C_1	1.6721 ± 0.0112	1.6212 ± 0.0104	1.5810 ± 0.0116	1.5540 ± 0.0146
D_2	-0.1721 ± 0.0048	-0.1651 ± 0.0045	-0.1569 ± 0.0050	-0.1468 ± 0.0064
s^a	0.0074	0.0069	0.0077	0.0096
	T = 353.15 K			
C_0	-4.1575 ± 0.0130			
C_1	1.5411 ± 0.0194			
D_2	-0.1348 ± 0.0086			
s^a	0.0127			

[a] Standard deviation of the regression, $cm^3 \cdot mol^{-1}$.

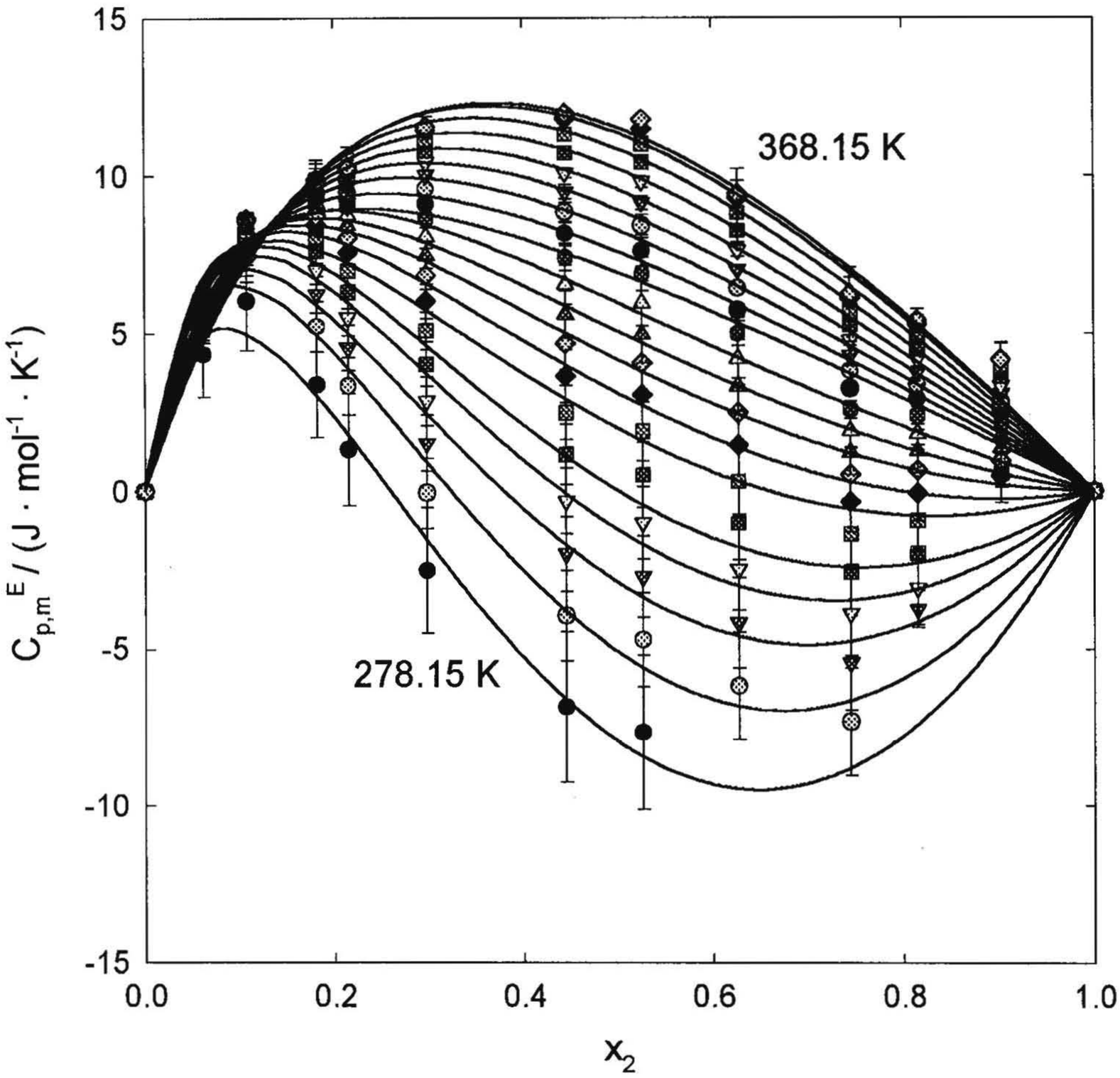

Figure 4.2 Excess molar heat capacities of aqueous AMP from 278.15 K to 368.15 K (at 5 K intervals) plotted against mole fraction. Symbols are experimental results, and lines are fitted values of Equation (4.8).

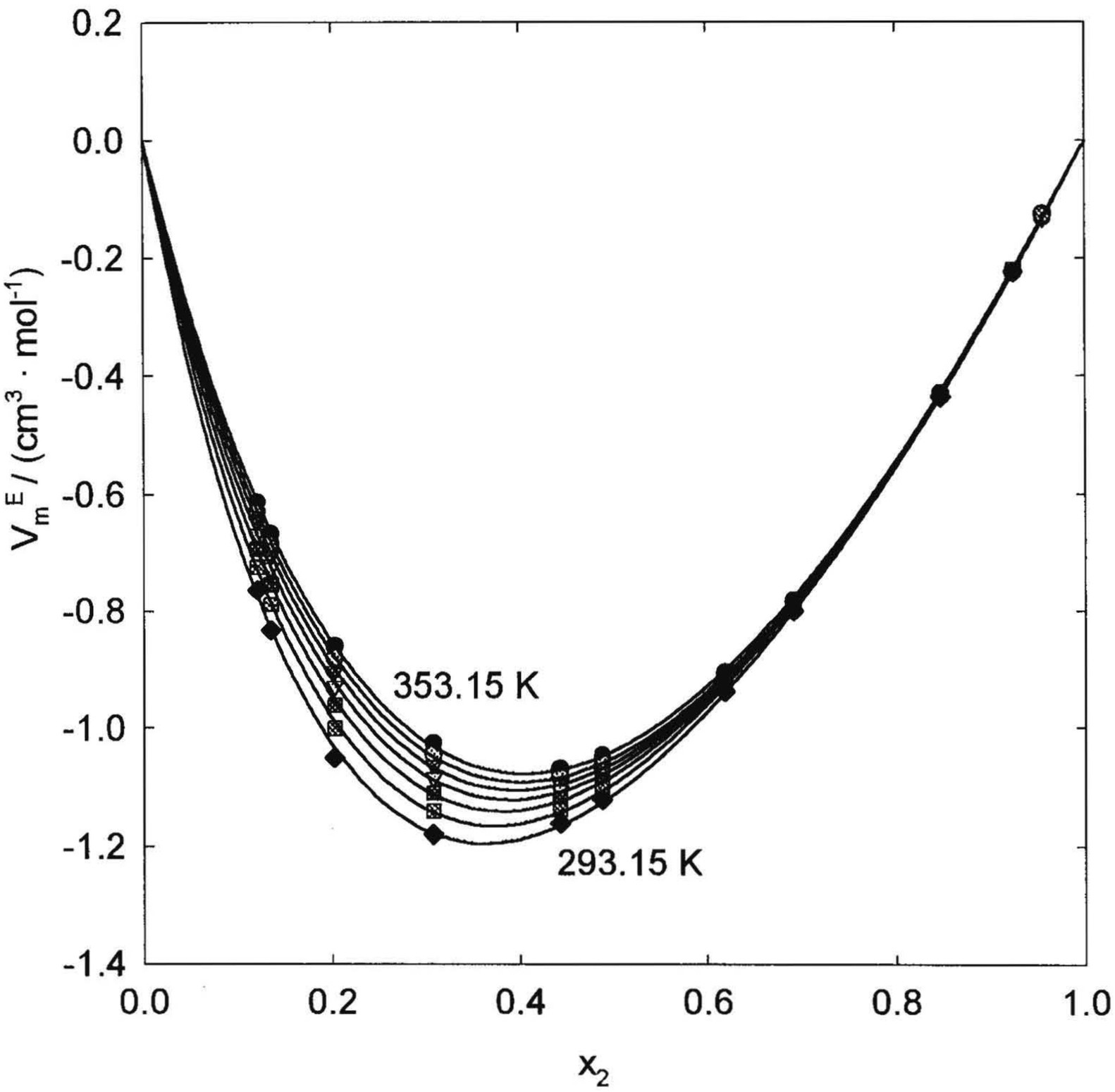

Figure 4.3 Excess molar volumes V_m^E of aqueous AMP from 293.15 K to 353.15 K (at 10 K intervals) plotted against mole fraction. Symbols are experimental results, and lines are fitted values of Equation (4.8).

(MDEA + H_2O) are positive over the whole mole fraction range. As temperature increases, the maximum in $C^E_{p,m}$ increases and moves to higher mole fractions. The values of V^E_m (MDEA + H_2O) at 298.15 K are negative over the whole mole fraction range, with a minimum at $x_2 \approx 0.35$. This corresponds approximately to the maximum in $C^E_{p,m}$ at T = 298.15 K, which occurs at $x_2 \approx 0.30$. The temperature dependance of V^E_m (MDEA + H_2O) has not been measured.

The behaviour of $C^E_{p,m}$ (AMP + H_2O) in Figure 4.2 differs from that of aqueous MDEA, in that it is sigmoid-shaped at low temperatures, passing through a maximum in the water-rich region then dropping to negative values at higher mole fractions of AMP. The maximum in $C^E_{p,m}$ (AMP + H_2O) increases and shifts towards higher mole fractions with increasing temperature so that, at $T \geq 308.15$ K, the values of $C^E_{p,m}$ (AMP + H_2O) at high mole fractions change sign to become positive. As shown in Figure 4.3, the values of V^E_m (AMP + H_2O) are negative at all temperatures, and have the same shape as those of (MDEA + H_2O) at 298.15 K (Hawrylak *et al.*, 2000). The magnitude of V^E_m (AMP + H_2O) decreases with increasing temperature.

Excess molar thermal expansibilities of (AMP + H_2O), $E^E_m = (\partial V^E_m/\partial T)_p$, calculated from the temperature dependence of the experimental V^E_m data, are shown in Figure 4.4. The shape of E^E_m (AMP + H_2O) is sigmoidal, and is somewhat similar to that of $C^E_{p,m}$ in composition dependence, but the temperature dependence is opposite. The fitted curves in Figure 4.4 are intended as a visual aid only.

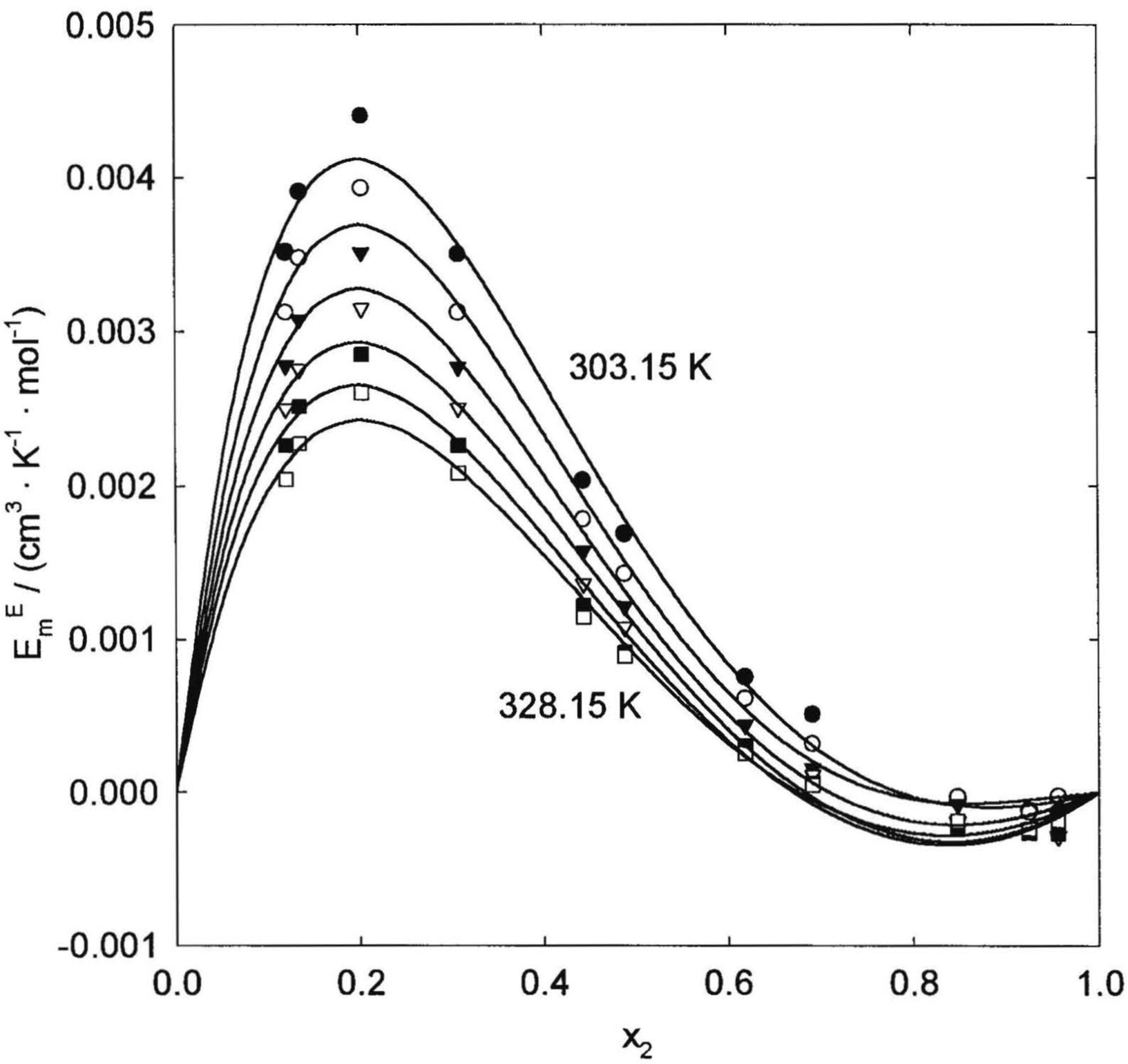

Figure 4.4 Experimental excess molar thermal expansibilities E_m^E of aqueous AMP from 303.15 K to 328.15 K (at 5 K intervals) plotted against mole fraction. Symbols are first derivatives of the experimental V_m^E results, and lines are fitted values of Equation (4.8).

4.4 Discussion

In the discussion that follows, we have used the reduced excess molar quantities, $Y_m^E/(x_1 \cdot x_2)$, proposed by Davis (1993) and Desnoyers and Perron (1997) in order to reveal the behaviour associated with specific solute-solvent and solute-solute interactions. At intermediate mole fractions, a linear dependance on mole fraction corresponds to the region, where the solute-solvent interactions for both components obey the Margules equation (Margules, 1895) for subregular solutions.

$$Y_m^E / \{x_2(1 - x_2)\} = A + B \cdot x_2 \qquad (4.9)$$

Here A and B are two interaction parameters. At low concentrations, the limiting behaviour of the excess properties is related to the corresponding standard molar and standard partial molar properties through the relationships:

$$\lim_{x2 \to 0} [Y_m^E / \{x_2(1 - x_2)\}] = Y_{2,m}^o - Y_{2,m}^* \qquad (4.10)$$

and

$$\lim_{x2 \to 1} [Y_m^E / \{x_2(1 - x_2)\}] = Y_{1,m}^o - Y_{1,m}^* \qquad (4.11)$$

Excess heat capacities are related to differences in the mean-square fluctuations in enthalpy and entropy between mixtures and the pure solvent, according to the expressions $<\sigma_H^2> = RT^2 \cdot C_{p,m}$ and $<\sigma_S^2> = R \cdot C_{p,m}$. Here, interpretation of the data for

both systems is based on the conceptual model proposed by Lumry *et al.* (1982), described in Section 1.4.3, which has been used by Pagé *et al.* (1993) and others to interpret the excess properties of water-alkanolamine systems. In Lumry's model, the composition is subdivided into three regions, as discussed in Section 1.4.3: (i) at low mole fractions, the AMP occupies "holes" in the open structure of water and disrupts the cooperative fluctuations of liquid water (typically at $x_2 \leq 0.1$); (ii) the AMP eliminates the extensive hydrogen-bonding connectivity between water molecules (typically at mole fractions $0.1 < x_2 \leq 0.3$); (iii) water-AMP interactions are gradually replaced by AMP-AMP interactions (typically at $x_2 \geq 0.3$). At very high mole fractions, a fourth region may also exist, in which water may occupy "holes" in the hydrogen-bonded structure of the liquid AMP. An idealized schematic plot for $C^E_{p,m}/\{x_2(1-x_2)\}$ is shown in Figure 4.5. The corresponding plots of $V^E_m/(x_1 \cdot x_2)$ provide a direct measure of the expansion or contraction of the mixture by hydrophilic or hydrophobic interactions.

Plots of the reduced excess molar heat capacities and reduced molar volumes of aqueous AMP are shown in Figures 4.6 and 4.7. Plots of the reduced excess molar heat capacities of aqueous MDEA are shown in Figure A.4.4. At high temperatures the change in slope of $C^E_{p,m}/\{x_2(1-x_2)\}$ for both systems is gradual and may be represented by a nearly constant Margules interaction parameter. This behaviour is also evident in the reduced molar volumes of (AMP + H_2O). Figure A.4.4 shows the emergence of a clear transition between region (ii) and region (iii) in the (MDEA + H_2O) system as the temperature is lowered from room temperature to 283 K. Figures 4.6 and 4.7 show the corresponding

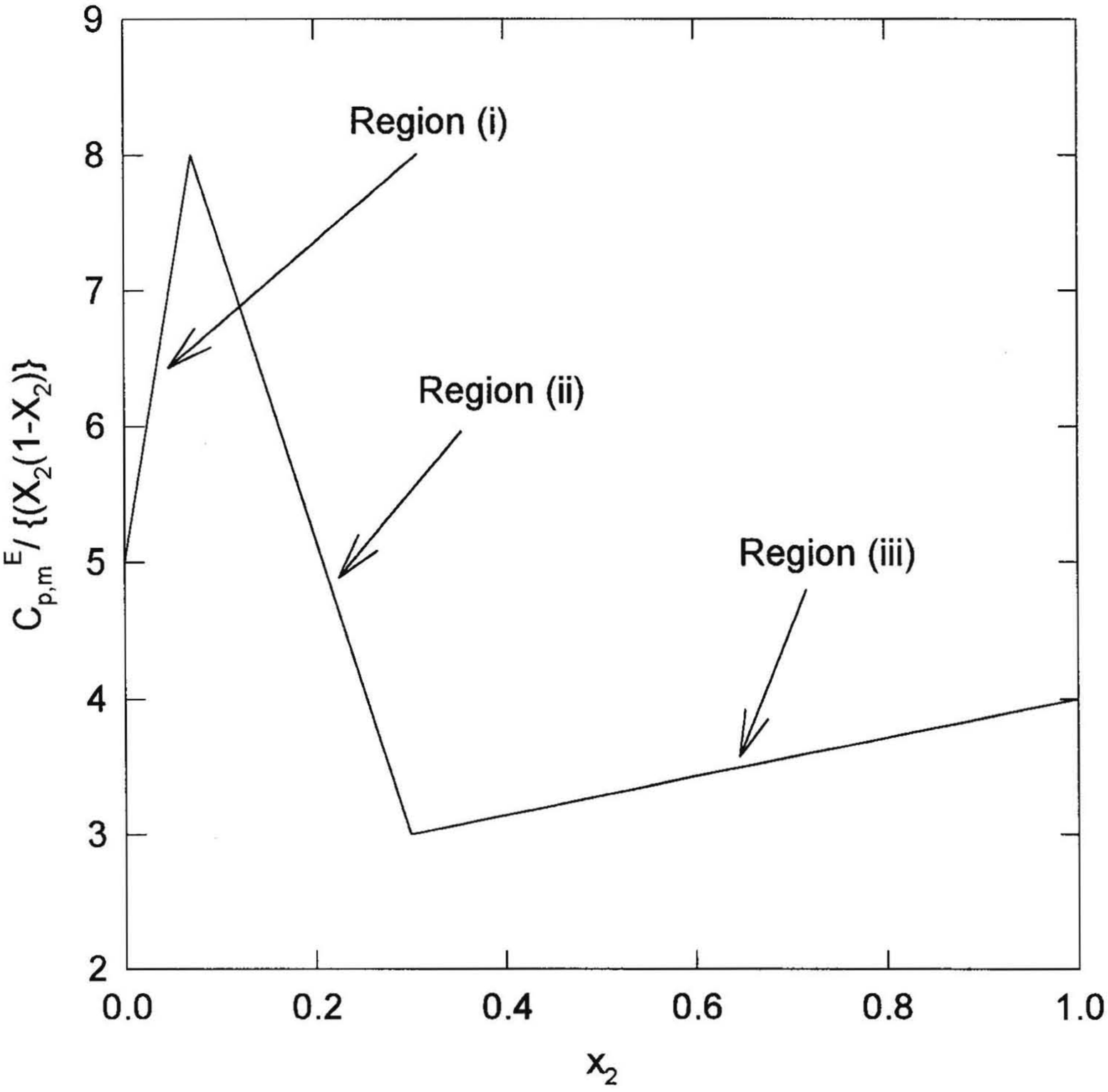

Figure 4.5 Idealized schematic of typical reduced excess molar heat capacity plot, showing regions (i), (ii), and (iii) according to Lumry *et al.* (1982). Reproduced from Hawrylak (1999).

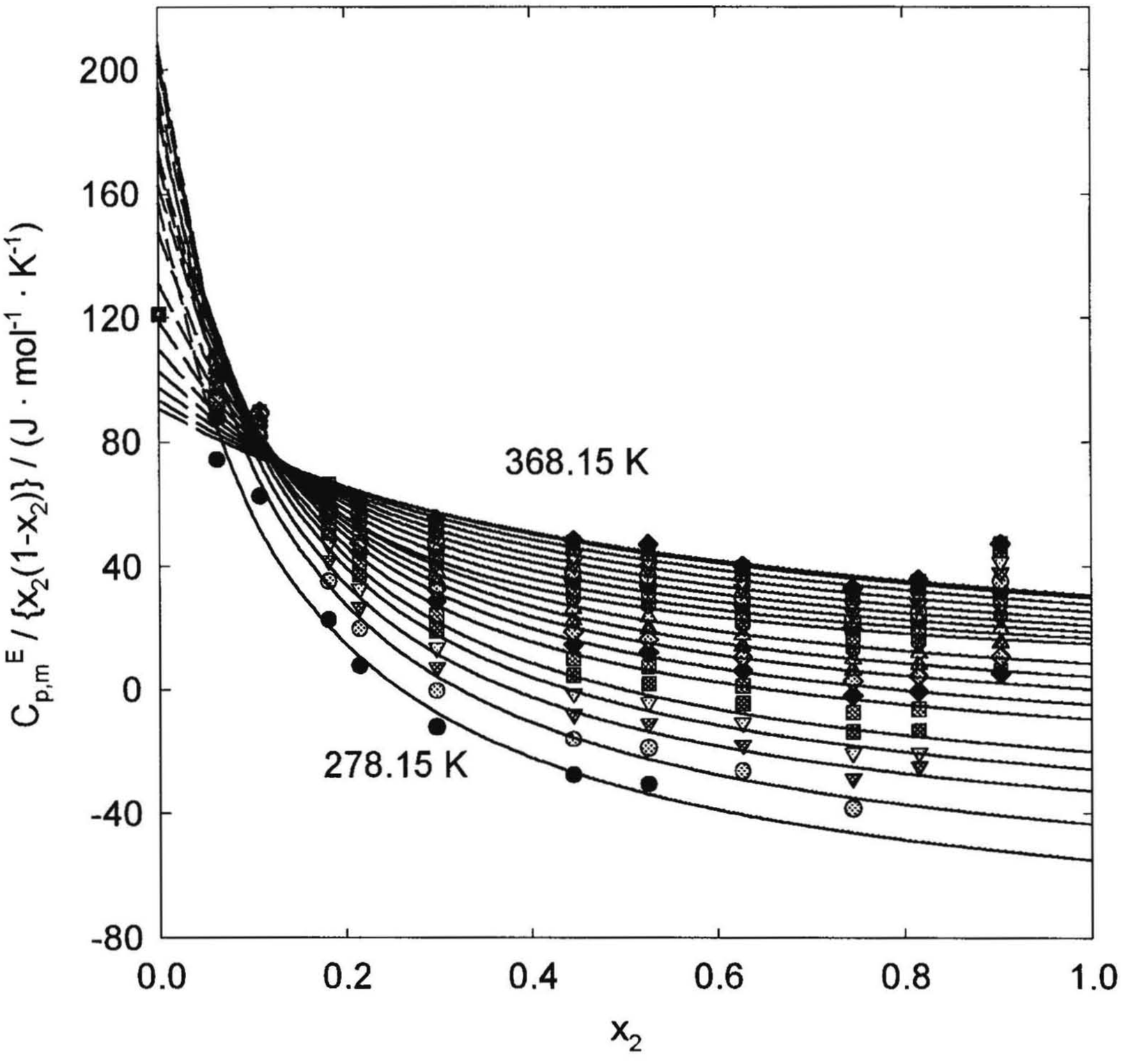

Figure 4.6 Reduced excess molar heat capacities of aqueous AMP from 278.15 K to 368.15 K (at 5 K intervals) plotted against mole fraction. Symbols are experimental results, and lines are fitted values of Equation (4.8). The point at $x_2 = 0$ is $(C^{o}_{p,m,2} - C^{*}_{p,m,2})$ at 298.15 K (Table 4.3).

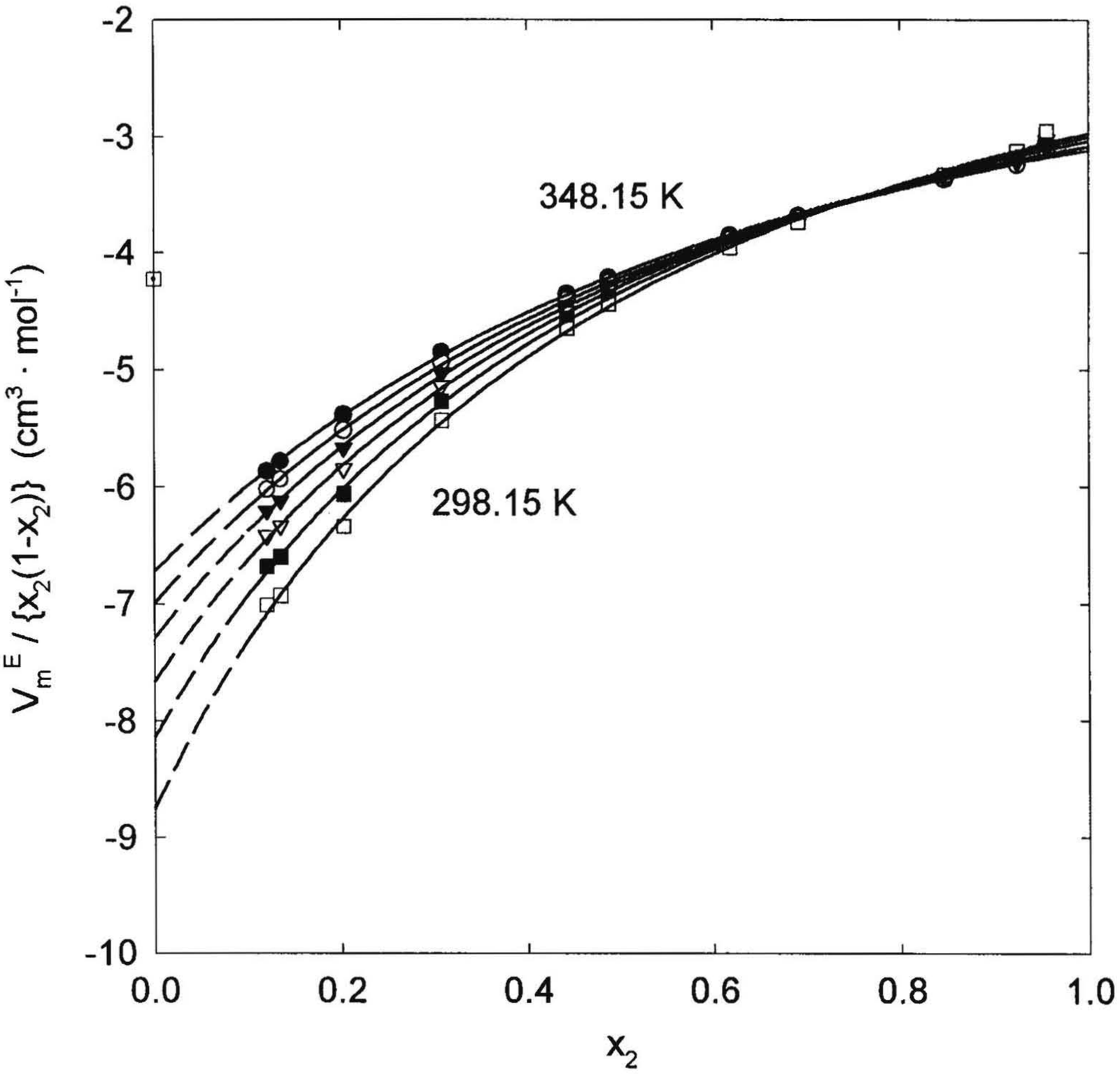

Figure 4.7 Reduced excess molar volumes of aqueous AMP from 298.15 K to 348.15 K (at 10 K intervals) plotted against mole fraction. Symbols are experimental results, and lines are fitted values of Equation (4.8). The point at $x_2 = 0$ is ($V^{o}_{m,2}$ - $V^{*}_{m,2}$) at 298.15 K (Table 4.3).

behaviour for (AMP + H_2O), which is similar although the change in slope at low temperature is not quite as sharp. In both systems the transition is much more pronounced and moves further into the water-rich region at temperatures below 298.15 K. The sigmoidal shape of $C^E_{p,m}$ (AMP + H_2O) in Figure 4.2 arises because the limiting values $C^o_{p,1}$-$C^*_{p,1}$ become negative at low temperatures.

To determine the extent of region (i) in these two systems, we have used data for $C^E_{p,m}$ and V^E_m at low mole fractions, $0.002 < x_2 < 0.05$, from measurements in the Picker calorimeter and the Sodev densimeter, to determine the standard partial molar properties $C^o_{p,2}$ and V^o_2. These are tabulated in Table 4.3 for T = 298.15 K. The measured values of $C^o_{p,2}$-$C^*_{p,2}$ for MDEA are identical to within experimental error with those obtained by extrapolating $C^E_{p,m}/\{x_2(1-x_2)\}$ to $x_2 = 0$ using the fitted parameters of Equation (4.8) reported by Hawrylak (1999), indicating that any maximum or minimum in the reduced properties must lie below the limit of measurements in the Picker calorimeter and densimeter ($x_2 < 0.002$). The same is true for V^o_2 - V^*_2 , using extrapolations of the parameters of Hawrylak (2000). The experimental values for $C^E_{p,m}$ and V^E_m for (AMP + H_2O) do display maxima and minima characteristic of region (i). These are plotted in Figures 4.8 and 4.9 respectively, along with the extrapolated curves corresponding to the parameters tabulated in Tables 4.4 and 4.5, which were fitted to data in the range $0.1 \leq x_2 \leq 0.9$. The values of $C^o_{p,2}$ (AMP, aq) and V^o_2 (AMP, aq) differ from the values extrapolated by fitting Equation (4.8) to data in the region ($0.1 \leq x_2 \leq 0.9$) by approximately -85 $J \cdot K^{-1} \cdot mol^{-1}$ and +4.5 $cm^3 \cdot mol^{-1}$, respectively. Earlier measurements by

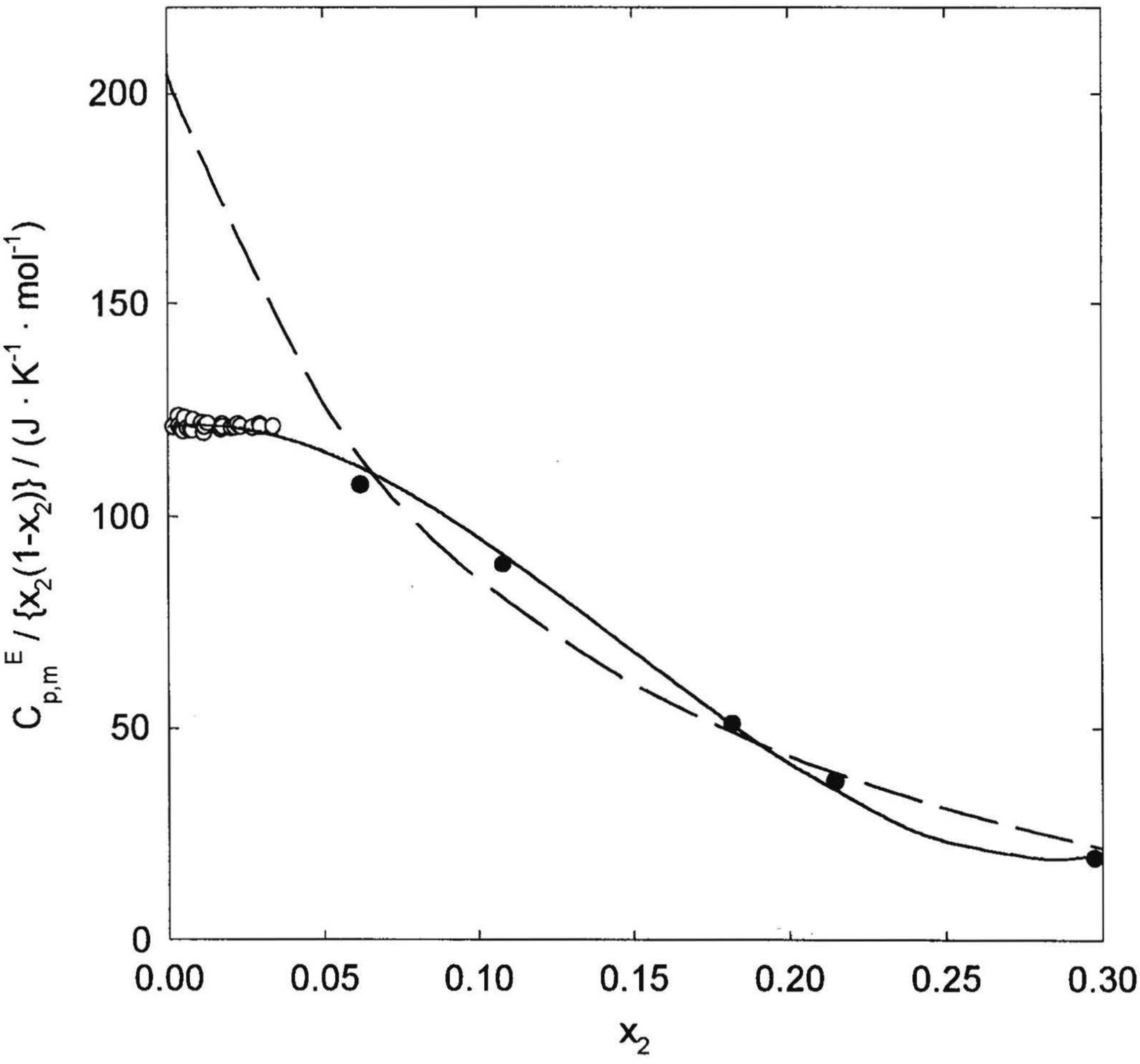

Figure 4.8 Reduced excess molar heat capacities of aqueous AMP at 298.15 K plotted against mole fraction. Symbols are experimental results: ○, Sodev CP-C Picker calorimeter; ●, CSC 4100 DSC. Lines are fitted values of Equation (4.8): ——— , $x_2 \leq 0.30$; – – – – , $0.05 \leq x_2 \leq 0.95$.

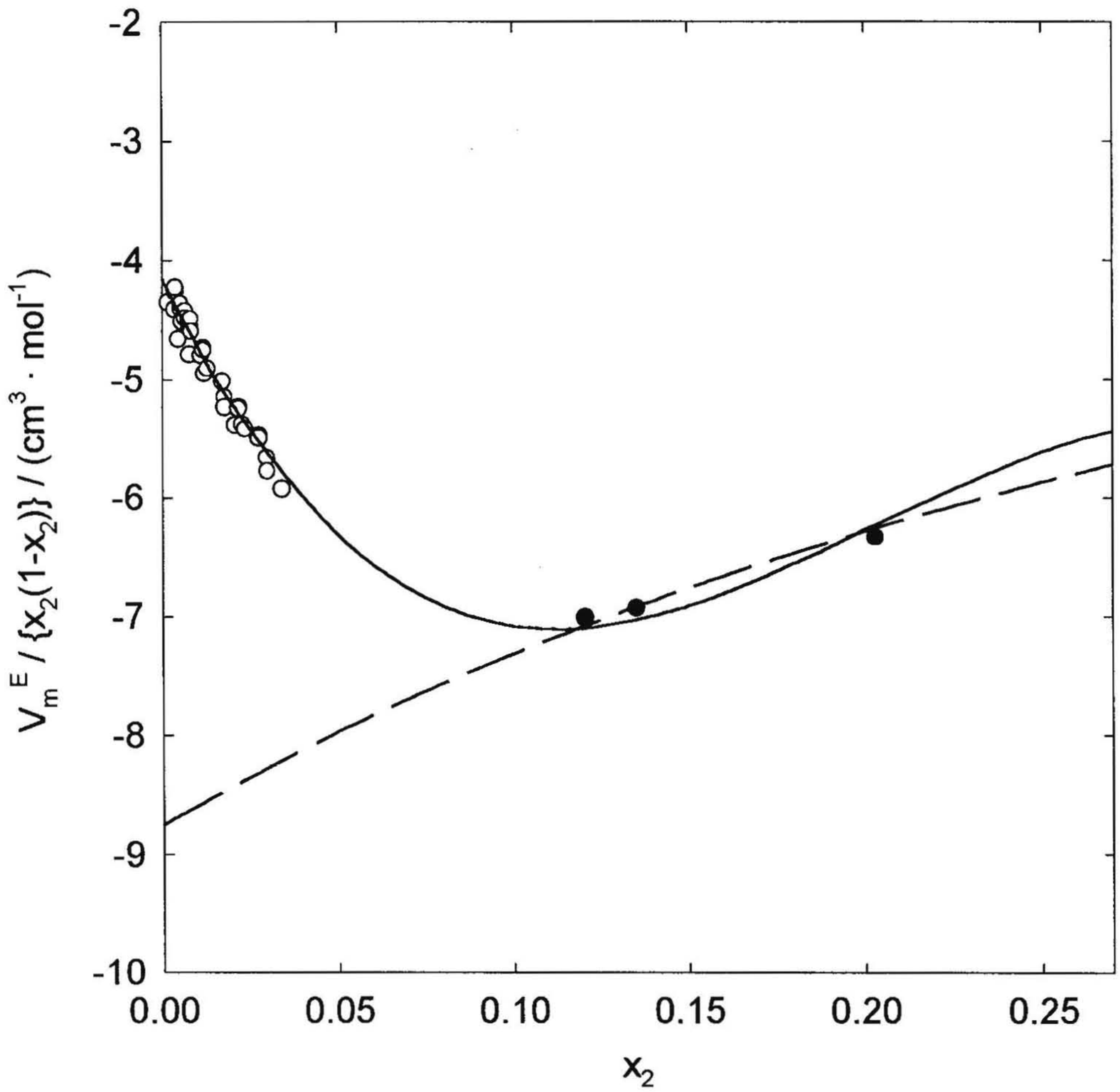

Figure 4.9 Reduced excess molar volumes of aqueous AMP at 298.15 K plotted against mole fraction. Symbols are experimental results: ○, Sodev vibrating flow densimeter; ●, DMA 5000. Lines are fitted values of Equation (4.8): ——— , $x_2 \leq 0.31$; – – – – , $0.05 \leq x_2 \leq 0.96$.

Roux *et al.* (1980) at 298.15 K have confirmed the existence of a maximum in $C^{E}_{p,m}/\{x_2(1-x_2)\}$ below x = 0.1 corresponding to the onset of region (i).

In Lumry's model, the stability of region (i) is correlated with the hydrophobicity of the solute molecule as, for example, in the case of aqueous surfactants in which the co-operative fluctuations are associated with "tail-to-tail" interactions. Cooperative fluctuations in aqueous amines and alcohols are thought to arise from the formation of time-average "clathrate-like" structures which break down when solute mole fractions exceed the stoichiometric value, or from Lewis acid-base interactions that stabilize hydrophobic solvation (Roux *et al.*, 1980; Pagé *et al.*, 1993). AMP is on the borderline of hydrophobic behaviour under these conditions while MDEA, which has two hydroxyl groups on flexible alkyl chains, is apparently more hydrophilic.

Roux *et al.* (1980) have identified the relative hydrophobicity of alcohols and amines with the difference between the standard partial molar property of the solute and the corresponding molar property of the pure liquid, $Y^{o}_{2} - Y^{*}_{2}$. The standard state properties in Table 4.3 show interesting differences between the properties of MDEA and AMP at infinite dilution relative to the pure liquid state. Both display positive values of $C^{o}_{p,2} - C^{*}_{p,2}$ and negative values of $V^{o}_{2} - V^{*}_{2}$, consistent with Lumry's suggestion that the hydrated molecules occupy "holes" in bulk water with a smaller volume and higher heat capacity than in the bulk liquid alkanolamine. The properties of dilute solutions of water in MDEA in Table 4.3, $C^{o}_{p,1} - C^{*}_{p,1}$ and $V^{o}_{1} - V^{*}_{1}$, show little change in volume but a significant increase in heat capacity relative to bulk water, suggesting that water also

restricts the cooperative fluctuations of hydrogen bonds in bulk MDEA. The negative values of both $C^{o}_{p,1}$ - $C^{*}_{p,1}$ and V^{o}_{1} - V^{*}_{1} for AMP in Table 4.3 suggest that, solvated water in AMP is significantly less "structured" than is the case in bulk water. A more comprehensive study of the type reported by Roux *et al.* (1980) that includes other thermodynamic functions, along with parallel spectroscopic studies, would clearly be of interest to explore the differences between these systems.

5. Conclusions

New data for $C^{E}_{p,m}$ (AMP + H_2O) in the range 278.15 ≤ T ≤ 368.15 K, and for V^{E}_{m} (AMP + H_2O) in the range 293.15 ≤ T ≤ 353.15 K have been reported in this study. These properties were compared with those of the mixtures composed of water and a tertiary amine MDEA. The results are consistent with Lumry's model, with MDEA being less hydrophobic than AMP. The mole-fraction dependence of the reduced excess heat capacities is most pronounced below 298.15 K, with clear differences in the behaviour of $C^{E}_{p,m}$ (MDEA + H_2O) and $C^{E}_{p,m}$ (AMP + H_2O) while the behaviour of V^{E}_{m} for the two aqueous alkanolamines is similar. The results suggest that interesting hydration effects take place in both the water-rich and alkanolamine-rich solutions and that further studies to examine other thermodynamic properties would be of interest, particularly at temperatures below 298.15 K.

Bibliography

Albert H.J. and Wood R.H. (1984) High-Precision Densimeter for Fluids at Temperatures to 700K and Pressures to 40 MPa. *Rev. Sci. Instrum.* **55**, 589-593.

Anderson G.M., Castet S., Schott J., and Mesmer R.E. (1991) The Density Model for Estimation of Thermodynamic Parameters of Reactions at High Temperatures and Pressures. *Geochim. Cosmochim. Acta.* **55**, 1769-1779.

Angell C.A. (1983) Supercooled Water. *Ann. Rev. Phys. Chem.* **34**, 593-630.

Anton Paar GmbH (1998) *DMA 5000 Density Meter Manual* (Anton Paar GmbH, Graz, Austria)

Archer D.G. and Wang P. (1990) The Dielectric Constant of Water and Debye-Hückel Limiting Slopes. *J. Phys. Chem. Ref. Data* **19**, 371-411.

Archer D.G. (1992) Thermodynamic Properties of the NaCl + H_2O System II. Thermodynamic Properties of NaCl(aq), NaCl·$2H_2O$(cr), and Phase Equilibria. *J. Phys. Chem. Ref. Data* **21**, 793-821.

Astarita G., Savage D.W., and Bisio A. (1983) *Gas Treating with Chemical Solvents.* John Wiley & Sons, New York.

Balakrishnan P.V. (1988) Liquid-Vapor Distribution of Amines and Acid Ionization Constants of Their Ammonium Salts in Aqueous Systems at High Temperature..*J. Solution Chem.* **17**, 825-840.

Bettin H. and Spieweck F. (1990) Die Dichte des Wassers als Funktion der Temperatur nach Einführung der Internationalen Temperaturskala von 1990. PTB-Mitt. **100**, pg. 195-196.

Blanc C., Eluge J., and Lallemand F.J. (1981) MDEA Process Selects H_2S. *Hydrocarbon Processing.* 111-116.

Bockris J.O. and Reddy A.K.N. (1998) *Modern Electrochemistry 2nd Edition, Vol. 1*; Plenum Press, New York.

Born M. (1920) Volumen und Hydratationswärme der Ionen. *Zeitschr. Physik* **1**, 45-48.

Budavari S., O'Neil M.J., Smith A., and Heckelman P.E. (1989) *The Merck Index: 11th edition*, Merck & Co., Inc, Rahway, N.J., U.S.A.

Chiu L.F., Liu H.F., and Li M.H. (1999) Heat Capacity of Alkanolamines by Differential Scanning Calorimetery. *J. Chem. Eng. Data* **44**, 631-636.

Chueh C.F. and Swanson A.C. (1973) Estimation of Liquid Heat Capacity. *Can. J. Chem. Eng.* **51**, 596-600.

Clarke, R.G.F. (2000) Amino Acids under Hydrothermal Conditions: Apparent Molar Volumes, Apparent Molar Heat Capacities, and Acid/Base Dissociation Constants for Aqueous α-Alanine, β-Alanine, Glycine, and Proline at Temperatures from 25 to 250°C and Pressures up to 30.0 MPa. *Ph.D. Thesis* Memorial University of Newfoundland.

Corti H.R., Fernandez-Prini R.J., and Svarc F. (1990) Densities and Partial Molar Volumes of Aqueous Solutions of Lithium, Sodium, and Potassium Hydroxides up to 250°C. *J. Solution Chem.* **19**, 793-809.

CSC (1995) *CSC 4100 Multi-Cell Differential Scanning Calorimeter, User's Manual*, Revision 2.0. ©1995 Calorimetry Sciences Corporation.

Davis, M. (1993) Thermodynamic and Related Studies of Amphiphile + Water Systems. *Chem. Soc. Rev.* **22**, 127-134.

Desnoyers J.E., de Visser C., Perron G., and Picker P. (1976) Reexamination of the Heat Capacities Obtained by Flow Microcalorimetry. Recommendation for the Use of a Chemical Standard. *J. Solution Chem.* **5**, 605-616.

Desnoyers J.E. and Perron G.(1997) Treatment of Excess Thermodynamic Quantities for Liquid Mixtures. *J. Solution Chem.* **26**, 749-755.

DIN 51 757 (04,1994) Testing of Mineral Oils and Related Materials; Determination of Density; cited from *DMA 5000 Density Meter Manual* (Anton Paar GmbH, Graz, Austria, 1998)

Féron D. and Lambert I. (1992) Thermal Stability of Three Amines in Pressurized Water Reactor Secondary Systems. Laboratory and Loop Experiments. *J. Solution Chem.* **21**, 919-932.

Franck E.U. (1956) Hochverdichteter Wasserdampf II. Ionendissociation von KCl in H_2O bis 750°C. *Z. Phys. Chem.* **8**, 107-126.

Franck E.U. (1961) Überkritisches Wasser als Electrolytisches Lösungsmittel. *Angew. Chem.* **73**, 309-322.

Harvey A.H., Peskin A.P., and Klein S.A. (1996) *NIST Standard Reference Database 10, NIST/ASME Steam Properties Database.* Version 2.11.

Hawrylak B. (1999) Thermodynamics of Aqueous Methyldiethanolamine and Methyldiethanolammonium Chloride over a Wide Range of Temperature and Pressure: Apparent Molar Volumes, Heat Capacities, Compressibilities, and Excess Molar Heat Capacities. *M.Sc. Thesis* Memorial University of Newfoundland.

Hawrylak B., Burke S. E., and Palepu R. (2000) Partial Molar and Excess Volumes and Adiabatic Compressibilities of Binary Mixtures of Ethanolamines with Water. *J. Solution Chem.* **29**, 575-594.

H & D Fitzgerald Ltd. (2000) Technical Assessment of the Anton Paar DMA5000 density meter. URL: *http://www.density.co.uk*

Helgeson H.C. and Kirkham D.H. (1976) Theoretical Prediction of the Thermodynamic Behaviour of Aqueous Electrolytes at High Temperatures and Pressures: III Equation of State for Aqueous Species at Infinite Dilution. *Amer. J. Sci.* **276**, 97-240.

Helgeson H.C., Kirkham D.H., and Flowers G.C. (1981) Theoretical Predictions of the Thermodynamic Behaviour of Aqueous Electrolytes at High Pressures and Temperatures. IV. Calculation of Activity Coefficients, Osmotic Coefficients, and Apparent Molar and Standard and Relative Partial Molar Properties to 600°C and 5kb. *Amer. J. Sci.* **281**, 1249-1516.

Hershey J.P., Damesceno R., and Millero F.J. (1984) Densities and Compressibilities of Aqueous HCl and NaOH from 0 to 45°C. The Effect of Pressure on the Ionization of Water. *J. Solution Chem.* **13**, 825-848.

Hill P.G. (1990) A Unified Fundamental Equation for the Thermodynamic Properties of H_2O. *J. Phys. Chem. Ref. Data* **19**, 1233-1274.

Hnědkovský L., Majer V., and Wood R.H. (1995) Volumes and Heat Capacities of H_3BO_3(aq) at Temperatures from 298.15 K to 705 K and at Pressures to 35 MPa. *J. Chem. Thermodyn.* **27**, 801-814.

Hovey J.K., Hepler L.G., and Tremaine P.R. (1988) Thermodynamics of Aqueous Aluminate Ion: Standard Partial Molar Heat Capacities and Volumes of $Al(OH)_4^-(aq)$ from 10 to 55°C. *J. Phys. Chem.* **92**, 1323-1332.

Hsu C.H. and Li M.H. (1997) Viscosities of Aqueous Blended Amines. *J. Chem. Eng. Data* **42**, 714-720.

Johnson J.W., Oelkers E.H., and Helgeson H.C. (1992) SUPCRT92: A Software Package for Calculating the Standard Molar Thermodynamic Properties of Minerals, Gases, Aqueous Species, and Reactions from 1 to 5000 bar and 0 to 1000°C. *Computers and Geosciences* **18**, 899-947.

Kratky O., Leopold H., and Stabinger H. (1969) Density Determinations of Liquids and Gases to an Accuracy of 10^{-6} g·cm^{-3}, with a Sample Volume of only 0.6 cm^3 (English Title from Chem. Abs.) *Angew. Phys.* **27**, 273-277.

Lewis G.N. and Randall M. (1961) *Thermodynamics, 2nd edition*. Revised by Pitzer K.S.; Brewer, L. McGraw-Hill, New York.

Lewis G.G. and Wetton E.A.M. (1987) Assessment of Amines for the Control of Steam-Water Circuit pH and Two-phase Erosion Corrosion. *Central Electricity Generating Board Report* Report No. OED/STN/87/20083/M.

Lide D.R. (1990) *Handbook of Chemistry and Physics: 71st edition*. CRC Press, Inc., U.S.A.

Lumry R., Battistel E., and Jolicoeur C. (1982) Geometric Relaxation in Water: Its Role in Hydrophobic Hydration. *Faraday Symp. Chem. Soc.* **17**, 93-108.

Maham Y., Hepler L., Mather A.E., Hakin A.W., and Marriott R.A. (1997) Molar Heat Capacities of Alkanolamines from 299.1 to 397.8 K. *J. Chem. Soc., Faraday Trans.* **93**, 1747-1750.

Mains G.J., Larson J.W. and Hepler L.G. (1984) General Thermodynamic Analysis of the Contributions of Temperature-Dependent Chemical Equilibria to Heat Capacities of Ideal Gases and Ideal Associated solutions. *J. Phys. Chem.* **88**, 1257-1261.

Margules M. (1895) *Sitzber. Akad. Wiss. Wien., Math-naturw. Kl., Abt. IIa* **104**, 1243; cited by Pitzer K. S. (1995), *Thermodynamics, 3rd edition*. McGraw-Hill, New York.

Marshall W.L and Franck E.U. (1981) Ion Product of Water Substance, 0-1000°C, 1-10,000 bars, New International Formulation and its Background. *J. Phys. Chem. Ref. Data* **10**, 295-304.

Mesmer R.E., Marshall W.L., Palmer D.A., Simonson J.M., and Holmes H.F. (1988) Thermodynamics of Aqueous Association and Ionization Reactions at High Temperatures and Pressures. *J. Solution Chem.* **17**, 699-718.

Millero F.J. (1979) *Activity Coefficients in Electrolyte Solutions: Vol. 2.* Pytkowicz, M. ed., CRC Press, Boca Raton, FL.

Missenard F.A. (1965) Chimie Physique. - Méthode Additive Pour la Détermination de la Chaleur Molarire des Liquids. *C. R. Acad. Sci.* **260**, 5521-5523.

Pagé M., Huot J-Y., and Jolicoeur C. (1993) A Comprehensive Thermodynamic Investigation of Water-Ethanolamine Mixtures at 10, 25, and 40°C. *Can. J. Chem.* **71**, 1064-1072.

Perrin D.D. and Armarego W.L.F. (1988) *Purification of Laboratory Chemicals: 3rd edition.* Pergamon Press, Great Britain.

Perron G., Couture L., and Desnoyers J.E. (1992) Correlation of the Volumes and Heat Capacities of Solutions with their Solid-Liquid Phase Diagrams. *J. Solution Chem.* **21**, 433-443.

Picker P., Leduc P.A., Philip P.R., and Desnoyers J.E. (1971) Heat Capacity of Solutions by Flow Microcalorimetry. *J. Chem. Thermodyn.* **3**, 631-642.

Picker P., Tremblay E., and Jolicoeur C. (1974) A High Precision Digital Readout Flow Densimeter for Liquids. *J. Solution Chem.* **3**, 377-384.

Pitzer K.S. (1973) Thermodynamics of Electrolytes. I. Theoretical basis and General Equations. *J. Phys. Chem.*, 77, 268-277.

Pitzer K.S. (1991) *Activity Coefficients in Electrolyte Solutions, 2nd Edition.* CRC Press, Boca Raton.

Pitzer K.S. (1995) *Thermodynamics, 3rd edition.* McGraw-Hill, Inc., New York.

Poole P.H., Sciortino F., Grande T., Stanley H.E., and Angell C.A. (1994) Effect of hydrogen Bonds on the Thermodynamic Behavior of Liquid Water. *Physical Review Letters* **73**, 1632-1635.

Roux G., Roberts D., Perron G., and Desnoyers J.E. (1980) Microheterogeneity in Aqueous-Organic Solutions: Heat Capacities, Volumes and Expansibilities of Some Alcohols, Aminoalcohol and Tertiary Amines in Water. *J. Solution Chem.* **9**, 629-647.

Sartori G. and Savage D.W. (1983) Sterically Hindered Amines for CO_2 Removal from Gases. *Ind. Eng. Chem. Fundam.* **22**, 239-249.

Sedlbauer J., O'Connell J.P., and Wood R.H. (2000) A New Equation of State for Correlation and Prediction of Standard Molal Thermodynamic Properties of Aqueous Species at High Temperatures and Pressures. *Chemical Geology*. **163**, 43-63.

Simonson J.M., Mesmer R.E., and Rogers P.S.Z. (1989) The Enthalpy of Dilution and Apparent Molar Heat Capacity of NaOH(aq) to 523 K and 40 MPa. *J. Chem. Thermodyn.* **21**, 561-584.

Shock E.L. and Helgeson H.C. (1988) Calculation of the Thermodynamic and Transport Properties of Aqueous Species at High Pressures and Temperatures: Correlation Algorithms for Ionic Species and Equation of State Predictions to 5 kb and 1000°C. *Geochim. Cosmochim. Acta.* **52**, 2009-2036.

Shock E.L. and Helgeson H.C. (1990) Calculation of the Thermodynamic and Transport Properties of Aqueous Species at High Pressures and Temperatures: Standard Partial Molar Properties of Organic Species. *Geochim. Cosmochim. Acta.* **54**, 915-945.

Shvedov D. and Tremaine P. R. (1997) Thermodynamic Properties of Aqueous Dimethylamine and Dimethylammonium Chloride at Temperatures from 283 K to 523 K-Apparent Molar Volumes, Heat-Capacities, and Temperature-Dependence of Ionization. *J. Solution Chem.* **26**, 1113-1143.

Tanger J.C. and Helgeson H.C. (1988) Calculation of the Thermodynamic and Transport Properties of Aqueous Species at High Pressures and Temperatures: Revised Equations of State for the Standard Partial Molar Properties of Ions and Electrolytes. *Am. J. Sci.* **288**, 19-98.

Tremaine P.R., Sway K., and Barbero J.A., (1986) The Apparent Molar Heat Capacity of Aqueous Hydrochloric Acid from 10 to 140°C. *J. Solution Chem.* **15**, 1-22.

Tremaine P.R., Shvedov D., and Xiao C. (1997) Thermodynamic Properties of Aqueous Morpholine and Morpholinium Chloride at Temperatures from 10 to 300°C: Apparent Molar Volumes, Heat Capacities, and Temperature Dependence of Ionization. *J. Phys. Chem. B* **101**, 409-419.

Van Ness H.C. and Abbott M.M. (1982) *Classical Thermodynamics of Nonelectrolyte Solutions: With Applications to Phase Equilibria*. McGraw-Hill, New York.

Woolley E.M. and Hepler L.G. (1977) Heat Capacity of Weak Electrolyte and Ion Association Reactions: Method and Application to Aqueous $MgSO_4$ and HIO_3 at 298K. *Can. J. Chem.* **55**, 158-163.

Xiao C. and Tremaine P.R. (1996) Apparent Molar Heat Capacities and Volumes of $LaCl_3$(aq), $La(ClO_4)_3$(aq) and $Gd(ClO_4)_3$(aq) from 283 to 338K. *J. Chem. Thermodyn.* **41**, 1075-1078.

Xiao C. (1997) Thermodynamics of Aqueous Electrolytes and Hydrogen-Bonded Non-Electrolytes over a Wide Range of Temperature and Pressure. *Ph.D. Thesis* Memorial University of Newfoundland.

Xiao C. and Tremaine P.R. (1997) Apparent Molar Volumes of Aqueous Sodium Trifluoromethanesulfonate and Trifluoromethanesulfonic Acid from 283 K to 600 K and Pressures up to 20 MPa. *J. Solution Chem.* **26**, 277-294.

Xu S., Otto F.D., and Mather A.E. (1991) Physical Properties of Aqueous AMP Solutions. *J. Chem. Eng. Data* **36**, 71-75.

Young T.F. and Smith M.B. (1954) Thermodynamic Properties of Mixtures of Electrolytes in Aqueous Solutions. *J. Phys. Chem.* **58**, 716-724.

Appendices

Appendix 1: Experimental Data Tables of Apparent Molar Properties for Dilute Aqueous AMP and $AMPH^+Cl^-$ 146

Appendix 2: Experimental Data Tables of Molar Properties for Pure AMP and Pure Water 161

Appendix 3: Experimental Data Tables of Molar Properties and Excess Molar Properties for the System (AMP + H_2O) 163

Appendix 4: Excess Molar Properties of (MDEA + H_2O) Mixtures from the Literature 170

Table A.1.1 Apparent molar volumes $V_{\phi,2}$ for aqueous AMP (ACROS), where m_2 is the molality; and $(\rho-\rho_1^*)$ is the relative density to water.

m_2	α	$(\rho-\rho_1^*)\cdot10^3$	V_ϕ^{exp}	$V_{\phi,2}$
$mol\cdot kg^{-1}$		$g\cdot cm^{-3}$	$cm^3\cdot mol^{-1}$	$cm^3\cdot mol^{-1}$
		T = 283.15 K		
1.6972	0.0046	-0.3840	89.42	89.54
1.3358	0.0051	-0.4544	89.54	89.67
1.2896	0.0052	-0.4087	89.52	89.65
0.99641	0.0060	-0.5131	89.72	89.87
0.72305	0.0070	-0.5737	90.01	90.19
0.61302	0.0076	-0.5739	90.15	90.34
0.46018	0.0087	-0.5493	90.41	90.63
0.30888	0.0107	-0.3259	90.25	90.52
0.30888	0.0107	-0.3942	90.48	90.75
0.20020	0.0132	-0.2381	90.37	90.72
		T = 298.15 K		
1.6972	0.0051	-1.2440	90.25	90.38
1.3358	0.0057	-1.2267	90.44	90.58
1.2896	0.0058	-1.2293	90.47	90.62
0.99641	0.0066	-1.1310	90.65	90.81
0.72305	0.0078	-0.9627	90.83	91.02
0.61302	0.0084	-0.8709	90.91	91.12
0.46018	0.0097	-0.7302	91.06	91.31
0.30888	0.0119	-0.5011	91.08	91.38
0.20020	0.0147	-0.3312	91.10	91.47
		T = 313.15 K		
1.6972	0.0052	-2.3469	91.46	91.59
1.3358	0.0059	-2.0854	91.62	91.76
1.2896	0.0060	-2.0546	91.65	91.80
0.99641	0.0068	-1.7258	91.76	91.93
0.72305	0.0080	-1.3548	91.87	92.07
0.61302	0.0087	-1.1768	91.90	92.12
0.46018	0.0101	-0.9114	91.93	92.19
0.30888	0.0123	-0.6181	91.93	92.24
0.20020	0.0152	-0.4452	92.14	92.53

Table A.1.1 Continued.

m_2 / mol·kg^{-1}	α	$(\rho-\rho_1^*)\cdot10^3$ / g·cm^{-3}	V_ϕ^{exp} / cm^3·mol^{-1}	$V_{\phi,2}$ / cm^3·mol^{-1}
		T = 328.15 K		
1.6972	0.0053	-3.2431	92.70	92.84
1.3358	0.0060	-2.7674	92.82	92.98
1.3358	0.0060	-2.7473	92.81	92.96
1.2896	0.0061	-2.6294	92.78	92.93
1.2896	0.0061	-2.6175	92.77	92.92
0.99641	0.0069	-2.1671	92.87	93.05
0.72305	0.0081	-1.6496	92.94	93.14
0.61302	0.0088	-1.4259	92.96	93.19
0.46018	0.0102	-1.0605	92.90	93.17
0.30888	0.0124	-0.7714	93.07	93.40
0.20020	0.0154	-0.4534	92.81	93.20
		T = 328.15 K		
1.6972	0.0053	-3.0453	92.56	92.70
1.3358	0.0060	-2.6511	92.72	92.88
0.99641	0.0069	-1.7965	92.46	92.63
0.72305	0.0081	-1.7144	93.03	93.24
0.61302	0.0088	-1.4655	93.03	93.26
0.46018	0.0102	-1.1122	93.02	93.29
0.30888	0.0124	-0.7602	93.04	93.36
0.20020	0.0154	-0.4901	93.00	93.40

Table A.1.2 Apparent molar heat capacities $C_{p,\phi,2}$ for aqueous AMP (ACROS), where m_2 is the molality; α is the degree of dissociation; ρ_1^*, ρ, $c_{p,1}^*$, and c_p are the densities and specific heat capacities of pure water and solution, respectively; and C_p^{rel} is the chemical relaxation contribution.

m_2 / mol·kg^{-1}	α	$[1-c_p\cdot\rho/(c_{p,1}^*\cdot\rho_1^*)]\cdot10^3$	$C_{p,\phi}^{exp}$ / J·K^{-1}·mol^{-1}	C_p^{rel} / J·K^{-1}·mol^{-1}	$C_{p,\phi,2}$ / J·K^{-1}·mol^{-1}
		T = 283.15 K			
1.6972	0.0046	8.8169	349.84	0.39	350.5
1.3358	0.0051	6.9503	351.01	0.44	351.7
1.2896	0.0052	6.7206	350.94	0.45	351.7
0.99641	0.0060	5.2090	352.31	0.51	353.1
0.72305	0.0070	3.7730	354.08	0.60	355.0
0.61302	0.0076	3.1924	354.94	0.65	356.0
0.46018	0.0087	2.3554	356.70	0.75	357.9
0.30888	0.0107	1.5411	356.88	0.92	358.4
0.30888	0.0107	1.5745	357.37	0.92	358.9
0.20020	0.0132	1.0310	356.93	1.13	358.8
		T = 298.15 K			
1.6972	0.0051	5.5908	360.26	0.12	361.2
1.3358	0.0057	4.7010	360.42	0.13	361.4
1.2896	0.0058	4.4097	361.10	0.13	362.1
0.99641	0.0066	3.5685	361.46	0.15	362.6
0.72305	0.0078	2.6759	362.06	0.18	363.5
0.61302	0.0084	2.3115	362.24	0.19	363.8
0.46018	0.0097	1.7460	363.00	0.22	364.8
0.30888	0.0119	1.1619	363.42	0.27	365.6
0.20020	0.0147	0.7556	363.59	0.33	366.3

Table A.1.2 Continued.

m_2 / mol·kg^{-1}	α	$[1-c_p \cdot \rho/(c^*_{p,1} \cdot \rho^*_1)] \cdot 10^3$	$C^{exp}_{p,\phi}$ / J·K^{-1}·mol^{-1}	C^{rel}_p / J·K^{-1}·mol^{-1}	$C_{p,\phi,2}$ / J·K^{-1}·mol^{-1}
		T = 313.15 K			
1.6972	0.0052	3.8074	368.26	0.01	369.3
1.3358	0.0059	3.0673	368.97	0.01	370.1
1.2896	0.0060	3.0620	368.76	0.01	369.9
0.99641	0.0068	2.4487	369.11	0.01	370.4
0.72305	0.0080	2.0358	368.22	0.01	369.7
0.61302	0.0087	1.7288	368.45	0.01	370.1
0.46018	0.0101	1.5048	366.81	0.01	368.7
0.30888	0.0123	1.0211	366.81	0.02	369.1
		T = 328.15 K			
1.6972	0.0053	3.2092	372.90	0.02	373.8
1.3358	0.0060	2.5516	373.57	0.02	374.6
1.2896	0.0061	2.5904	372.95	0.02	374.0
1.2896	0.0061	2.4741	373.33	0.02	374.4
0.99641	0.0069	2.0185	373.50	0.03	374.7
0.72305	0.0081	1.5773	373.27	0.03	374.7
0.61302	0.0088	1.2805	373.87	0.03	375.4
0.46018	0.0102	1.0797	372.64	0.04	374.4
0.30888	0.0124	0.8400	371.87	0.05	374.1
		T = 328.15 K			
1.6972	0.0053	3.0511	372.78	0.02	373.7
1.3358	0.0060	2.4457	373.53	0.02	374.6
0.99641	0.0069	1.7585	372.97	0.03	374.2
0.72305	0.0081	1.5725	373.70	0.03	375.1
0.61302	0.0088	1.3868	373.39	0.03	375.0
0.46018	0.0102	1.2165	371.84	0.04	373.6
0.30888	0.0124	0.8422	371.68	0.05	373.9

Table A.1.3 Apparent molar volumes $V_{\phi,2}$ for aqueous AMP (Fluka), where m_2 is the molality of AMP; m_3 is the molality of NaOH; $(\rho-\rho_1^*)$ is the relative density of solution to water; $V_{\phi,3}$ is the apparent molar volume of NaOH; and $F_3 = m_3/(m_2 + m_3)$.

m_2 / mol·kg^{-1}	m_3 / mol·kg^{-1}	α	$(\rho-\rho_1^*)\cdot10^3$ / g·cm^{-3}	V_ϕ^{exp} / cm^3·mol^{-1}	$F_3V_{\phi,3}$ / cm^3·mol^{-1}	$V_{\phi,2}$ / cm^3·mol^{-1}
			T = 298.15 K			
0.21027	0.00418	0.00756	-0.2288	89.53	-0.11	91.62
0.28592	0.00407	0.00715	-0.3486	89.95	-0.08	91.49
0.36171	0.00380	0.00693	-0.4932	90.29	-0.06	91.47
0.42519	0.00182	0.00821	-0.6479	90.78	-0.02	91.40
0.45273	0.00396	0.00638	-0.6011	90.35	-0.05	91.35
0.65424	0.00200	0.00679	-0.9080	90.73	-0.02	91.19
0.96519	0.00196	0.00579	-1.1481	90.60	-0.01	90.94
1.2314	0.00174	0.00530	-1.2637	90.48	-0.01	90.74
1.5605	0.00206	0.00468	-1.3143	90.30	-0.01	90.54
			T = 298.15 K			
0.21027	0.00418	0.00756	-0.2366	89.57	-0.11	91.66
0.28592	0.00407	0.00715	-0.3582	89.99	-0.08	91.53
0.36171	0.00380	0.00693	-0.4722	90.23	-0.06	91.41
0.42519	0.00182	0.00821	-0.6256	90.72	-0.02	91.34
0.45273	0.00396	0.00638	-0.6270	90.41	-0.05	91.41
0.65424	0.00200	0.00679	-0.8960	90.71	-0.02	91.17
0.96519	0.00196	0.00579	-1.1442	90.60	-0.01	90.94
1.2314	0.00174	0.00530	-1.2516	90.47	-0.01	90.73
1.5605	0.00206	0.00468	-1.2894	90.28	-0.01	90.53

Table A.1.4 Apparent molar heat capacities $C_{p,\phi,2}$ for aqueous AMP (Fluka), where m_2 is the molality of AMP; m_3 is the molality of NaOH; α, ρ_1^*, ρ, $c_{p,1}^*$, and c_p denote the same as those in Table A.1.1; $C_{p,\phi,3}$ is the apparent molar heat capacity of NaOH; $F_3 = m_3/(m_2 + m_3)$; and C_p^{rel} is the chemical relaxation contribution.

m_2 / mol·kg^{-1}	m_3 / mol·kg^{-1}	α	$[1-c_p\rho/(c_{p,1}^*\rho_1^*)]\cdot10^3$	$C_{p,\phi}^{exp}$ / (J·K^{-1}·mol^{-1})	$F_3C_{p,\phi,3}$ / (J·K^{-1}·mol^{-1})	C_p^{rel} / (J·K^{-1}·mol^{-1})	$C_{p,\phi,2}$ / (J·K^{-1}·mol^{-1})
			T = 298.15 K				
0.21027	0.00418	0.00756	0.9836	353.60	-1.90	0.17	363.9
0.28592	0.00407	0.00715	1.3524	354.88	-1.37	0.16	362.6
0.36171	0.00380	0.00693	1.6284	357.07	-1.01	0.16	363.1
0.42519	0.00182	0.00821	1.8637	359.37	-0.42	0.19	362.8
0.45273	0.00396	0.00638	2.0088	357.41	-0.85	0.15	362.5
0.65424	0.00200	0.00679	2.8488	358.89	-0.30	0.15	361.5
0.96519	0.00196	0.00579	3.8078	359.69	-0.20	0.13	361.7
1.2314	0.00174	0.00530	4.5514	359.93	-0.14	0.12	361.5
1.5605	0.00206	0.00468	5.5757	359.33	-0.13	0.11	360.8

Table A.1.5 Apparent molar volumes $V_{\phi,2}$ for aqueous $AMPH^+Cl^-$, where subscripts "2" and "3" denote $AMPH^+Cl^-$ and HCl, respectively; $(\rho-\rho_1^*)$ is the relative density of solution to water; and $F_3 = m_3/(m_2 + m_3)$. Unless otherwise specified, $AMPH^+Cl^-$ solutions were made by mixing AMP (ACROS) solution with standard HCl solution.

m_2 / mol·kg^{-1}	m_3 / mol·kg^{-1}	$(\rho-\rho_1^*)\cdot10^3$ / g·cm^{-3}	V_ϕ^{exp} / cm^3·mol^{-1}	$F_3V_{\phi,3}$ / cm^3·mol^{-1}	$V_{\phi,2}$ / cm^3·mol^{-1}
		T = 283.15 K			
0.20255	0.00206	3.9668	104.92	0.18	105.81
0.30415	0.00309	5.8895	104.94	0.18	105.83
0.40486	0.00411	7.7465	104.97	0.18	105.86
0.50007	0.00508	9.4346	105.06	0.18	105.94
0.60337	0.00613	11.250	105.09	0.18	105.97
0.79726	0.00810	14.626	105.03	0.18	105.91
0.99522	0.01011	17.926	105.01	0.18	105.90
		T = 283.15 K			
0.20255	0.00206	3.9266	105.12	0.18	106.01
0.30415	0.00309	5.8832	104.96	0.18	105.85
0.40486	0.00411	7.7344	105.00	0.18	105.89
0.50007	0.00508	9.4526	105.02	0.18	105.91
0.60337	0.00613	11.299	105.00	0.18	105.89
0.79726	0.00810	14.601	105.06	0.18	105.95
0.99522	0.01011	17.915	105.03	0.18	105.91
		T = 298.15 K			
0.20255	0.00206	3.8700	105.63	0.19	106.52
0.30415	0.00309	5.7189	105.74	0.19	106.63
0.40486	0.00411	7.5131	105.79	0.19	106.68
0.50007	0.00508	9.1527	105.87	0.19	106.76
0.60337	0.00613	10.8941	105.93	0.19	106.82
0.79726	0.00810	14.1303	105.92	0.19	106.80
0.99522	0.01011	17.2556	105.97	0.19	106.86

Table A.1.5 Continued.

m_2 / mol·kg^{-1}	m_3 / mol·kg^{-1}	$(\rho-\rho_1^*)\cdot10^3$ / g·cm^{-3}	V_ϕ^{exp} / cm^3·mol^{-1}	$F_3V_{\phi,3}$ / cm^3·mol^{-1}	$V_{\phi,2}$ / cm^3·mol^{-1}
		T = 298.15 K[a]			
0.20657	0.00927	4.0631	102.78	0.79	106.56
0.31242	0.01402	6.0401	102.89	0.80	106.68
0.42416	0.01754	8.0711	103.20	0.74	106.70
0.54358	0.02439	10.2163	102.98	0.81	106.76
0.67006	0.02771	12.3978	103.26	0.75	106.75
0.89337	0.04008	16.1675	103.04	0.81	106.81
1.27177	0.05706	22.1517	103.07	0.82	106.84
1.82922	0.07564	30.0643	103.42	0.76	106.91
		T = 313.15 K			
0.20255	0.00206	3.8375	106.22	0.19	107.11
0.30415	0.00309	5.6477	106.40	0.19	107.29
0.40486	0.00411	7.4062	106.49	0.19	107.38
0.50007	0.00508	9.0502	106.51	0.19	107.40
0.60337	0.00613	10.7295	106.65	0.19	107.53
0.79726	0.00810	13.9374	106.60	0.19	107.49
0.99522	0.01011	17.0211	106.65	0.20	107.54
		T = 328.15 K			
0.20255	0.00206	3.8709	106.62	0.19	107.52
0.30415	0.00309	5.6330	107.03	0.19	107.93
0.40486	0.00411	7.4601	106.93	0.19	107.82
0.50007	0.00508	9.0737	107.04	0.19	107.93
0.60337	0.00613	10.8527	107.01	0.19	107.90
0.79726	0.00810	14.0057	107.09	0.19	107.98
0.99522	0.01011	17.0423	107.21	0.19	108.10

Table A.1.5 Continued.

m_2 / mol·kg^{-1}	m_3 / mol·kg^{-1}	$(\rho-\rho_1^*)\cdot10^3$ / g·cm^{-3}	V_ϕ^{exp} / cm^3·mol^{-1}	$F_3V_{\phi,3}$ / cm^3·mol^{-1}	$V_{\phi,2}$ / cm^3·mol^{-1}
		T = 328.15 K			
0.20212	0.00205	3.8481	106.70	0.19	107.59
0.20255	0.00206	3.8250	106.86	0.19	107.75
0.30415	0.00309	5.6764	106.88	0.19	107.78
0.30636	0.00311	5.7078	106.91	0.19	107.81
0.40486	0.00411	7.4444	106.97	0.19	107.87
0.50007	0.00508	9.0730	107.04	0.19	107.94
0.60337	0.00613	10.8074	107.09	0.19	107.98
0.79726	0.00810	13.9196	107.21	0.19	108.10
0.99522	0.01011	16.9490	107.31	0.19	108.21

[a] $AMPH^+Cl^-$ was obtained from Fluka.

Table A.1.6 Apparent molar heat capacities $C_{p,\phi,2}$ for aqueous $AMPH^+Cl^-$, where subscripts "2" and "3" denote $AMPH^+Cl^-$ and HCl, respectively; ρ_1^*, ρ, $c_{p,1}^*$, and c_p are the densities and specific heat capacities of pure water and solution, respectively; and $F_3 = m_3/(m_2 + m_3)$. Unless otherwise specified, $AMPH^+Cl^-$ solutions were made by mixing AMP (ACROS) solution with standard HCl solution.

m_2 / mol·kg^{-1}	m_3 / mol·kg^{-1}	$[1-c_p\cdot\rho/(c_{p,1}^*\cdot\rho_1^*)]\cdot10^3$	$C_{p,\phi}^{exp}$ / J·K^{-1}·mol^{-1}	$F_3C_{p,\phi,3}$ / J·K^{-1}·mol^{-1}	$C_{p,\phi,2}$ / J·K^{-1}·mol^{-1}
		T = 283.15 K			
0.40486	0.00411	18.2762	244.66	-1.33	248.49
0.50007	0.00508	22.2281	246.15	-1.31	249.97
0.60337	0.00613	26.8227	244.22	-1.29	248.00
0.79726	0.00810	35.1517	241.83	-1.25	245.55
0.99522	0.01011	43.5137	239.61	-1.22	243.27
		T = 283.15 K			
0.20255	0.00206	9.1972	248.18	-1.38	252.10
0.30415	0.00309	13.9014	244.19	-1.35	248.04
0.40486	0.00411	18.3693	243.79	-1.33	247.61
0.50007	0.00508	22.6572	242.24	-1.31	246.03
0.60337	0.00613	27.1139	241.74	-1.29	245.50
0.79726	0.00810	35.5063	239.96	-1.25	243.67
0.99522	0.01011	43.7933	238.37	-1.22	242.02
		T = 298.15 K			
0.20255	0.00206	8.7250	258.16	-1.15	261.95
0.30415	0.00309	13.0153	257.88	-1.13	261.64
0.40486	0.00411	17.1595	257.96	-1.11	261.71
0.50007	0.00508	21.0959	257.37	-1.10	261.09
0.60337	0.00613	25.1463	257.93	-1.08	261.65
0.79726	0.00810	32.7578	256.96	-1.06	260.64
0.99522	0.01011	40.2564	256.49	-1.04	260.15

Table A.1.6 Continued.

m_2 / mol·kg^{-1}	m_3 / mol·kg^{-1}	$[1-c_p \cdot \rho/(c^*_{p,1} \cdot \rho^*_1)] \cdot 10^3$	$C^{exp}_{p,\phi}$ / J·K^{-1}·mol^{-1}	$F_3C_{p,\phi,3}$ / J·K^{-1}·mol^{-1}	$C_{p,\phi,2}$ / J·K^{-1}·mol^{-1}
		T = 298.15 K [a]			
0.20657	0.00927	9.3731	242.80	-4.91	258.82
0.31242	0.01402	13.9709	243.94	-4.81	259.91
0.42416	0.01754	18.5482	246.60	-4.37	261.36
0.54358	0.02439	23.4624	246.45	-4.65	262.37
0.67006	0.02771	28.3693	248.21	-4.24	262.88
0.89337	0.04008	37.4069	245.85	-4.48	261.56
1.27177	0.05706	51.5148	245.39	-4.33	260.93
1.82922	0.07564	70.5244	245.88	-3.85	260.05
		T = 313.15 K			
0.20255	0.00206	8.4899	263.18	-1.03	266.90
0.30415	0.00309	12.4710	265.96	-1.00	269.67
0.40486	0.00411	16.5609	264.91	-0.99	268.60
0.50007	0.00508	20.4005	263.75	-0.97	267.42
0.60337	0.00613	24.2241	265.29	-0.96	268.95
0.79726	0.00810	31.3940	265.14	-0.94	268.78
0.99522	0.01011	38.4172	265.44	-0.92	269.06
		T = 328.15 K			
0.20212	0.00205	8.2980	266.14	-0.97	269.82
0.20255	0.00206	8.2865	267.39	-0.97	271.09
0.30415	0.00309	12.2965	267.71	-0.95	271.39
0.30636	0.00311	12.3465	268.34	-0.95	272.03
0.40486	0.00411	16.0666	269.49	-0.93	273.17
0.50007	0.00508	19.5686	270.53	-0.91	274.19
0.60337	0.00613	23.2595	271.50	-0.89	275.16
0.79726	0.00810	30.2692	271.30	-0.87	274.94
0.99522	0.01011	37.0331	271.86	-0.85	275.48

[a] $AMPH^+Cl^-$ was obtained from Fluka.

Table A.1.7 Apparent molar volumes $V_{\phi,2}$ for aqueous AMP (Fluka) at high temperatures, where subscripts "2" and "3" denote AMP and NaOH, respectively; $(\rho-\rho_1^*)$ is the relative density of solution to water; $V_{\phi,3}$ is the apparent molar volume of NaOH; and $F_3 = m_3/(m_2 + m_3)$.

m_2 / mol·kg^{-1}	m_3 / mol·kg^{-1}	α	$(\rho-\rho_1^*)\cdot10^3$ / g·cm^{-3}	V_ϕ^{exp} / cm^3·mol^{-1}	$F_3V_{\phi,3}$ / cm^3·mol^{-1}	$V_{\phi,2}$ / cm^3·mol^{-1}
			T = 378.79 K, p = 20.36 MPa			
0.21027	0.00418	0.0069	-0.4958	94.04	-0.47	96.75
0.36171	0.00380	0.0064	-1.2178	95.68	-0.25	97.27
0.45273	0.00396	0.0059	-1.4941	95.73	-0.21	97.08
0.65424	0.00200	0.0064	-2.5452	96.78	-0.07	97.48
0.96519	0.00196	0.0054	-3.5439	96.70	-0.05	97.22
1.23142	0.00174	0.0050	-4.4513	96.76	-0.03	97.19
1.56048	0.00206	0.0044	-5.4778	96.76	-0.03	97.14
			T = 429.97 K, p = 19.47 MPa			
0.28592	0.00407	0.0038	-1.3137	101.49	-0.49	103.68
0.65424	0.00200	0.0041	-3.4164	103.11	-0.11	103.80
0.96519	0.00196	0.0036	-5.3676	103.79	-0.07	104.31
1.23142	0.00174	0.0033	-6.1330	103.23	-0.05	103.64
			T = 480.37 K, p = 19.62 MPa			
0.65424	0.00200	0.0022	-3.8596	110.59	-0.16	111.28
0.96519	0.00196	0.0020	-5.8891	111.18	-0.11	111.69
1.23142	0.00174	0.0019	-7.1479	110.99	-0.08	111.39
1.56048	0.00206	0.0016	-9.0634	111.25	-0.07	111.61
			T = 530.32 K, p = 19.61 MPa			
0.21027	0.00418	0.00054	-1.2244	118.43	-1.69	122.58
0.65424	0.00200	0.00090	-4.4573	121.60	-0.26	122.34
0.96519	0.00196	0.00084	-6.5978	122.03	-0.18	122.56
1.23142	0.00174	0.00084	-8.1831	122.02	-0.12	122.42
1.56048	0.00206	0.00073	-10.1911	122.16	-0.11	122.52

Table A.1.7 Continued.

m_2 / mol·kg^{-1}	m_3 / mol·kg^{-1}	α	$(\rho-\rho_1^*)\cdot10^3$ / g·cm^{-3}	V_ϕ^{exp} / cm^3·mol^{-1}	$F_3V_{\phi,3}$ / cm^3·mol^{-1}	$V_{\phi,2}$ / cm^3·mol^{-1}
			T = 555.59K, p = 19.63 MPa			
0.21027	0.00418	0.00027	-1.4847	127.15	-2.27	132.04
0.65424	0.00200	0.00049	-5.2986	130.83	-0.35	131.66
0.96519	0.00196	0.00047	-7.5506	130.82	-0.24	131.39
1.23142	0.00174	0.00048	-9.4186	130.89	-0.16	131.32
1.56048	0.00206	0.00041	-11.6987	131.03	-0.15	131.42
			T = 480.89 K, p = 10.21 MPa			
0.21027	0.00418	0.0015	-1.2655	110.38	-1.04	113.78
0.36171	0.00380	0.0016	-2.0123	110.46	-0.56	112.32
0.45273	0.00396	0.0015	-2.7949	111.49	-0.46	113.06
0.65424	0.00200	0.0020	-4.0112	111.96	-0.16	112.64
0.96519	0.00196	0.0018	-5.8668	112.20	-0.11	112.69
1.23142	0.00174	0.0018	-7.5482	112.53	-0.08	112.92
1.56048	0.00206	0.0015	-9.2381	112.47	-0.07	112.83
			T = 530.88 K, p = 10.33 MPa			
0.21027	0.00418	0.00047	-1.3967	121.53	-1.71	125.75
0.65424	0.00200	0.00079	-5.5104	126.20	-0.27	126.95
0.96519	0.00196	0.00075	-7.5534	125.65	-0.18	126.17
1.23142	0.00174	0.00075	-9.5247	125.86	-0.12	126.26
1.56048	0.00206	0.00065	-11.6475	125.78	-0.12	126.14

Table A.1.8 Apparent molar volumes $V_{\phi,2}$ for aqueous $AMPH^+Cl^-$ (Fluka) at high temperatures, where subscripts "2" and "3" denote $AMPH^+Cl^-$ and HCl, respectively; $(\rho-\rho_1^*)$ is the relative density of solution to water; and $F_3 = m_3/(m_2 + m_3)$.

m_2 / mol·kg^{-1}	m_3 / mol·kg^{-1}	$(\rho-\rho_1^*)\cdot10^3$ / g·cm^{-3}	V_ϕ^{exp} / cm^3·mol^{-1}	$F_3V_{\phi,3}$ / cm^3·mol^{-1}	$V_{\phi,2}$ / cm^3·mol^{-1}
		T = 378.75 K, p = 20.36 MPa			
0.10278	0.00461	2.2617	103.44	0.69	107.36
0.20657	0.00927	4.4133	103.87	0.69	107.81
0.31242	0.01402	6.5928	103.90	0.69	107.84
0.54358	0.02439	10.6719	104.97	0.69	108.95
0.89337	0.04008	16.4168	105.62	0.69	109.64
1.27177	0.05706	22.5631	105.60	0.69	109.62
1.82922	0.07564	29.6373	106.63	0.64	110.37
		T = 434.69 K, p = 20.31 MPa			
0.10278	0.00461	2.4461	104.97	0.49	109.17
0.20657	0.00927	4.7279	105.95	0.49	110.20
0.31242	0.01402	7.5572	104.23	0.49	108.40
0.54358	0.02439	12.4762	105.13	0.49	109.33
0.89337	0.04008	19.6003	105.48	0.49	109.71
1.27177	0.05706	26.5605	105.89	0.49	110.13
1.82922	0.07564	35.0368	107.08	0.45	111.04
		T = 480.37 K, p = 19.62 MPa			
0.10278	0.00461	3.4565	97.08	0.15	101.27
0.20657	0.00927	6.3379	100.46	0.15	104.81
0.42416	0.01754	12.0197	102.95	0.14	107.05
0.89337	0.04008	23.7175	103.60	0.15	108.09
1.27177	0.05706	31.8958	104.45	0.15	108.98
1.82922	0.07564	41.8641	106.18	0.14	110.42

Table A.1.8 Continued.

m_2 / mol·kg^{-1}	m_3 / mol·kg^{-1}	$(\rho-\rho_1^*)\cdot10^3$ / g·cm^{-3}	V_ϕ^{exp} / cm^3·mol^{-1}	$F_3V_{\phi,3}$ / cm^3·mol^{-1}	$V_{\phi,2}$ / cm^3·mol^{-1}
		T = 530.32 K, p = 19.61 MPa			
0.10278	0.00461	4.6782	83.54	-0.68	88.01
0.42416	0.01754	15.6059	95.23	-0.63	99.82
0.54358	0.02439	19.5287	95.85	-0.68	100.86
0.89337	0.04008	29.5938	98.68	-0.68	103.82
1.27177	0.05706	39.6184	100.28	-0.68	105.49
1.82922	0.07564	51.6760	103.10	-0.63	108.02
		T = 480.89 K, p = 10.21 MPa			
0.20657	0.00927	6.5302	99.78	0.09	104.16
0.31242	0.01402	9.2590	101.99	0.09	106.47
0.54358	0.02439	15.3884	102.95	0.09	107.48
0.89337	0.04008	23.8465	104.00	0.09	108.57
1.27177	0.05706	31.9043	105.05	0.09	109.67
1.82922	0.07564	42.4410	106.36	0.08	110.68
		T = 530.88 K, p = 10.33 MPa			
0.20657	0.00927	8.8933	87.02	-0.90	91.86
0.31242	0.01402	12.2675	92.31	-0.90	97.39
0.54358	0.02439	20.6061	93.37	-0.90	98.50
0.89337	0.04008	31.2024	96.52	-0.90	101.79
1.27177	0.05706	41.7886	98.28	-0.90	103.63
1.82922	0.07564	54.8550	101.04	-0.83	106.08

Table A.2.1 Experimental molar heat capacities of water $C^*_{p,m,1}$ and AMP $C^*_{p,m,2}$.

T	$C^*_{p,m,1}$	$C^*_{p,m,2}$
K	$J \cdot K^{-1} \cdot mol^{-1}$	$J \cdot K^{-1} \cdot mol^{-1}$
278.15	75.74	
283.15	75.50	
288.15	75.29	
293.15	75.11	
298.15	74.96	
303.15	74.83	243.98
308.15	74.74	245.53
313.15	74.69	247.15
318.15	74.66	249.11
323.15	74.65	250.41
328.15	74.68	252.42
333.15	74.73	254.65
338.15	74.81	257.10
343.15	74.92	259.64
348.15	75.06	262.31
353.15	75.25	265.23
358.15	75.44	268.27
363.15	75.69	271.29
368.15	75.97	273.79

Table A.2.2 Densities ρ and molar volumes V_m^* of pure AMP.

T / (K)	ρ / (g·cm^{-3})	(ρ - ρ_1^*) / (g·cm^{-3})	V_m^* / (cm^3·mol^{-1})
353.147	0.882754	-0.089031	100.976
348.153	0.887180	-0.087658	100.472
343.151	0.891586	-0.086173	99.976
338.155	0.895953	-0.084593	99.488
333.155	0.900288	-0.082903	99.009
328.155	0.904586	-0.081102	98.539
323.154	0.908855	-0.079175	98.076
318.154	0.913095	-0.077113	97.621
313.153	0.917304	-0.074908	97.173
308.154	0.921482	-0.072547	96.732
303.155	0.925723	-0.069922	96.289

Table A.3.1 Molar heat capacities $C_{p,m}$ and excess molar heat capacities $C^E_{p,m}$ of aqueous AMP.

x_2	$C_{p,m}$ / $J \cdot K^{-1} \cdot mol^{-1}$	$C^E_{p,m}$ / $J \cdot K^{-1} \cdot mol^{-1}$	$C_{p,m}$ / $J \cdot K^{-1} \cdot mol^{-1}$	$C^E_{p,m}$ / $J \cdot K^{-1} \cdot mol^{-1}$	$C_{p,m}$ / $J \cdot K^{-1} \cdot mol^{-1}$	$C^E_{p,m}$ / $J \cdot K^{-1} \cdot mol^{-1}$
	T = 278.15 K		T = 283.15 K		T = 288.15 K	
0.06209	90.39	4.337	91.40	5.518	91.73	5.947
0.10797	99.68	6.026	100.96	7.467	101.47	8.051
0.18173	109.26	3.383	110.95	5.229	111.92	6.242
0.21466	112.65	1.320	114.53	3.347	115.71	4.556
0.29765	122.56	-2.517	124.89	-0.065	126.48	1.529
0.44499	142.64	-6.847	145.44	-3.948	147.46	-1.988
0.52581	155.23	-7.652	158.08	-4.713	160.18	-2.712
0.62683			173.37	-6.176	175.51	-4.181
0.74485			191.80	-7.319	193.87	-5.435
0.81506					207.24	-3.748
	T = 293.15 K		T = 298.15 K		T = 303.15 K	
0.06209	91.91	6.159	92.01	6.258	92.07	6.282
0.10797	101.78	8.376	102.01	8.558	102.17	8.631
0.18173	112.72	7.004	113.43	7.602	114.07	8.071
0.21466	116.73	5.521	117.67	6.317	118.55	6.991
0.29765	127.93	2.864	129.31	4.037	130.67	5.094
0.44499	149.35	-0.312	151.16	1.162	152.95	2.495
0.52581	162.15	-0.999	164.07	0.510	166.00	1.894
0.62683	177.52	-2.495	179.49	-1.016	181.47	0.302
0.74485	195.82	-3.893	197.75	-2.563	199.73	-1.363
0.81506	208.36	-3.076	210.11	-1.979	212.02	-0.939
0.90240					228.27	0.567

Table A.3.1 Continued.

x_2	$C_{p,m}$ / $J \cdot K^{-1} \cdot mol^{-1}$	$C^E_{p,m}$ / $J \cdot K^{-1} \cdot mol^{-1}$	$C_{p,m}$ / $J \cdot K^{-1} \cdot mol^{-1}$	$C^E_{p,m}$ / $J \cdot K^{-1} \cdot mol^{-1}$	$C_{p,m}$ / $J \cdot K^{-1} \cdot mol^{-1}$	$C^E_{p,m}$ / $J \cdot K^{-1} \cdot mol^{-1}$
	T = 308.15 K		T = 313.15 K		T = 318.15 K	
0.06209	92.11	6.247	92.11	6.153	92.11	6.034
0.10797	102.30	8.636	102.41	8.572	102.50	8.473
0.18173	114.67	8.446	115.23	8.730	115.77	8.957
0.21466	119.39	7.568	120.17	8.022	120.94	8.419
0.29765	131.98	6.028	133.25	6.849	134.39	7.482
0.44499	154.69	3.665	156.38	4.685	158.06	5.606
0.52581	167.84	3.068	169.64	4.073	171.43	4.974
0.62683	183.43	1.462	185.39	2.482	187.31	3.339
0.74485	201.70	-0.349	203.70	0.532	205.65	1.223
0.81506	213.94	-0.063	215.89	0.667	217.86	1.261
0.90240	229.33	0.469	231.17	0.952	233.10	1.355
	T = 323.15 K		T = 328.15 K		T = 333.15 K	
0.06209	92.11	5.895	92.13	5.763	92.17	5.632
0.10797	102.60	8.352	102.73	8.229	102.87	8.100
0.18173	116.31	9.139	116.86	9.290	117.40	9.404
0.21466	121.69	8.744	122.44	9.033	123.17	9.259
0.29765	135.56	8.075	136.75	8.636	137.90	9.103
0.44499	159.84	6.541	161.64	7.414	163.39	8.157
0.52581	173.42	5.959	175.44	6.891	177.35	7.614
0.62683	189.35	4.195	191.48	5.022	193.59	5.733
0.74485	207.74	1.905	209.96	2.590	212.28	3.254
0.81506	219.96	1.817	222.21	2.397	224.55	2.920
0.90240	235.20	1.758	237.43	2.137	239.79	2.499

Table A.3.1 Continued.

x_2	$C_{p,m}$ / J·K^{-1}·mol^{-1}	$C^E_{p,m}$ / J·K^{-1}·mol^{-1}	$C_{p,m}$ / J·K^{-1}·mol^{-1}	$C^E_{p,m}$ / J·K^{-1}·mol^{-1}	$C_{p,m}$ / J·K^{-1}·mol^{-1}	$C^E_{p,m}$ / J·K^{-1}·mol^{-1}
	T = 338.15 K		T = 343.15 K		T = 348.15 K	
0.06209	92.24	5.513	92.33	5.405	92.45	5.307
0.10797	103.05	7.987	103.26	7.882	103.49	7.778
0.18173	117.98	9.512	118.56	9.594	119.16	9.665
0.21466	123.93	9.482	124.70	9.675	125.49	9.845
0.29765	139.11	9.580	140.33	10.017	141.56	10.416
0.44499	165.14	8.832	166.94	9.485	168.75	10.083
0.52581	179.40	8.403	181.48	9.141	183.57	9.810
0.62683	195.77	6.418	197.97	7.017	200.26	7.629
0.74485	214.62	3.811	216.99	4.298	219.46	4.784
0.81506	226.94	3.373	229.39	3.767	231.97	4.180
0.90240	242.26	2.820	244.81	3.099	247.45	3.347
	T = 353.15 K		T = 358.15 K		T = 363.15 K	
0.06209	92.62	5.248	92.82	5.201	93.02	5.134
0.10797	103.79	7.721	104.12	7.675	104.46	7.613
0.18173	119.80	9.749	120.46	9.828	121.12	9.874
0.21466	126.31	10.019	127.11	10.145	127.95	10.270
0.29765	142.81	10.792	144.07	11.138	145.31	11.431
0.44499	170.66	10.721	172.58	11.308	174.46	11.809
0.52581	185.67	10.414	187.81	11.002	189.91	11.472
0.62683	202.64	8.243	205.06	8.814	207.44	9.281
0.74485	222.03	5.269	224.66	5.715	227.33	6.119
0.81506	234.69	4.625	237.44	4.994	240.23	5.311
0.90240	250.27	3.648	253.22	3.975	256.15	4.178

Table A.3.1 Continued.

x_2	$C_{p,m}$ / $J \cdot K^{-1} \cdot mol^{-1}$	$C^E_{p,m}$ / $J \cdot K^{-1} \cdot mol^{-1}$
	T = 368.15 K	
0.06209	93.29	5.125
0.10797	104.70	7.436
0.18173	121.65	9.762
0.21466	128.63	10.218
0.29765	146.42	11.542
0.44499	176.06	11.970
0.52581	191.90	11.779
0.62683	209.57	9.418
0.74485	229.81	6.252
0.81506	242.90	5.416
0.90240	258.97	4.170

Table A.3.2 Relative densities ($\rho - \rho_1^*$) and excess molar volumes V_m^E of aqueous AMP.

x_2	$(\rho - \rho_1^*)$ / g·cm^{-3}	V_m^E / cm^3·mol^{-1}	$(\rho - \rho_1^*)$ / g·cm^{-3}	V_m^E / cm^3·mol^{-1}	$(\rho - \rho_1^*)$ / g·cm^{-3}	V_m^E / cm^3·mol^{-1}
	T = 293.15 K		T = 298.15 K		T = 303.15 K	
0.12042	0.000867	-0.764	-0.001348	-0.743	-0.003384	-0.724
0.13505	0.000085	-0.833	-0.002289	-0.810	-0.004470	-0.789
0.20286	-0.006020	-1.051	-0.008732	-1.024	-0.011237	-1.001
0.30836	-0.017569	-1.180	-0.020357	-1.159	-0.022942	-1.141
0.44335	-0.030528	-1.162	-0.033323	-1.149	-0.035924	-1.138
0.48809	-0.034325	-1.122	-0.037125	-1.111	-0.039730	-1.102
0.61844	-0.044027	-0.939	-0.046831	-0.935	-0.049455	-0.931
0.69131	-0.048706	-0.801	-0.051527	-0.799	-0.054168	-0.796
0.84726	-0.057315	-0.436	-0.060240	-0.431	-0.062915	-0.431
0.92429	-0.061004	-0.225	-0.063968	-0.218	-0.066654	-0.220
0.95563			-0.065413	-0.125	-0.068106	-0.126
	T = 308.15 K		T = 313.15 K		T = 318.15 K	
0.12042	-0.005262	-0.707	-0.007004	-0.693	-0.008622	-0.679
0.13505	-0.006486	-0.770	-0.008351	-0.754	-0.010082	-0.740
0.20286	-0.013555	-0.980	-0.015711	-0.962	-0.017716	-0.945
0.30836	-0.025353	-1.124	-0.027600	-1.109	-0.029703	-1.096
0.44335	-0.038346	-1.128	-0.040616	-1.120	-0.042739	-1.113
0.48809	-0.042164	-1.094	-0.044435	-1.088	-0.046566	-1.082
0.61844	-0.051907	-0.927	-0.054200	-0.925	-0.056343	-0.923
0.69131	-0.056642	-0.794	-0.058944	-0.793	-0.061104	-0.792
0.84726	-0.065415	-0.431	-0.067753	-0.431	-0.069938	-0.432
0.92429	-0.069171	-0.220	-0.071517	-0.221	-0.073712	-0.222
0.95563	-0.070631	-0.127	-0.072989	-0.127	-0.075188	-0.128

Table A.3.2 Continued.

x_2	$(\rho - \rho_1^*)$ / g·cm^{-3}	V_m^E / cm^3·mol^{-1}	$(\rho - \rho_1^*)$ / g·cm^{-3}	V_m^E / cm^3·mol^{-1}	$(\rho - \rho_1^*)$ / g·cm^{-3}	V_m^E / cm^3·mol^{-1}
	T = 323.15 K		T = 328.15 K		T = 333.15 K	
0.12042	-0.010134	-0.668	-0.011545	-0.657	-0.012869	-0.647
0.13505	-0.011698	-0.726	-0.013212	-0.714	-0.014625	-0.704
0.20286	-0.019591	-0.930	-0.021345	-0.916	-0.022994	-0.904
0.30836	-0.031674	-1.084	-0.033525	-1.073	-0.035269	-1.063
0.44335	-0.044732	-1.106	-0.046605	-1.100	-0.048373	-1.094
0.48809	-0.048563	-1.077	-0.050440	-1.073	-0.052211	-1.068
0.61844	-0.058355	-0.921	-0.060245	-0.920	-0.062021	-0.919
0.69131	-0.063125	-0.792	-0.065025	-0.792	-0.066806	-0.791
0.84726	-0.071980	-0.433	-0.073894	-0.434	-0.075689	-0.435
0.92429	-0.075764	-0.224	-0.077686	-0.225	-0.079484	-0.226
0.95563	-0.077242	-0.130	-0.079168	-0.131	-0.080970	-0.132
	T = 338.15 K		T = 343.15 K		T = 348.15 K	
0.12042	-0.014116	-0.638	-0.015287	-0.630	-0.016398	-0.621
0.13505	-0.015954	-0.694	-0.017205	-0.684	-0.018391	-0.675
0.20286	-0.024542	-0.892	-0.026000	-0.881	-0.027383	-0.871
0.30836	-0.036916	-1.054	-0.038468	-1.044	-0.039945	-1.035
0.44335	-0.050042	-1.089	-0.051617	-1.083	-0.053113	-1.077
0.48809	-0.053879	-1.064	-0.055458	-1.059	-0.056954	-1.053
0.61844	-0.063695	-0.917	-0.065274	-0.914	-0.066766	-0.911
0.69131	-0.068486	-0.790	-0.070063	-0.789	-0.071556	-0.786
0.84726	-0.077372	-0.435	-0.078951	-0.435	-0.080438	-0.433
0.92429	-0.081168	-0.227	-0.082746	-0.227	-0.084232	-0.225
0.95563	-0.082655	-0.132	-0.084238	-0.132	-0.085724	-0.130

Table A.3.2 Continued.

x_2	$(\rho - \rho_1^*)$ / g·cm^{-3}	V_m^E / cm^3·mol^{-1}
	T = 353.15 K	
0.12042	-0.017446	-0.614
0.13505	-0.019504	-0.667
0.20286	-0.028683	-0.861
0.30836	-0.041337	-1.026
0.44335	-0.054526	-1.069
0.48809	-0.058367	-1.047
0.61844	-0.068171	-0.906
0.69131	-0.072959	-0.782
0.84726	-0.081834	-0.429
0.92429	-0.085618	-0.221
0.95563	-0.087110	-0.126

Appendix 4: Excess Molar Properties of (MDEA + H_2O) Mixtures from the Literature

Methyldiethanolamine (MDEA) is another alkanolamine that has been used in gas processing plants. As shown in Figure A.4.1, it is a tertiary amine that cannot form carbamates, so the bicarbonate formation is dominant in reacting with carbon dioxide. MDEA is commonly used for the selective removal of H_2S from gas streams which contain both CO_2 and H_2S (Blanc *et al.*, 1981). This process takes advantage of the difference in reaction rates between CO_2 and H_2S, as well as the high H_2S absorption capacity of MDEA and its ease of regeneration.

Hawrylak (1999) measured excess molar heat capacities of aqueous MDEA, using the same equipment (CSC 4100 DSC) and method as described in this study. These excess heat capacities were plotted in Figure A.4.2, and used to calculated reduced excess heat capacities at four temperatures, as shown in Figure A.4.4. Hawrylak *et al.* (2000) also reported the excess molar volumes V_m^E of aqueous MDEA at 298.15 K plotted in Figure A.4.3.

The figures for (MDEA + H_2O) shown in this appendix are presented for comparison with the properties of (AMP + H_2O) in Figures 4.2, 4.3 and 4.6.

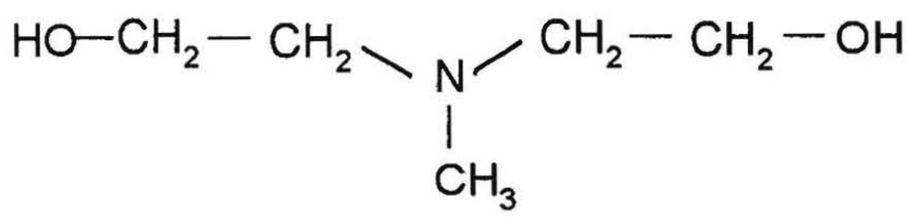

Figure A.4.1 Structure of methyldiethanolamine (MDEA).

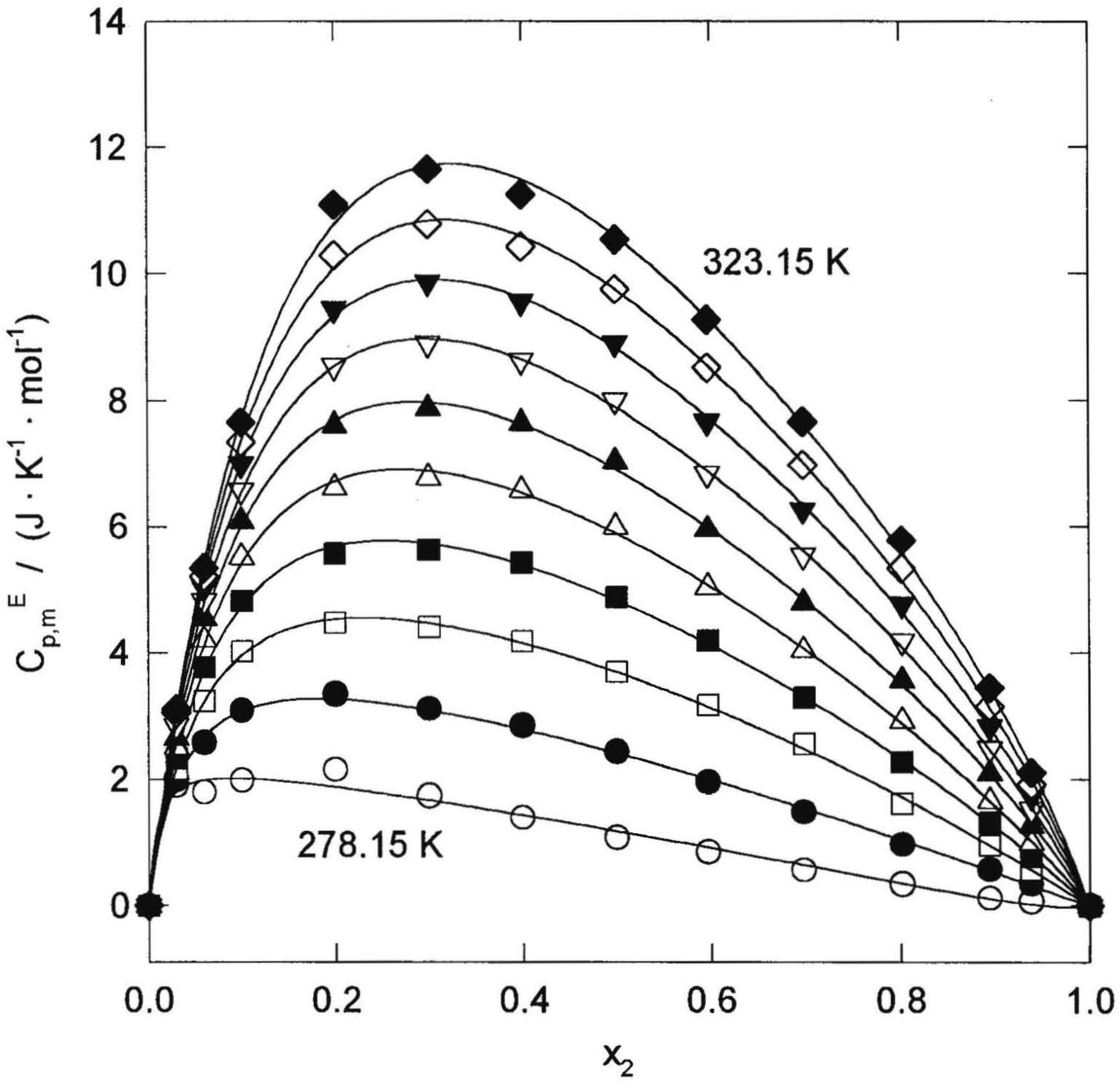

Figure A.4.2 Excess molar heat capacities $C_{p,m}^{E}$ of aqueous MDEA from 278.15 K to 323.15 K (at 5 K intervals) plotted against mole fraction (Hawrylak, 1999). Symbols are experimental results, and lines are fitted values of Equation (4.8).

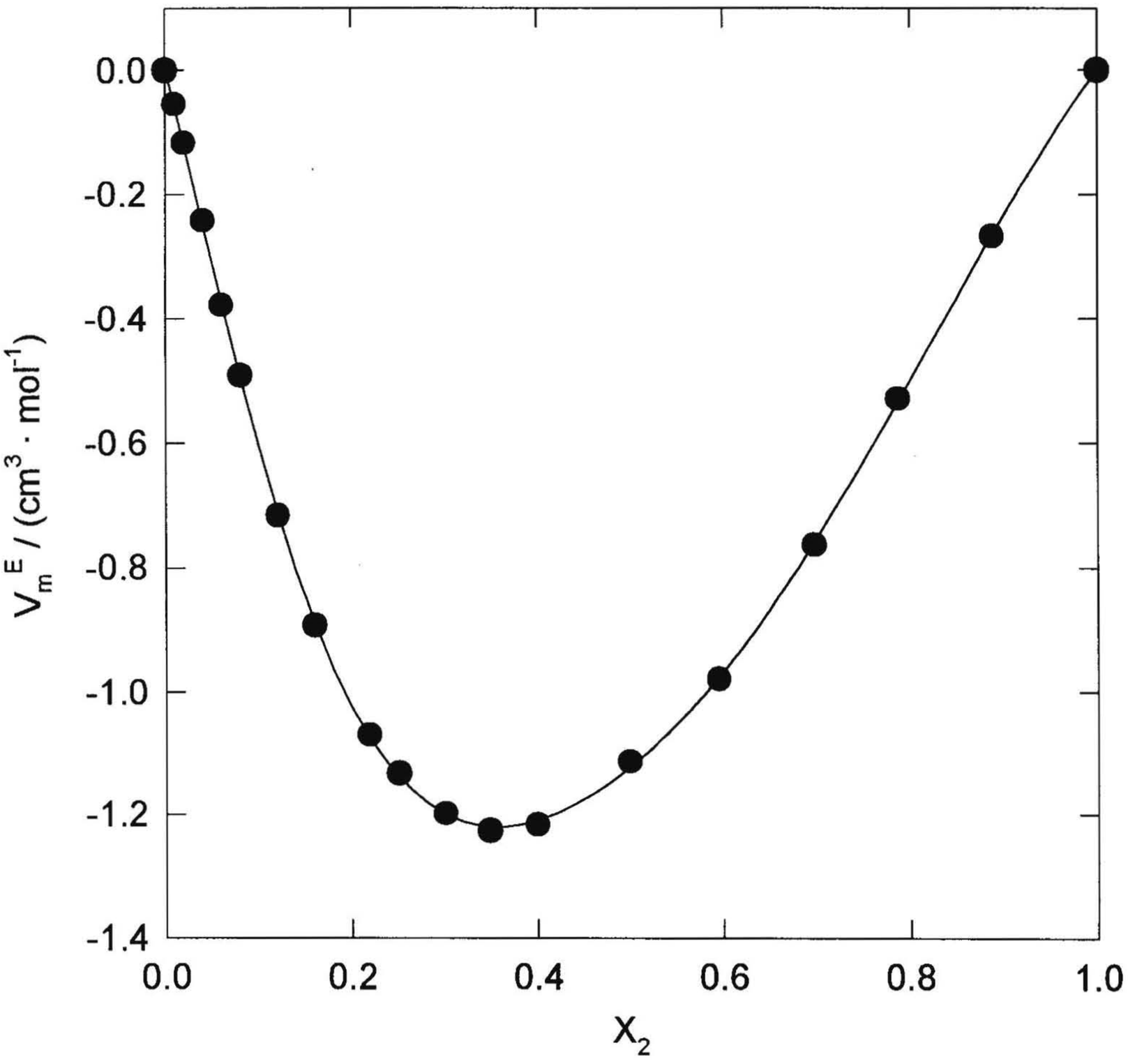

Figure A.4.3 Excess molar volumes V_m^E of aqueous MDEA at 298.15 K (Hawrylak *et al.*, 2000).

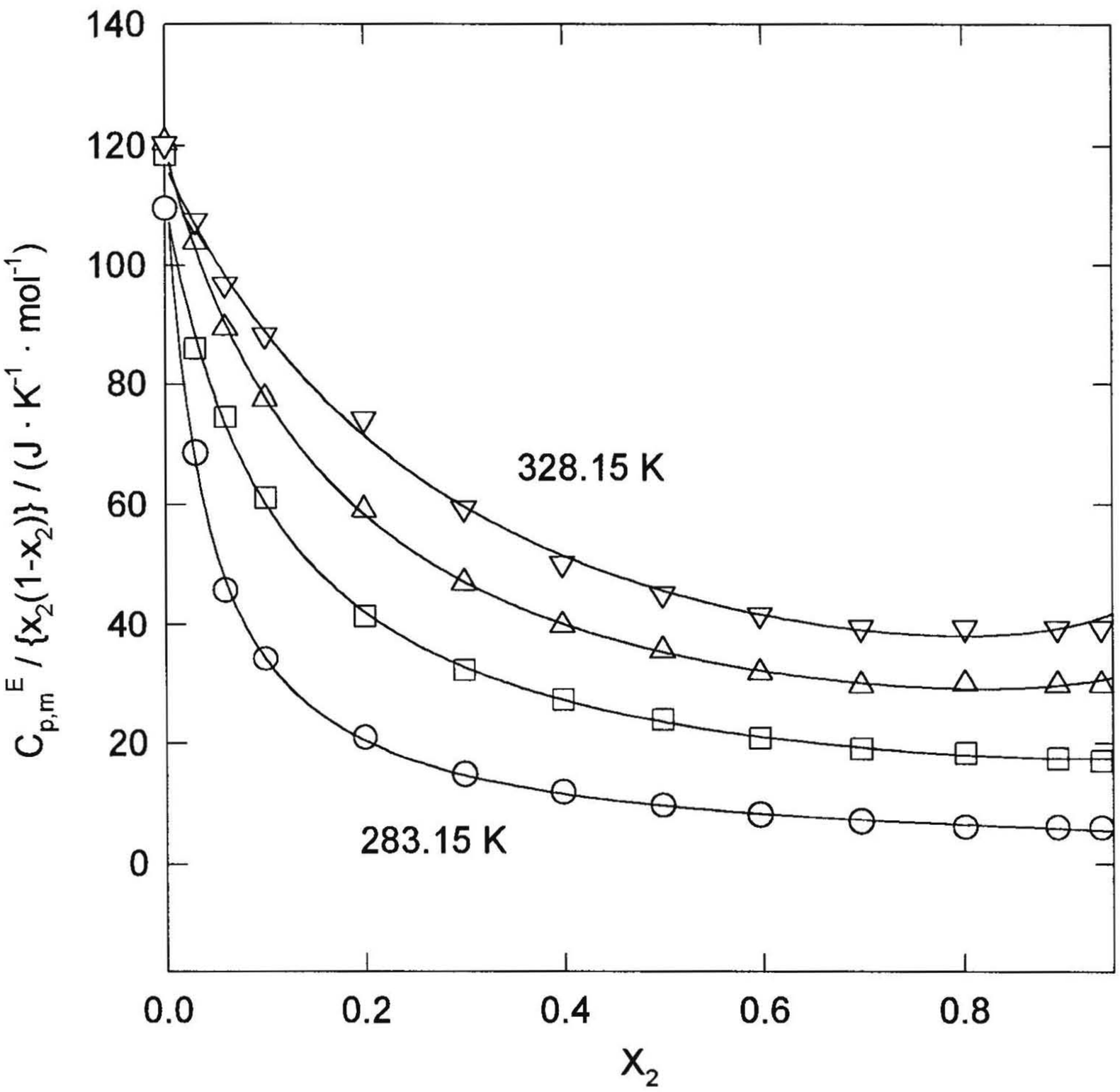

Figure A.4.4 Reduced excess molar heat capacities of aqueous MDEA from 283.15 K to 328.15 K (at 15 K intervals) plotted against mole fraction (Hawrylak, 1999). Symbols are experimental results; ($C^{o}_{p,m,2}$ - $C^{*}_{p,m,2}$) values at $x_2 \rightarrow 0$ were taken from Hawrylak (1999). Lines are fitted values of Equation (4.8).